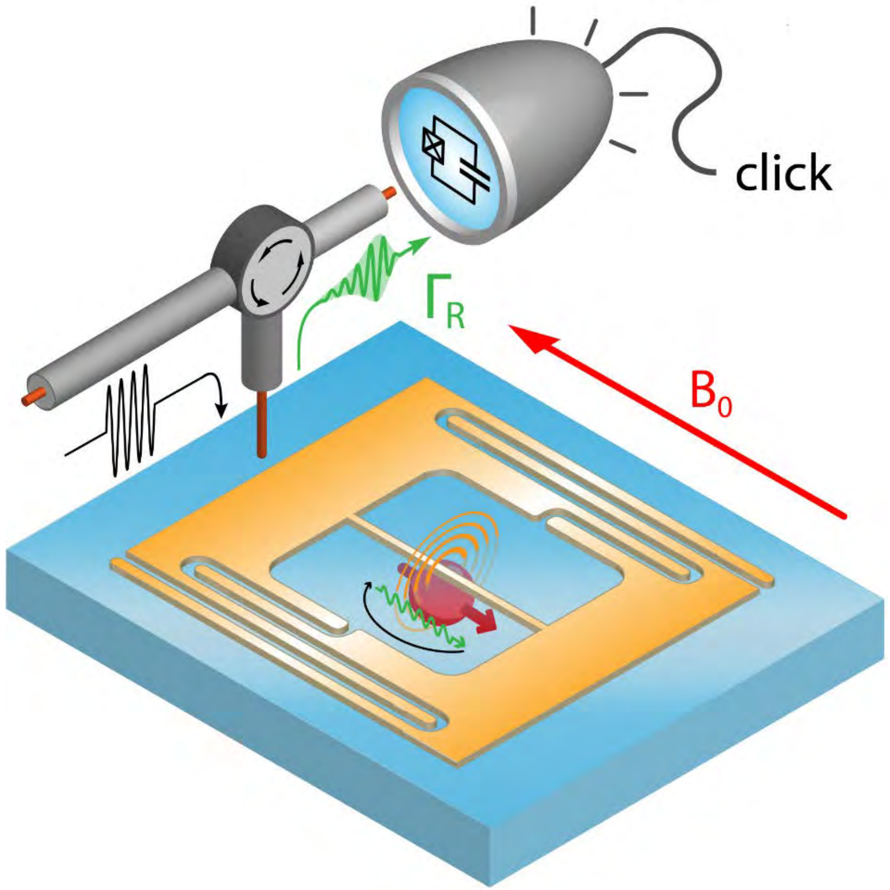

Quantum control of individual nuclear spins in solids

P. Bertet

Quantronics group, SPEC, CEA, Université Paris-Saclay

Individual nuclear spins for quantum computing and spectroscopy

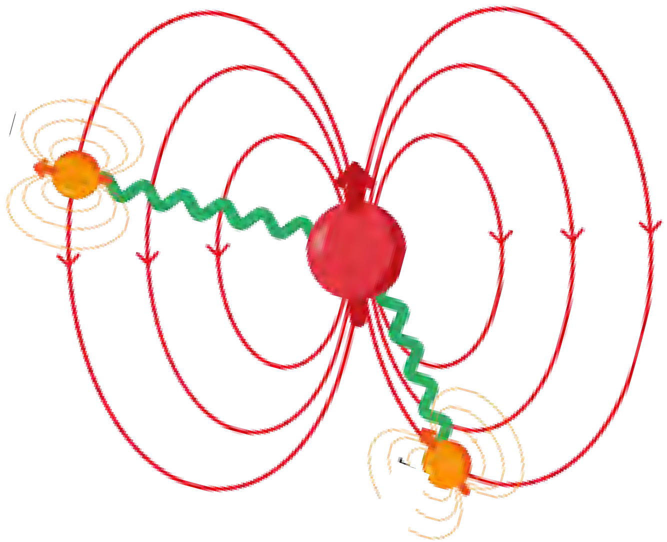

Nuclear spins in solids have long coherence times (up to hours) and narrow spectral lines.
The quantum control of individual nuclear spins opens new perspectives for quantum computing and sensing

Individual nuclear spins for quantum computing and spectroscopy

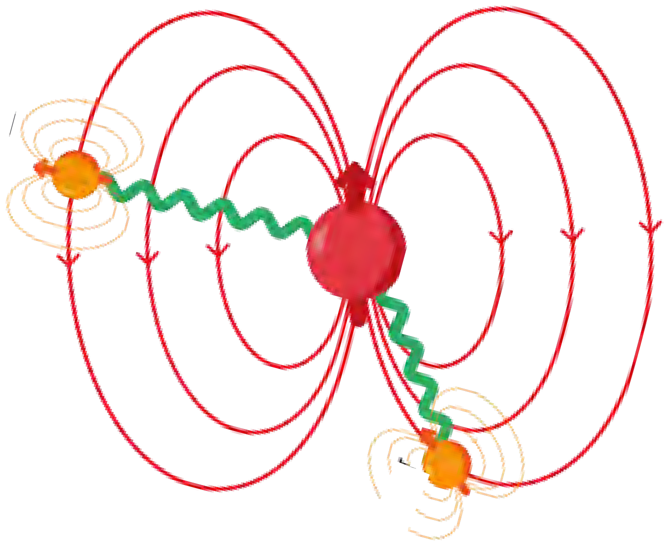

Nuclear spins in solids have long coherence times (up to hours) and narrow spectral lines.
The quantum control of individual nuclear spins opens new perspectives for quantum computing and sensing

1) All-microwave methods to control the quantum state and readout individual nuclear spins at 10mK, using an electron-spin as an ancilla *J. Travesedo et al., Science Advances (2025)*

2) Application to quantum computing : demonstration of a two-nuclear-spin-qubit processor
J. O'Sullivan et al., Nature Phys. (2025)

3) Application to spectroscopy of high-spin nuclei : observation of higher-order terms in the spin Hamiltonian
J. Travesedo et al., arxiv (2026)

Single-spin magnetic resonance : state-of-the-art

Optically-Detected Magnetic Resonance

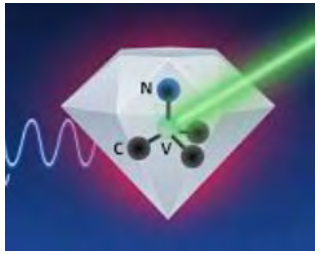

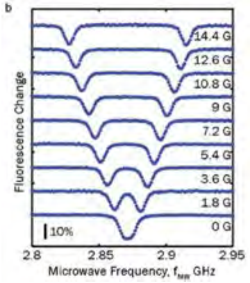

Gruber et al., Science (1997)
Jelezko et al., Phys. Rev. Lett. (2004)
Robledo et al., Nature (2011)

Spin-to-charge conversion Electrical Transport

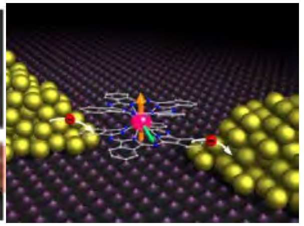

J. Elzerman et al., Nature (2004)
R. Vincent et al., Nature (2012)
Morello et al., Nature (2010)

Scanning probes (mechanical resonators, NVs, STM ..)

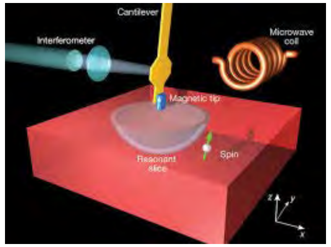

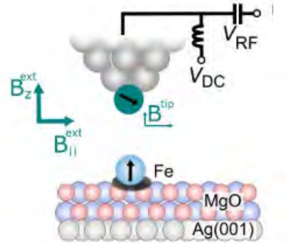

D. Rugar et al., Nature (2004)
M.Grinolds et al., Nature Phys. (2013)
S. Baumann et al., Science (2015)

System-specific / Small detection volume ($\sim 10^4 nm^3$ max)

All-microwave single-spin magnetic resonance method using superconducting quantum circuits

Main experimental constraint : $T \ll \frac{\hbar\omega_0}{k_B}$ (well satisfied at T=10mK and $\frac{\omega_0}{2\pi}$ =7GHz)

Single electron spin detection by microwave fluorescence

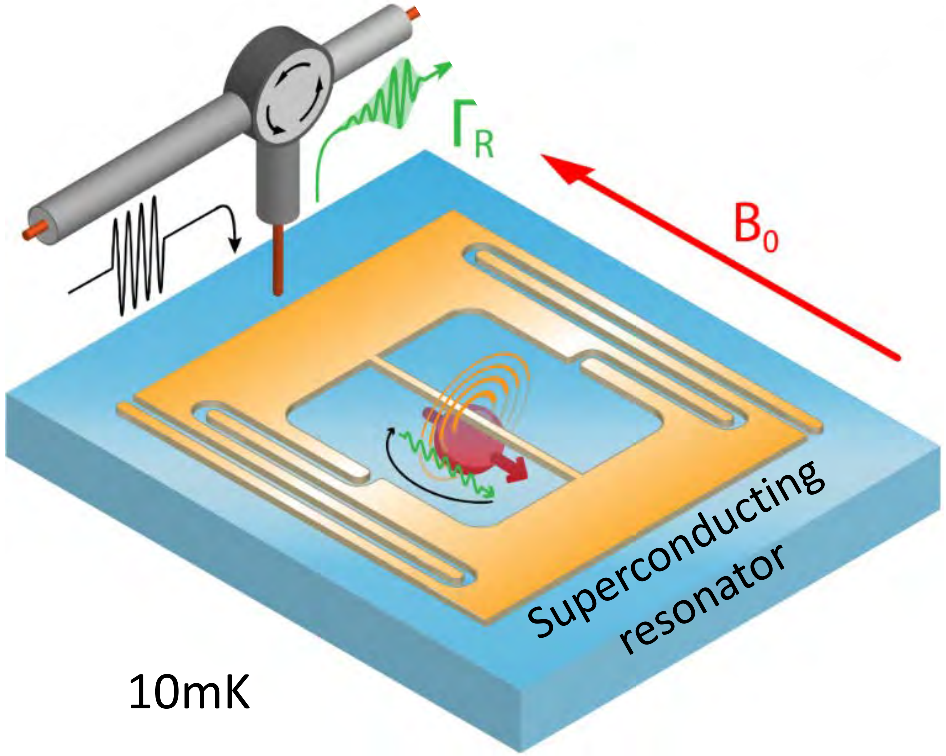

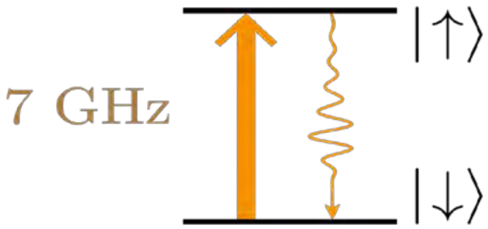

In free-space : $\Gamma_R \sim 10^{-12}s^{-1}$
Enhanced up to $\Gamma_R \sim 10^{3}s^{-1}$ by resonator coupling (Purcell effect)

A. Bienfait et al., Nature (2016)
E. Albertinale et al., Nature (2021)
Z. Wang et al., Nature (2023)

Single electron spin detection by microwave fluorescence

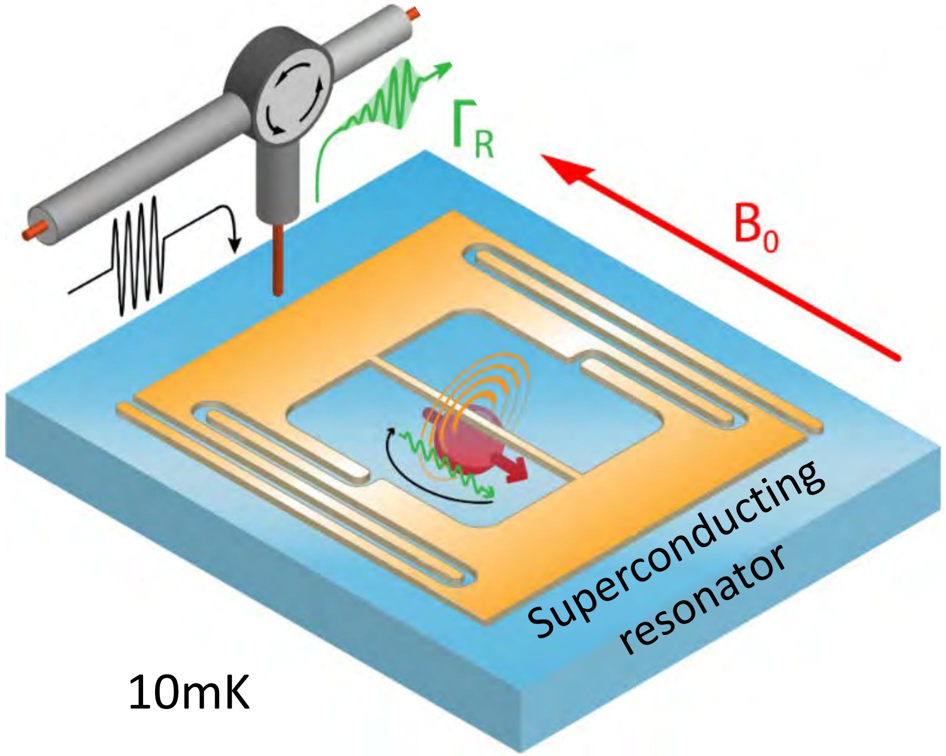

A. Bienfait et al., Nature (2016)
E. Albertinale et al., Nature (2021)
Z. Wang et al., Nature (2023)

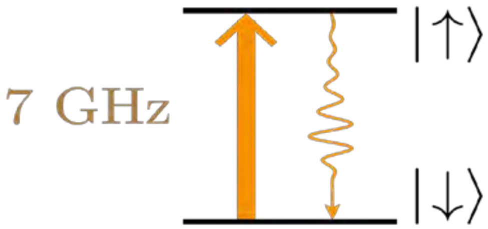

In free-space : $\Gamma_R \sim 10^{-12} s^{-1}$
Enhanced up to $\Gamma_R \sim 10^{3} s^{-1}$ by resonator coupling (Purcell effect)

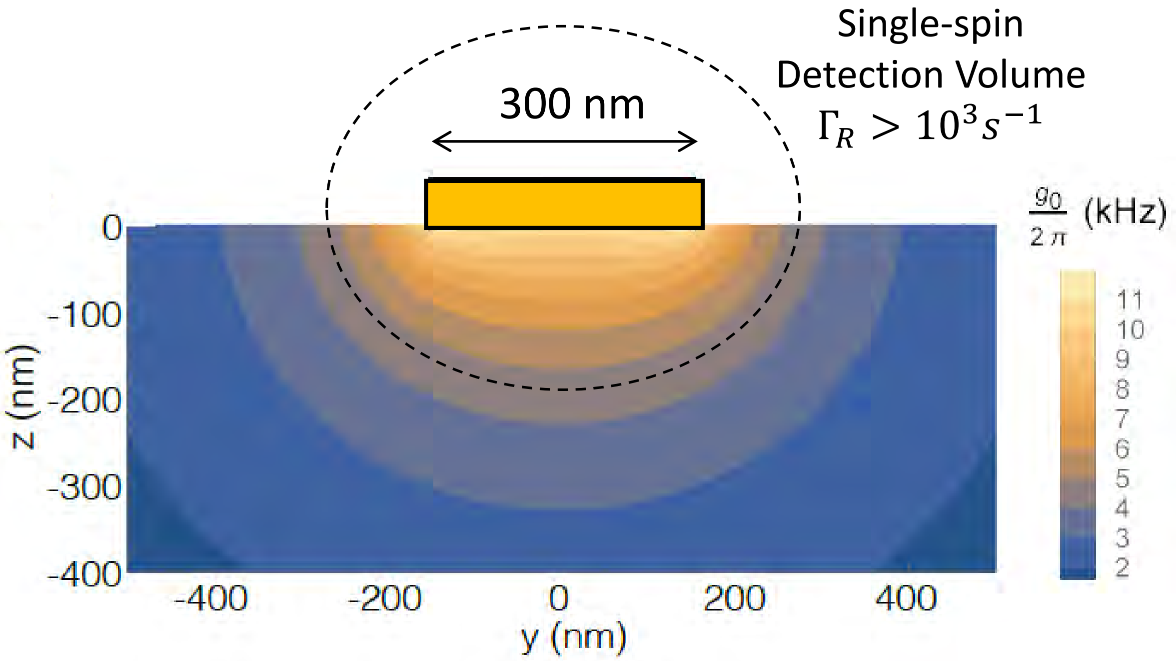

Single electron spin detection by microwave fluorescence

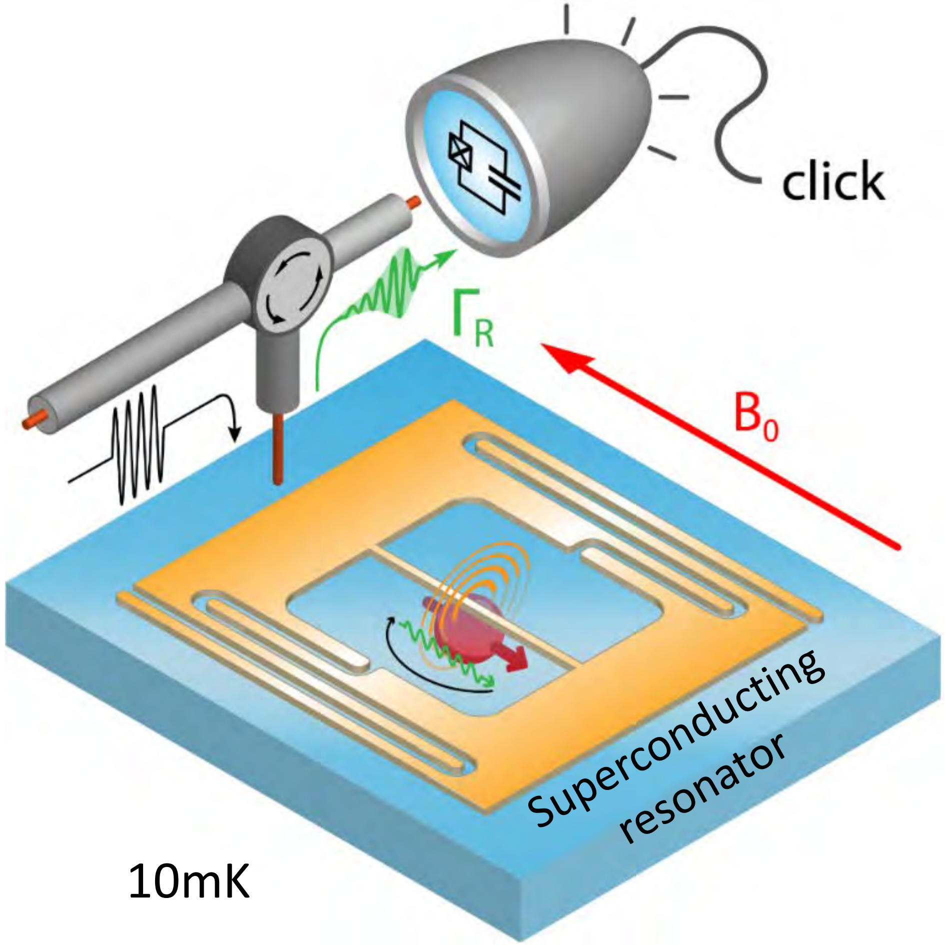

A. Bienfait et al., Nature (2016)
E. Albertinale et al., Nature (2021)
Z. Wang et al., Nature (2023)

Single Microwave Photon Detector

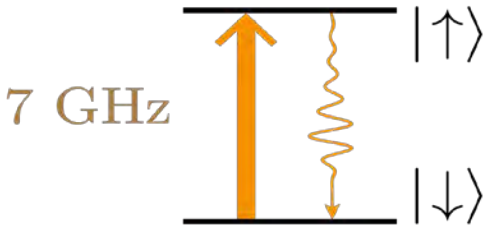

In free-space : $\Gamma_R \sim 10^{-12} s^{-1}$
Enhanced up to $\Gamma_R \sim 10^{3} s^{-1}$ by resonator coupling (Purcell effect)

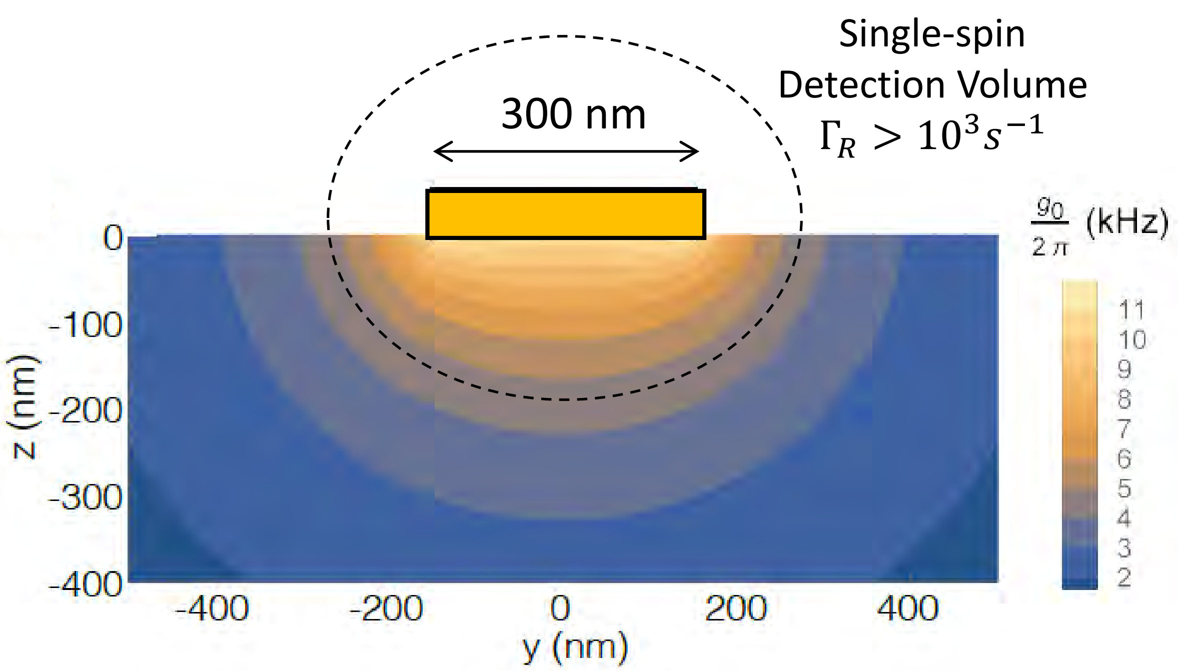

Single Microwave Photon Detector (SMPD)

E. Flurin

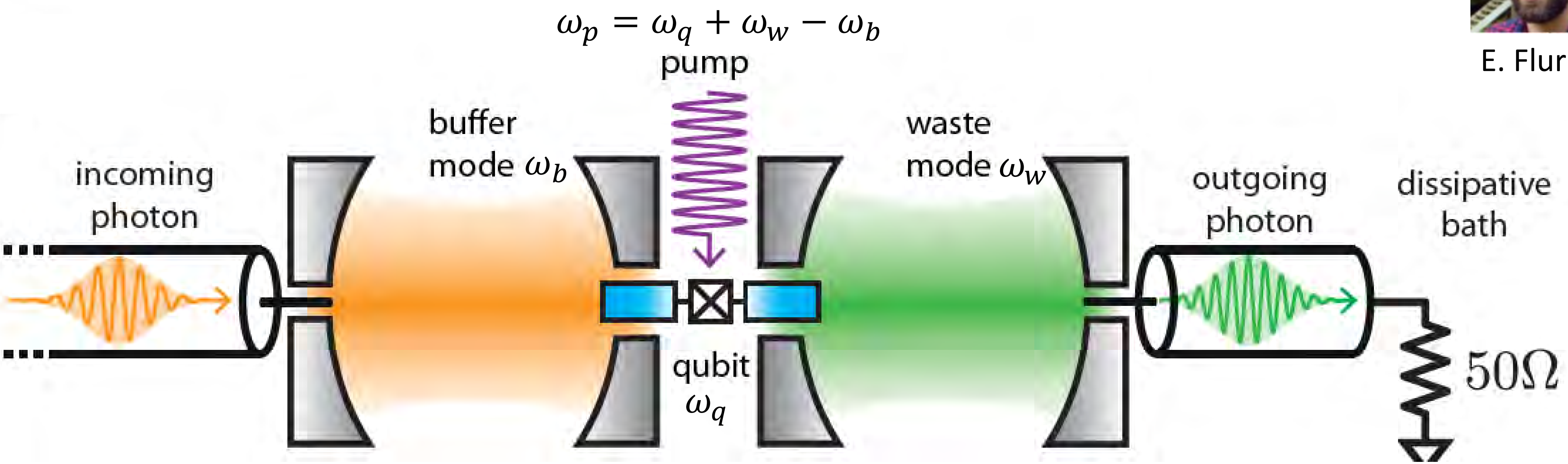

- Four-Wave-Mixing with transmon qubit
- Narrow-band detector with tunable input freq ω_b

Other circuit-QED-based SMPD designs

K. Inomata et al. Nature com (2016)

J.-C. Besse et al. Phys. Rev. X (2018)

Kono, S, et al. Nature Physics 14.6 (2018)

Opremcak, A., et al., Science 361.6408 (2018)

Lescanne et al., PRX (2020)

Balembois et al., PRAppl (2023)

Pallegoix et al., arxiv (2025)

Time traces for increasing input power

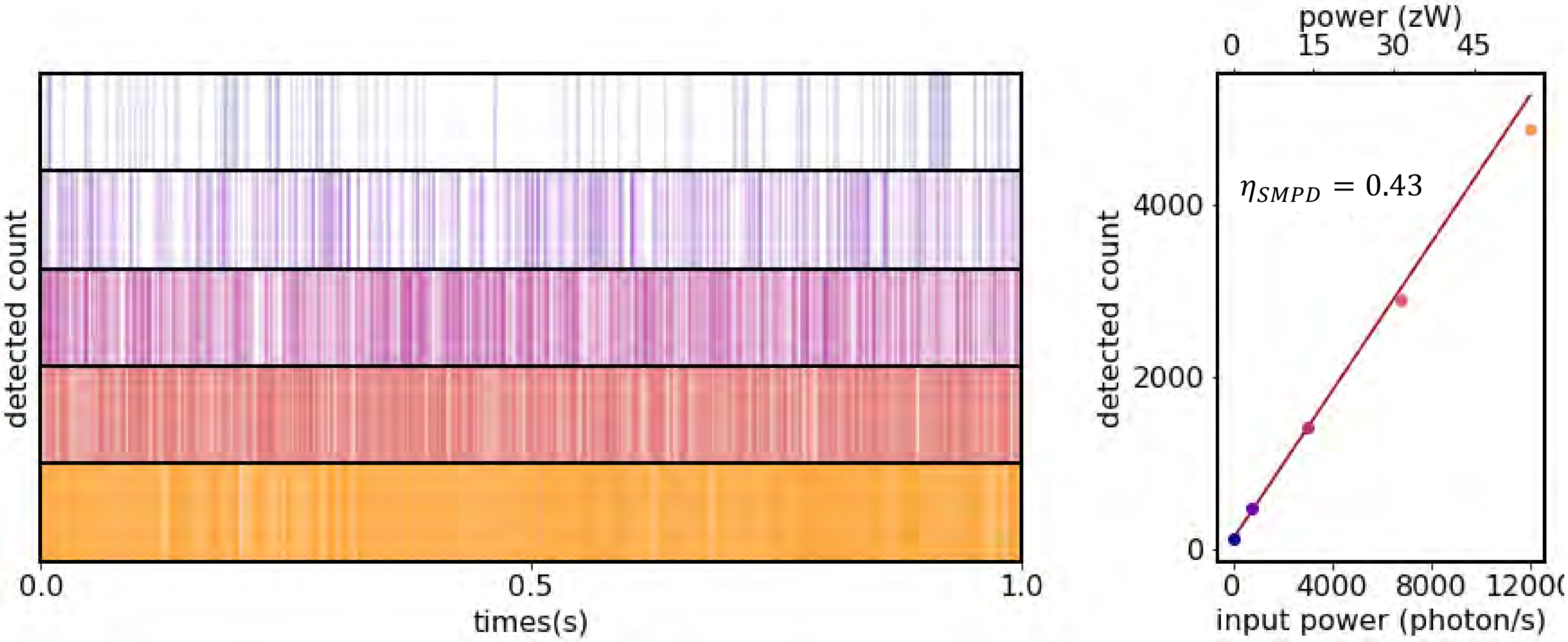

L. Balembois et al., Phys. Rev. Appl. (2025)

Best detector performance

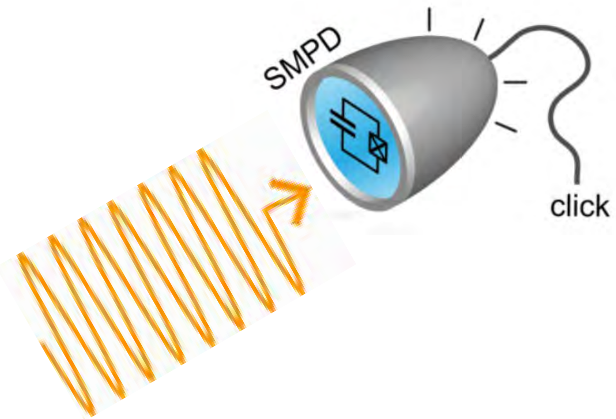

Dark-count rate	$\alpha = 40\ s^{-1}$
Quantum efficiency	0.8
Tunable bandwidth	$100 - 500$ kHz

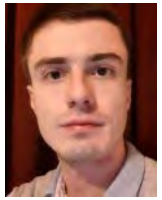

L. Pallegoix

E. Flurin

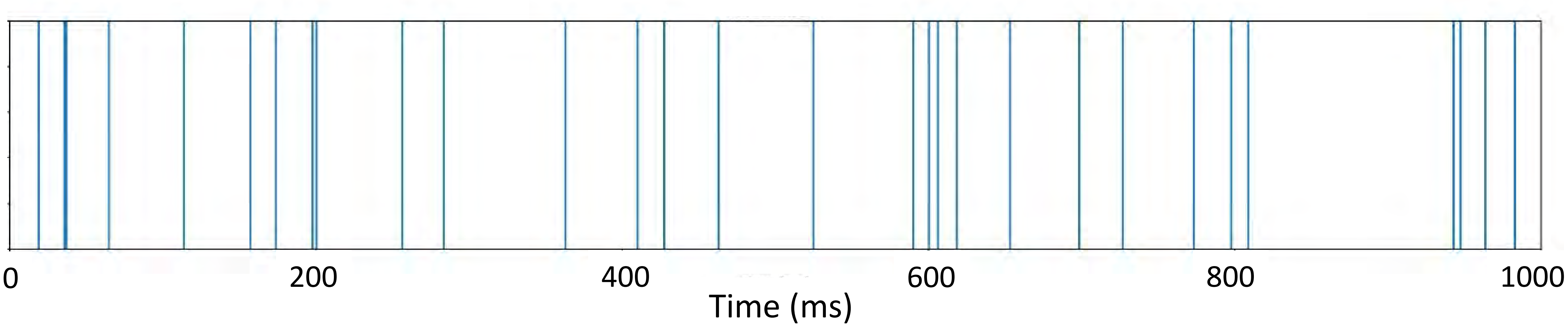

Most sensitive energy detector at microwave frequencies

Applications : single spin detection, Axion Dark Matter Search, …

L. Pallegoix et al., Phys.Rev. Appl (2026)

$CaWO_4$

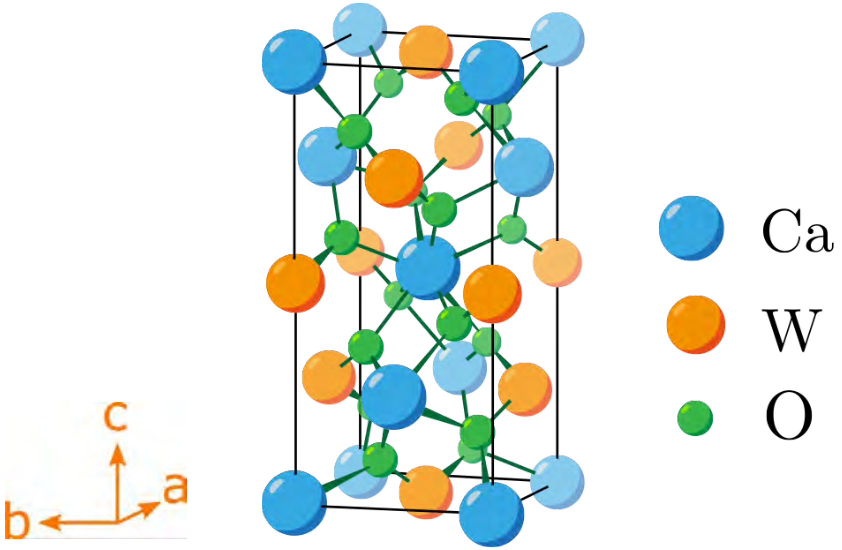

S_4 symmetry site

- Tetragonal symmetry
- Low nuclear magnetic moment density

  14% abundance ^{183}W (I=1/2, $\mu_W = 0.12\mu_N$)

➡ Narrow electron and nuclear spin linewidth

Er^{3+}:$CaWO_4$

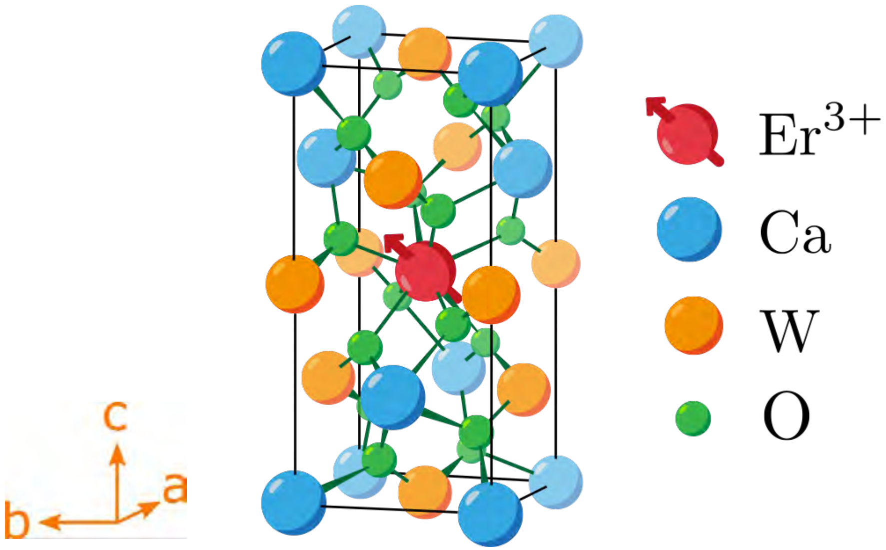

S_4 symmetry site

Effective $S = \frac{1}{2}$ (Kramers doublet)

$$\begin{array}{cc} & \begin{array}{ccc} a & b & c \end{array} \\ \dfrac{\gamma}{2\pi} = & \begin{pmatrix} 117.3 & 0 & 0 \\ 0 & 117.3 & 0 \\ 0 & 0 & 17.45 \end{pmatrix} GHz/T \end{array}$$

4x larger than free-electron

Favorable for large Γ_R

- Tetragonal symmetry
- Low nuclear magnetic moment density
  14% abundance ^{183}W (I=1/2, $\mu_W = 0.12\mu_N$)

➡ Narrow electron and nuclear spin linewidth

Undoped $CaWO_4$ sample grown by P. Goldner at Chimie ParisTech

Residual [Er] $\approx$ 3ppb

Experiment

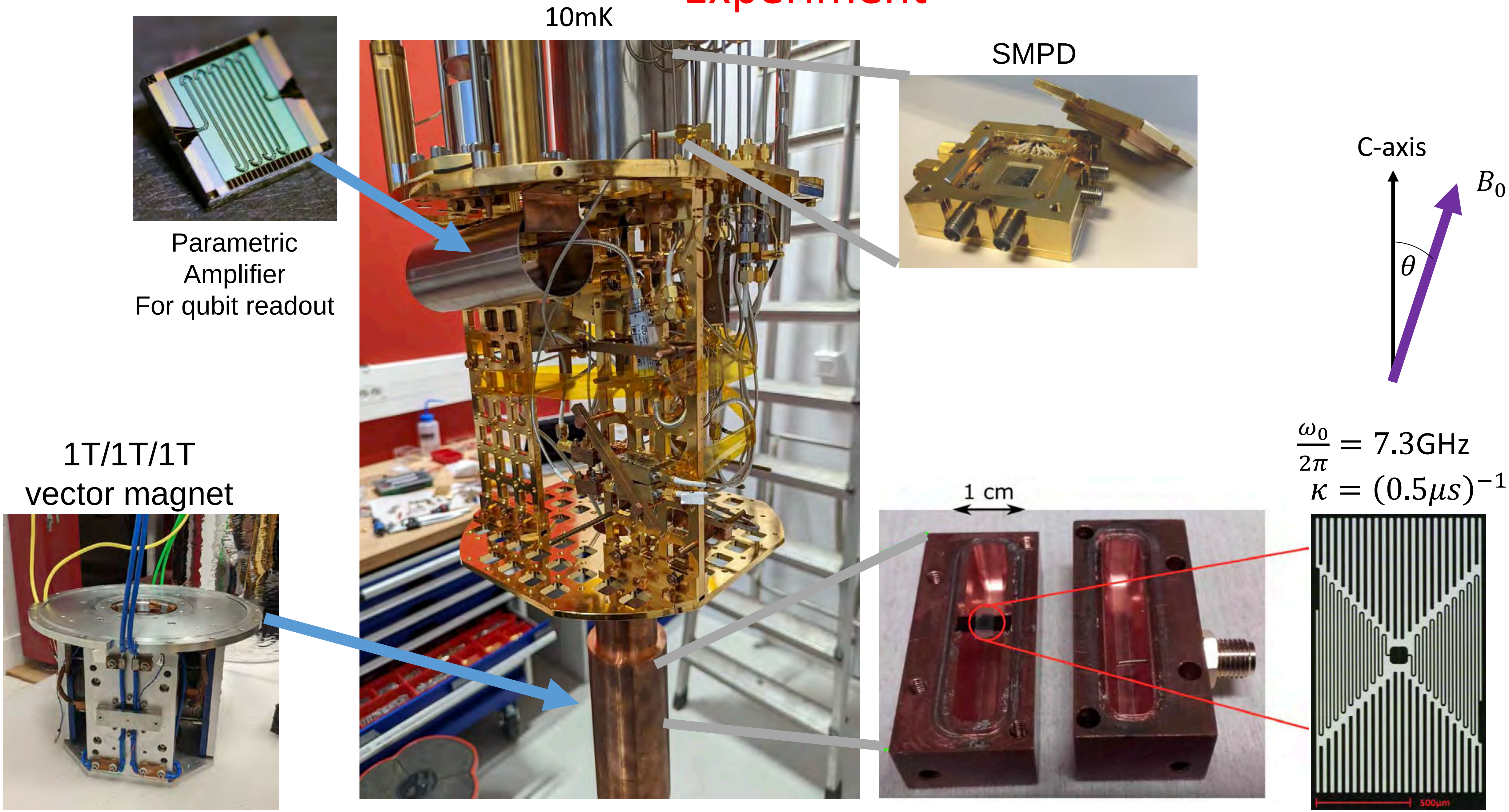
10mK
Parametric Amplifier For qubit readout
SMPD
C-axis
B_0
θ
1T/1T/1T vector magnet
1 cm
$\frac{\omega_0}{2\pi} = 7.3\text{GHz}$
$\kappa = (0.5\mu s)^{-1}$
500μm

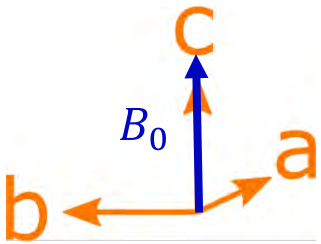

Single Er^{3+}-resolved spectroscopy

Z. Wang

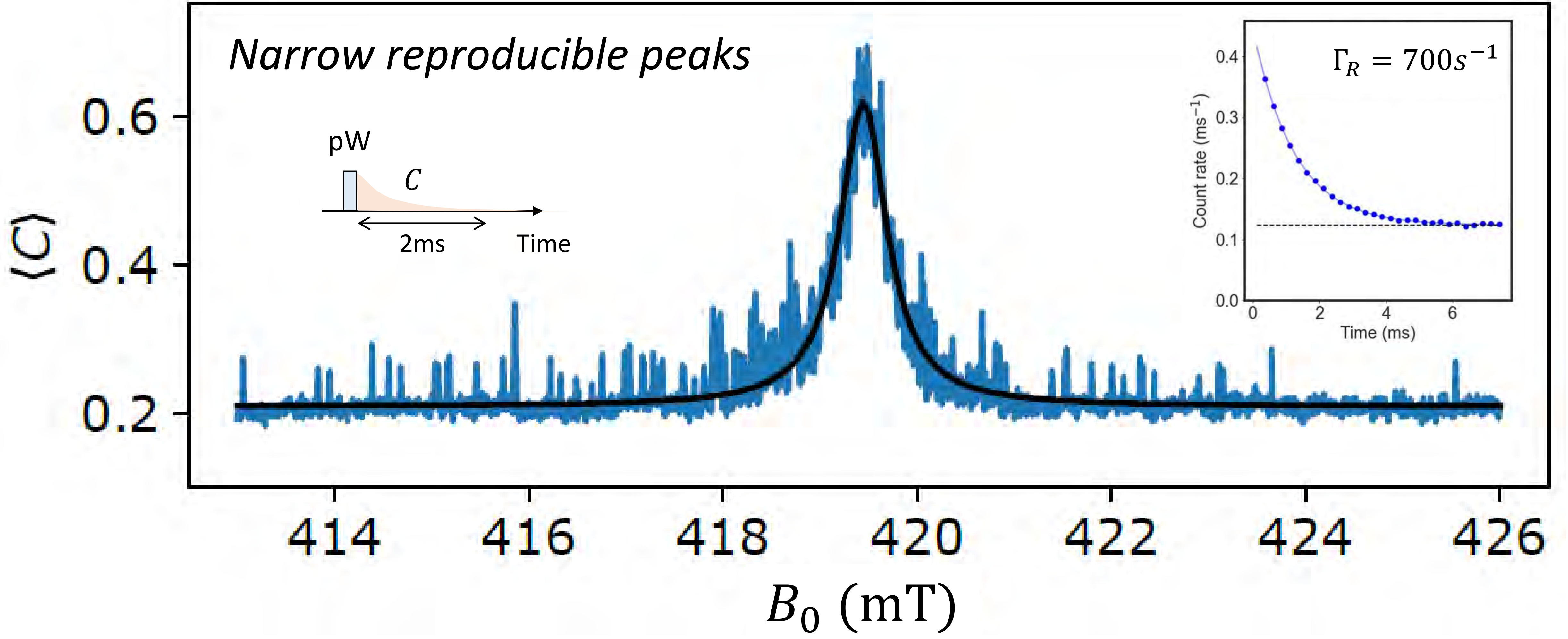

Z. Wang et al., Nature (2023)

Intensity-intensity correlation function

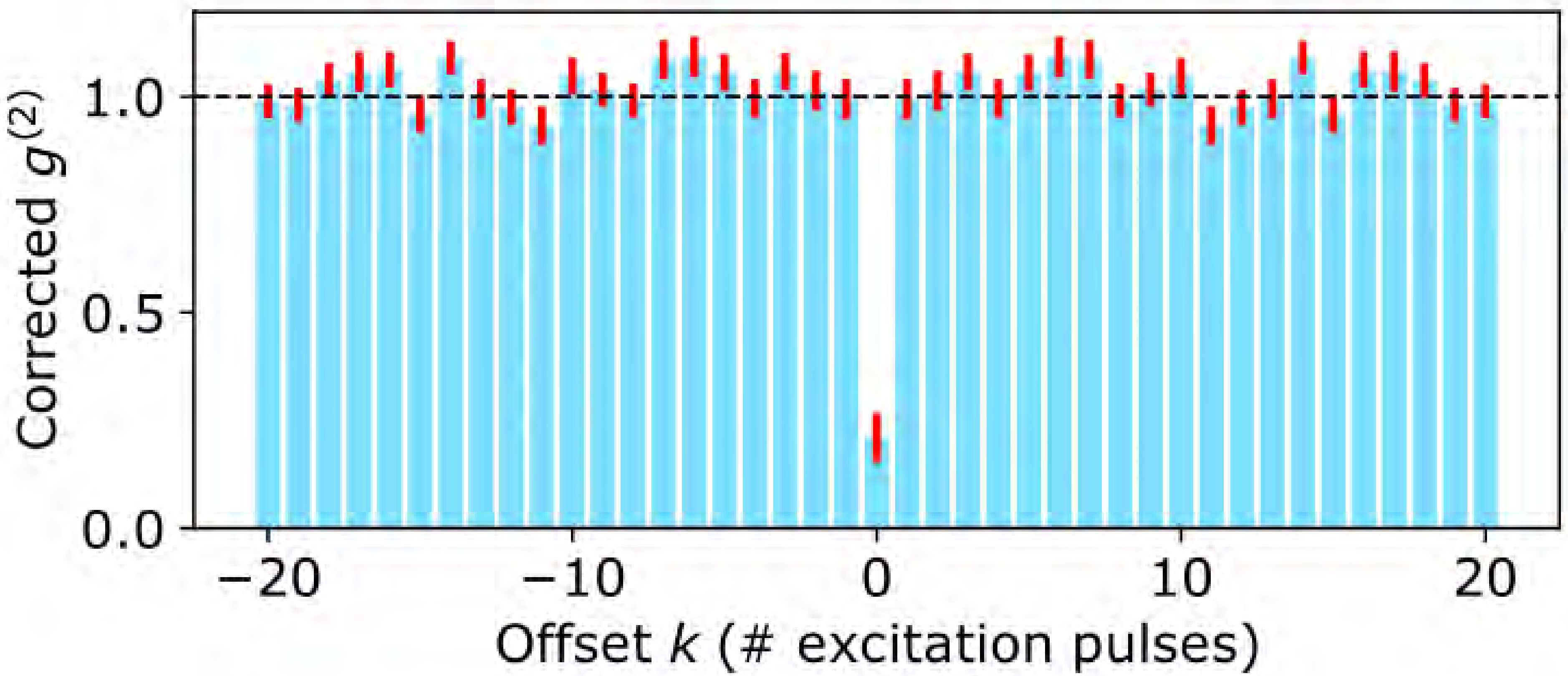

$g^2(0) = 0.23 \pm 0.06 < 0.5$ → Single-electron-spin emission

Z. Wang et al., Nature (2023)

Single-spin-resolved Er^{3+}:$CaWO_4$ spectrum

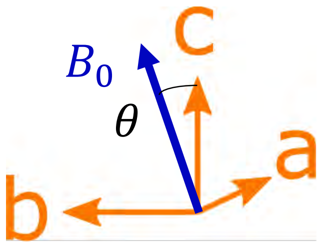

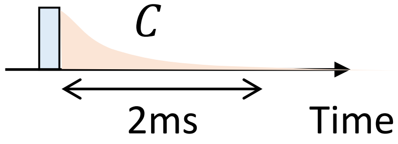

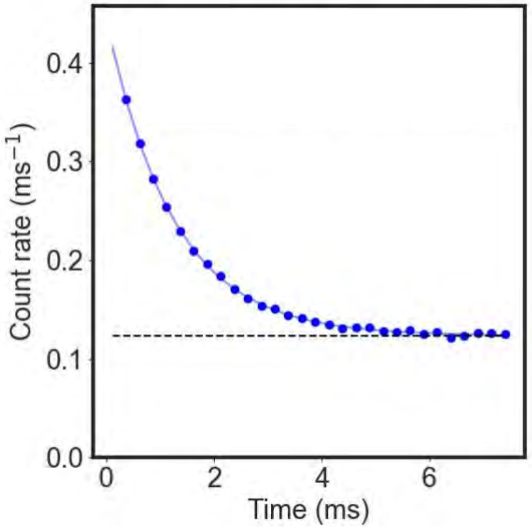

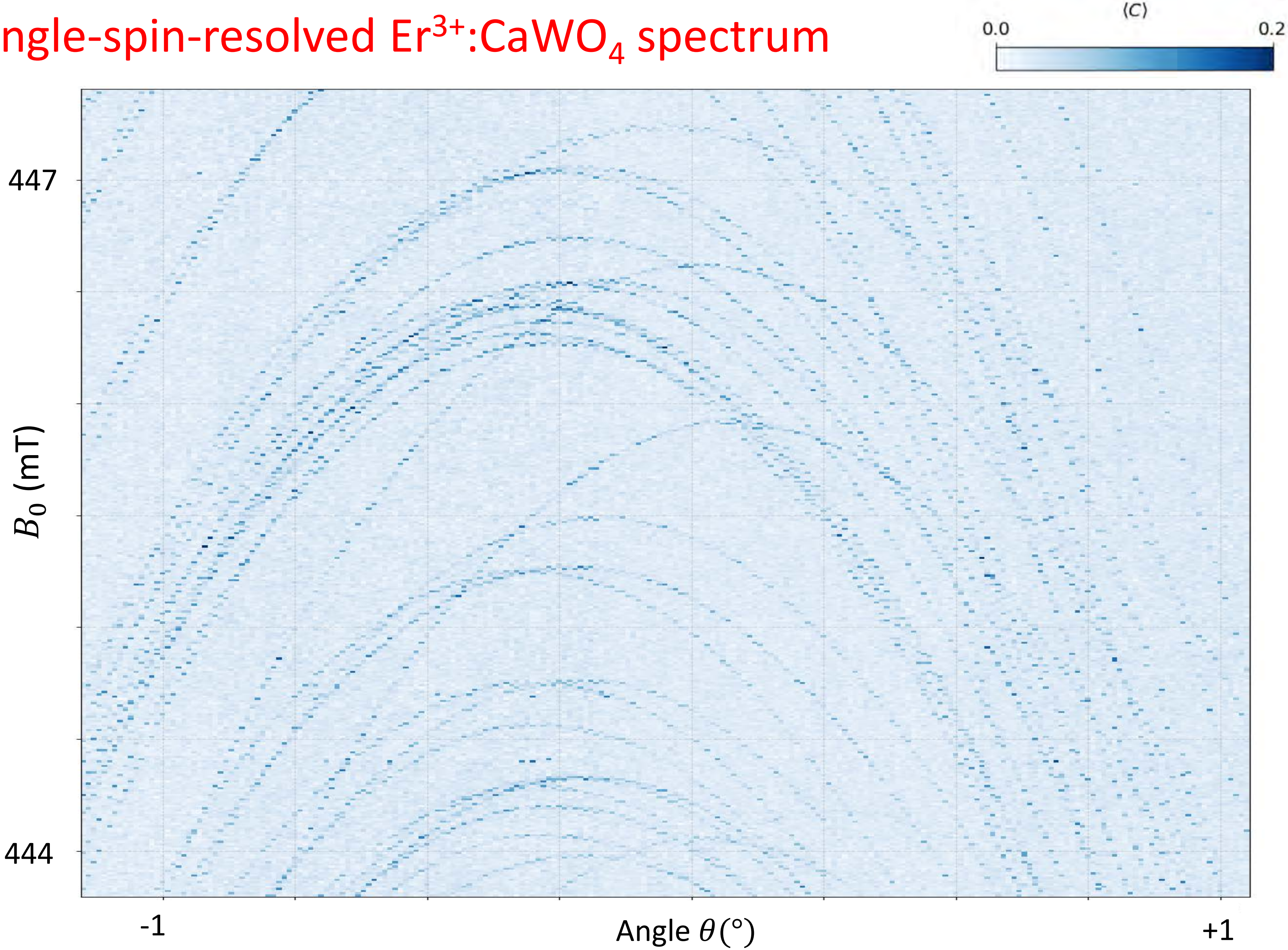

Z. Wang et al., Nature (2023)
J. Travesedo et al., arxiv (2026)

Interacting paramagnetic impurity and nuclear spin : Spin Hamiltonian

- « Standard model » of paramagnetic NMR and EPR spectroscopy
  (Dynamic Nuclear Polarization, ENDOR, ESEEM, ….)
- Spin-based Quantum Information Processing

Interacting paramagnetic impurity and nuclear spin 1/2 : Spin Hamiltonian

$$\mathcal{H} = \mathcal{H}_{eZ} + \mathcal{H}_{hf} + \mathcal{H}_{nZ}$$

Electron spin 1/2

$$\mathcal{H}_{eZ} = \omega_S S_z$$

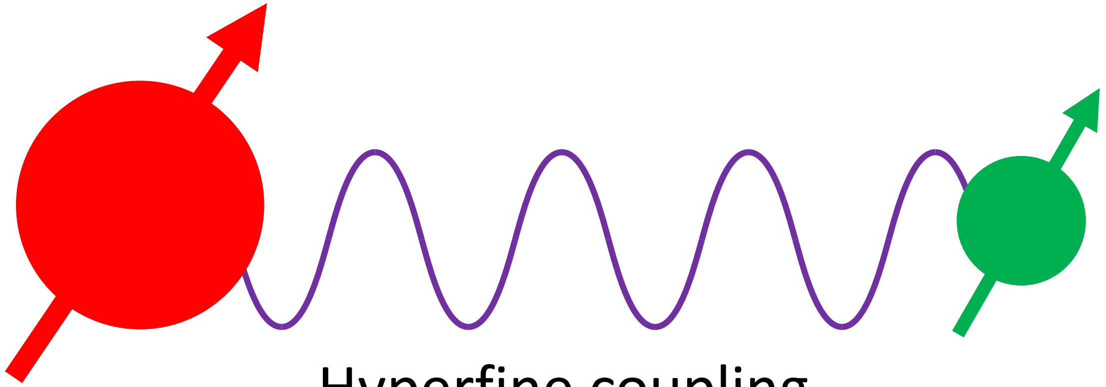

Nuclear spin 1/2

$$\mathcal{H}_{nZ} = \omega_I I_z$$

Hyperfine coupling
(dipolar + Fermi contact)

$$\mathcal{H}_{hf} = S \cdot \bar{\bar{A}} \cdot I$$

- « Standard model » of paramagnetic NMR and EPR spectroscopy
  (Dynamic Nuclear Polarization, ENDOR, ESEEM, ….)
- Spin-based Quantum Information Processing

Energy levels of coupled electron-nuclear spin system

$$\hat{H} = \omega_S \hat{S}_z + \omega_I \hat{I}_z + A_\parallel \hat{S}_z \hat{I}_z + A_\perp \hat{S}_z \hat{I}_x$$

High-field limit $|\omega_I| \gg A_\parallel, A_\perp$

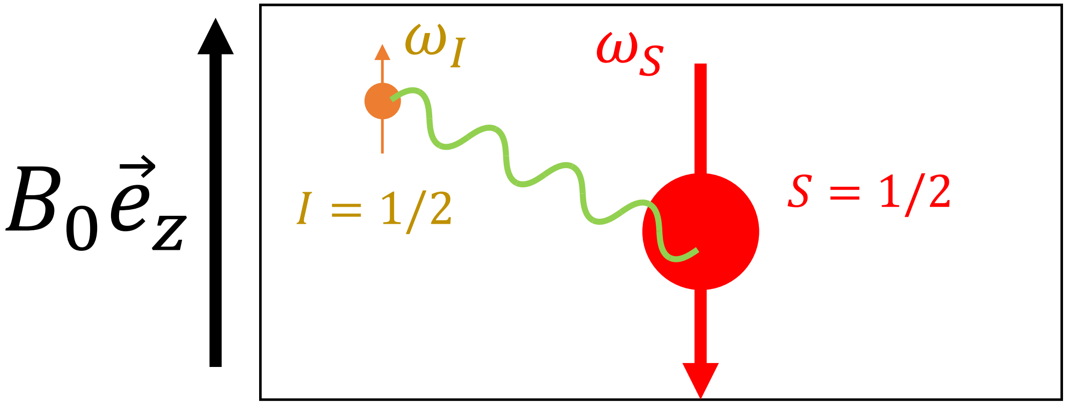

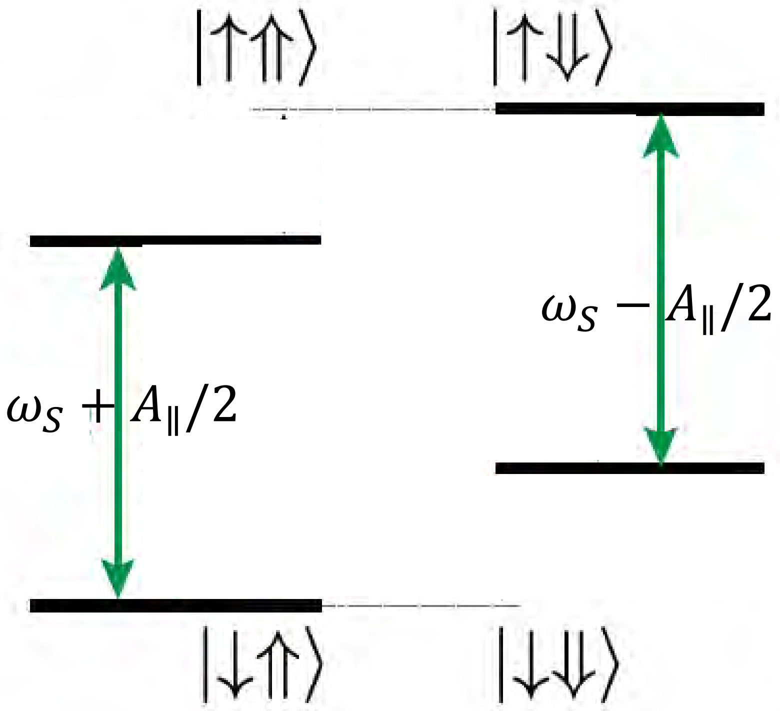

- Electron spin frequency depends on NS state

→ NS detection

Energy levels of coupled electron-nuclear spin system

$$\hat{H} = \omega_S \hat{S}_z + \omega_I \hat{I}_z + A_\parallel \hat{S}_z \hat{I}_z + A_\perp \hat{S}_z \hat{I}_x$$

High-field limit $|\omega_I| \gg A_\parallel, A_\perp$

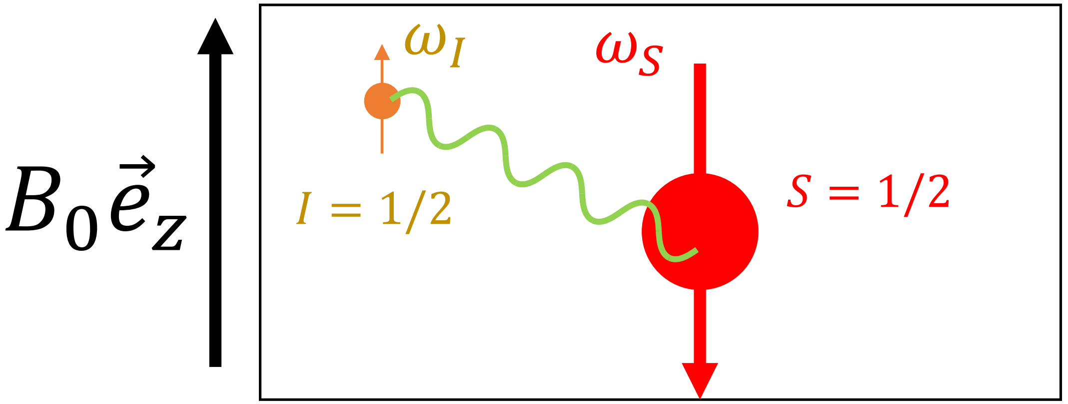

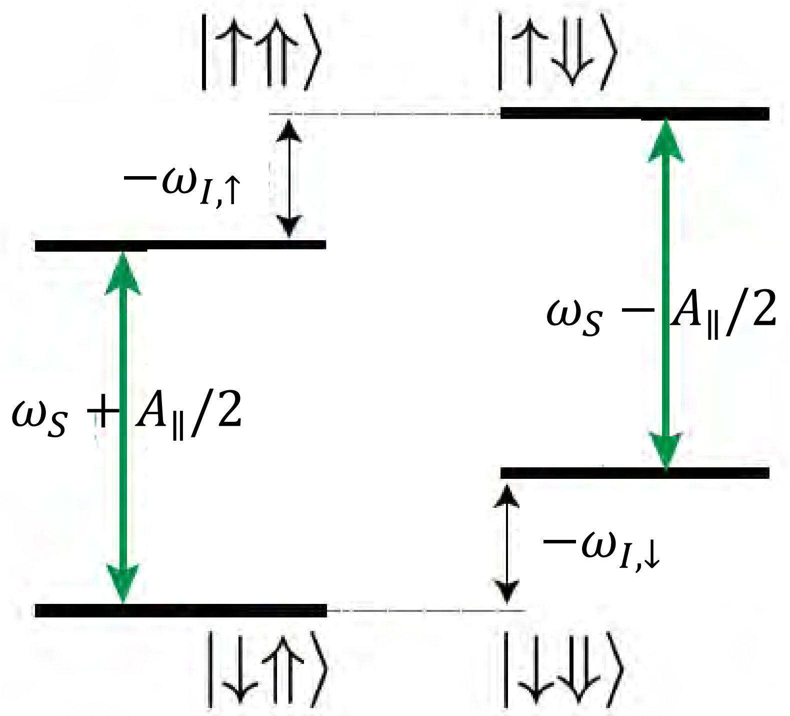

- Electron spin frequency depends on NS state

  ⇒ NS detection

- Nuclear spin frequency depends on electron spin state

  $\omega_{I,\downarrow} = \omega_I - A_\parallel/2$ $\omega_{I,\uparrow} = \omega_I + A_\parallel/2$

  ⇒ Need to measure both to access ω_I
  Also allows spectral addressing

Energy levels of coupled electron-nuclear spin system

$$\hat{H} = \omega_S \hat{S}_z + \omega_I \hat{I}_z + A_\parallel \hat{S}_z \hat{I}_z + A_\perp \hat{S}_z \hat{I}_x$$

High-field limit $|\omega_I| \gg A_\parallel, A_\perp$

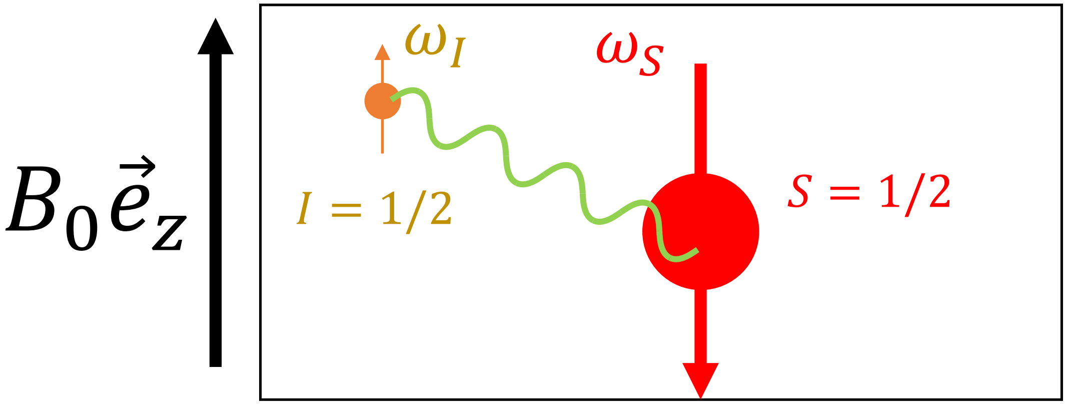

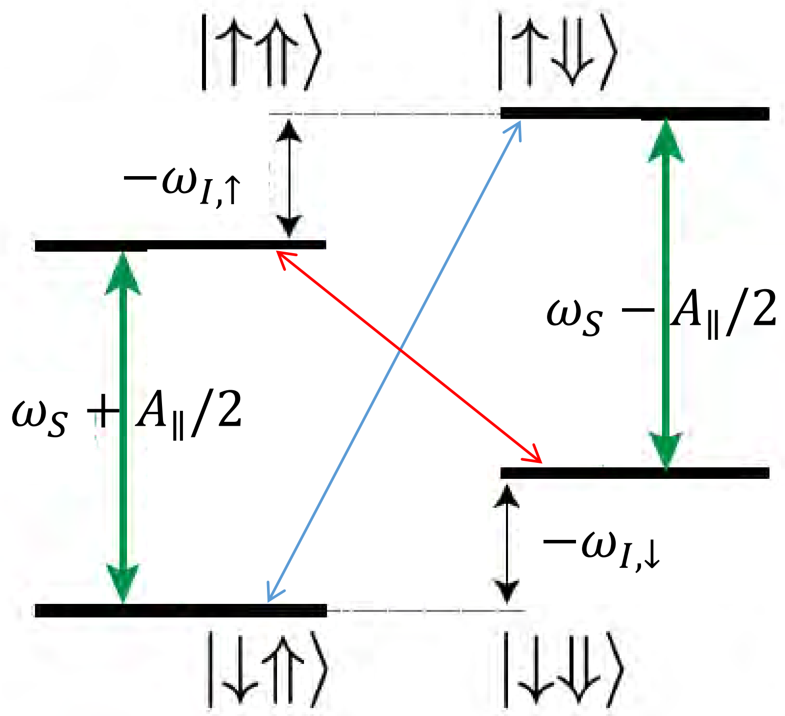

- Electron spin frequency depends on NS state

  ⟹ NS detection

- Nuclear spin frequency depends on electron spin state

  $\omega_{I,\downarrow} = \omega_I - A_\parallel/2 \qquad \omega_{I,\uparrow} = \omega_I + A_\parallel/2$

  ⟹ Need to measure both to access ω_I
  Also allows spectral addressing

- Crossed transitions are weakly allowed

matrix element $|\langle\downarrow\Uparrow|S_x|\uparrow\Downarrow\rangle| = |\langle\downarrow\Downarrow|S_x|\uparrow\Uparrow\rangle| = \left|\frac{A_\perp}{4\omega_I}\right|$

Single-Er^{3+} high-resolution spectroscopy, time dependence

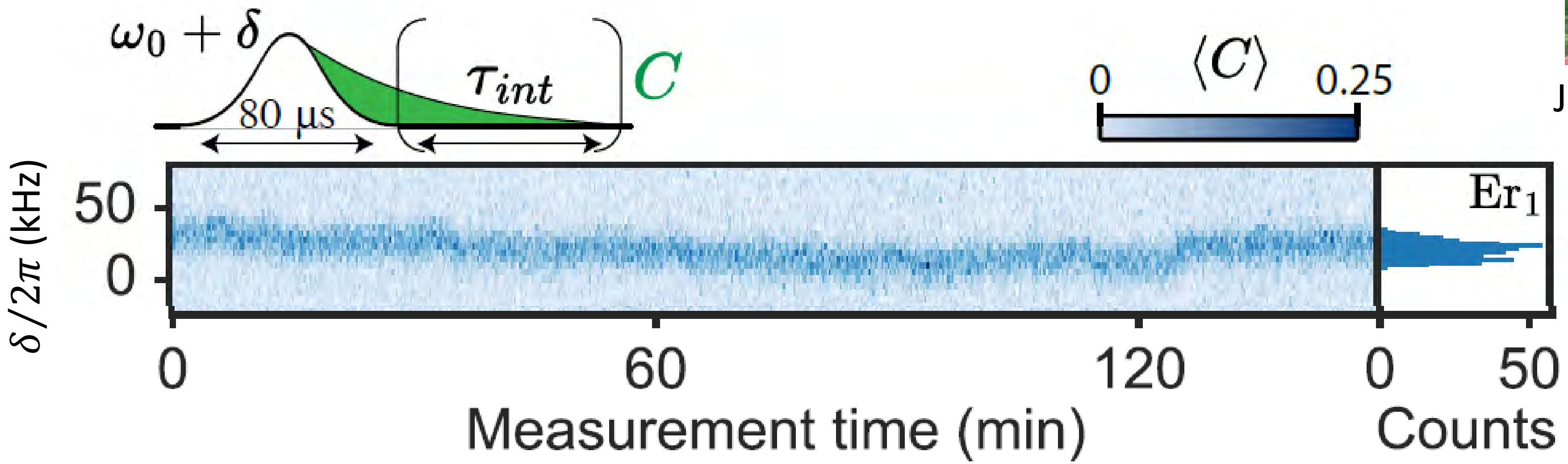

J. Travesedo

J. O'Sullivan

Quantum jumps of individual ^{183}W nuclear spins

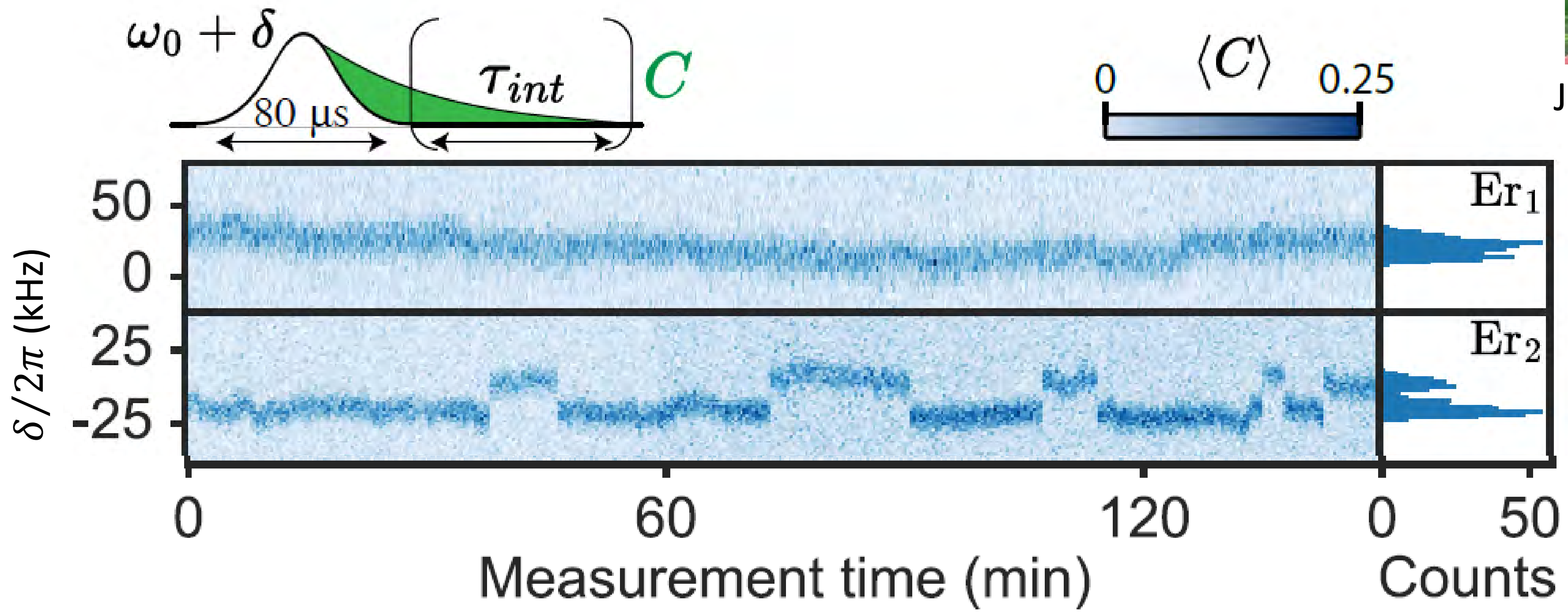

J. Travesedo

J. O'Sullivan

Quantum jumps of individual ^{183}W nuclear spins


J. Travesedo J. O'Sullivan

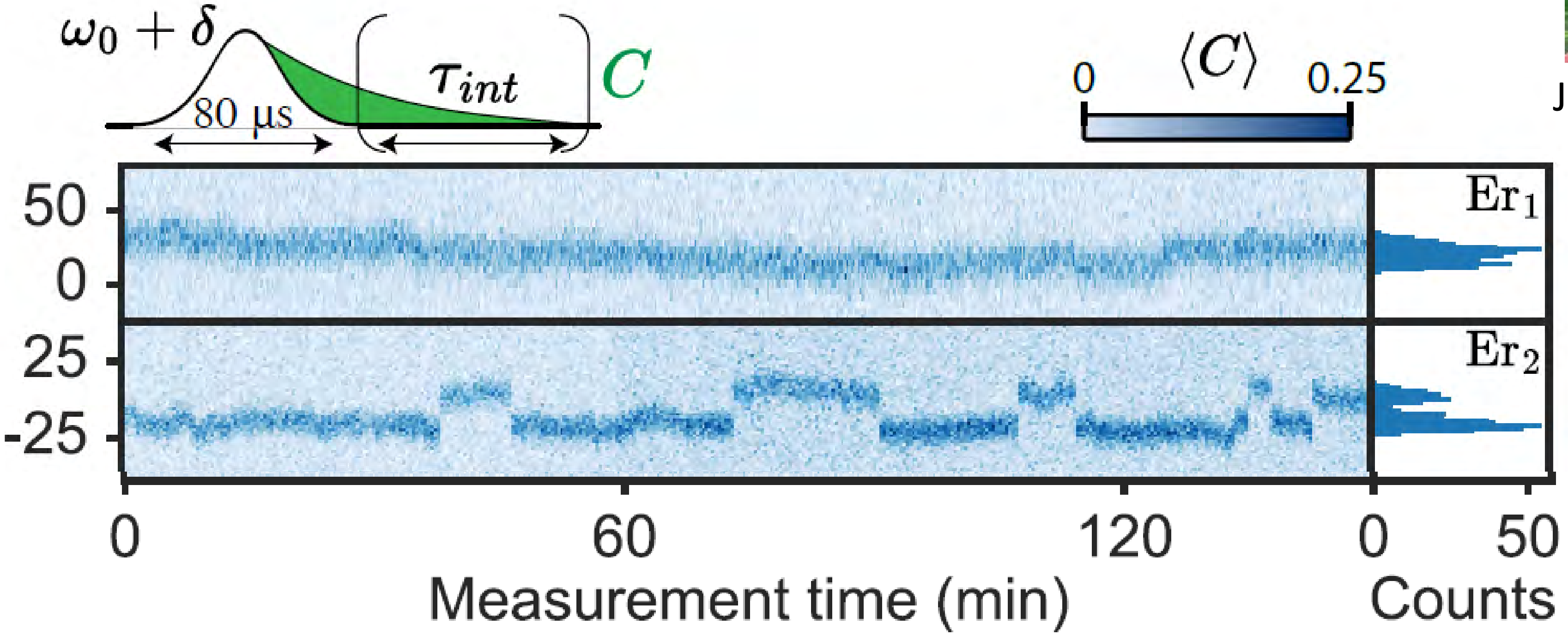

$$\hat{H} = \omega_S \hat{S}_z + \omega_I \hat{I}_z + A_\parallel \hat{S}_z \cdot \hat{I}_z + A_\perp \hat{S}_z \cdot \hat{I}_x$$

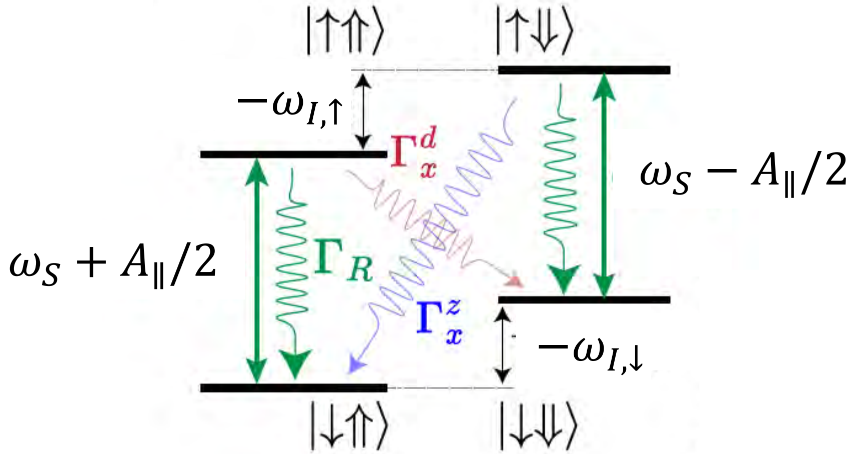

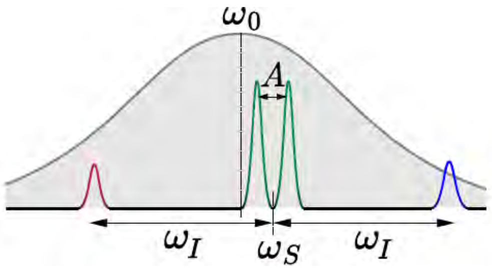

$$\frac{\Gamma_x^{z,d}}{\Gamma_R} = \frac{A_\perp^2}{4\omega_I^2} \frac{1}{1 + 4[\omega_I \pm (\omega_S - \omega_0)]^2/\kappa^2}$$

Quantum jumps of individual ^{183}W nuclear spins

J. Travesedo

J. O'Sullivan

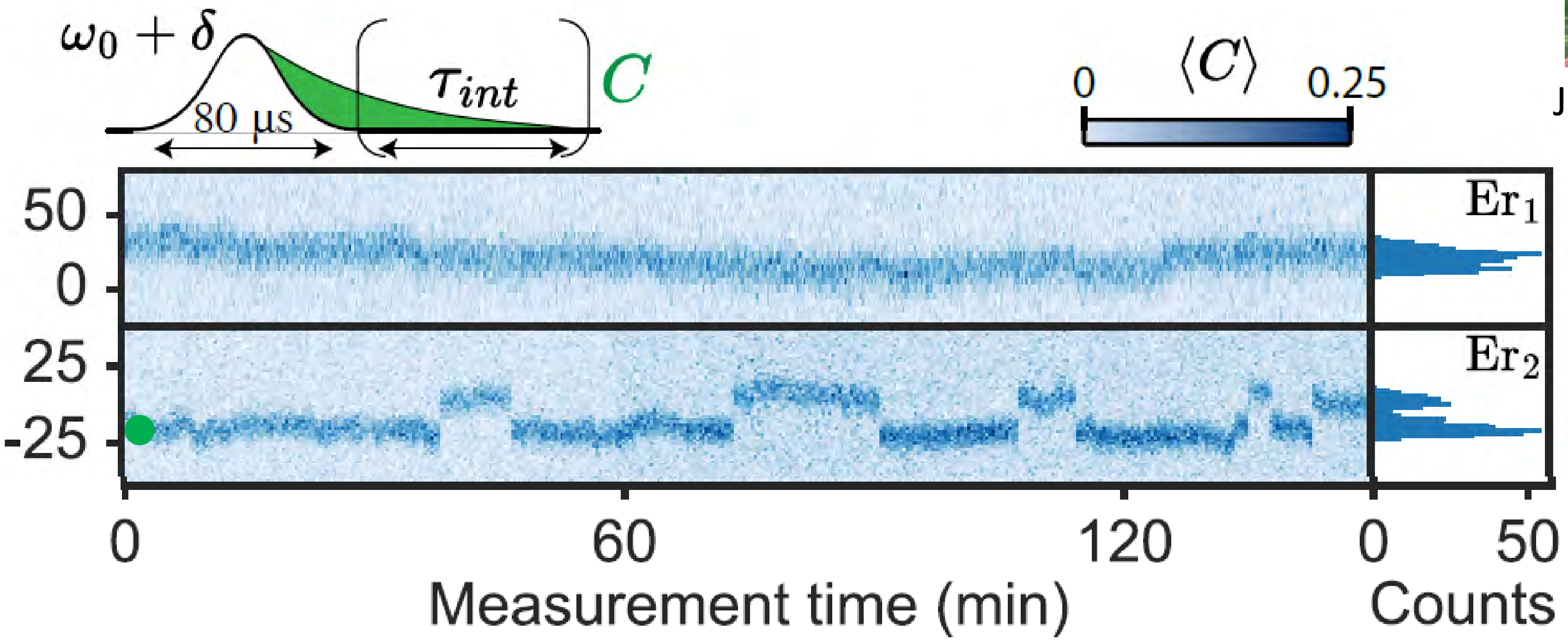

$$\widehat{H} = \omega_S \hat{S}_z + \omega_I \hat{I}_z + A_{\parallel} \hat{S}_z \cdot \hat{I}_z + A_{\perp} \hat{S}_z \cdot \hat{I}_x$$

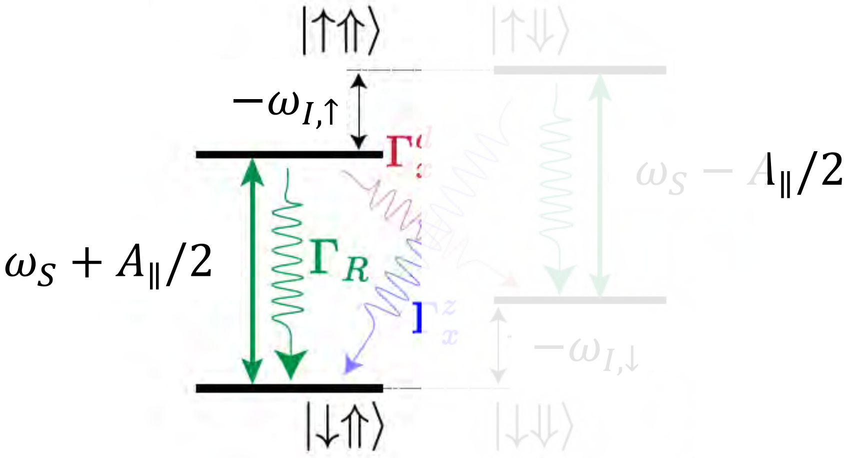

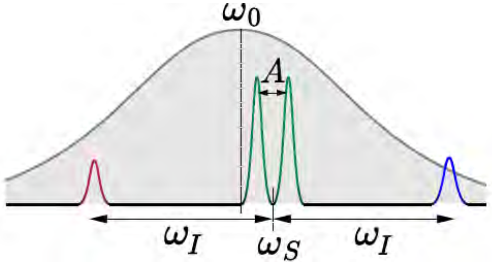

$$\frac{\Gamma_x^{z,d}}{\Gamma_R} = \frac{A_\perp^2}{4\omega_I^2} \frac{1}{1 + 4[\omega_I \pm (\omega_S - \omega_0)]^2/\kappa^2}$$

Quantum jumps of individual ^{183}W nuclear spins

J. Travesedo

J. O'Sullivan

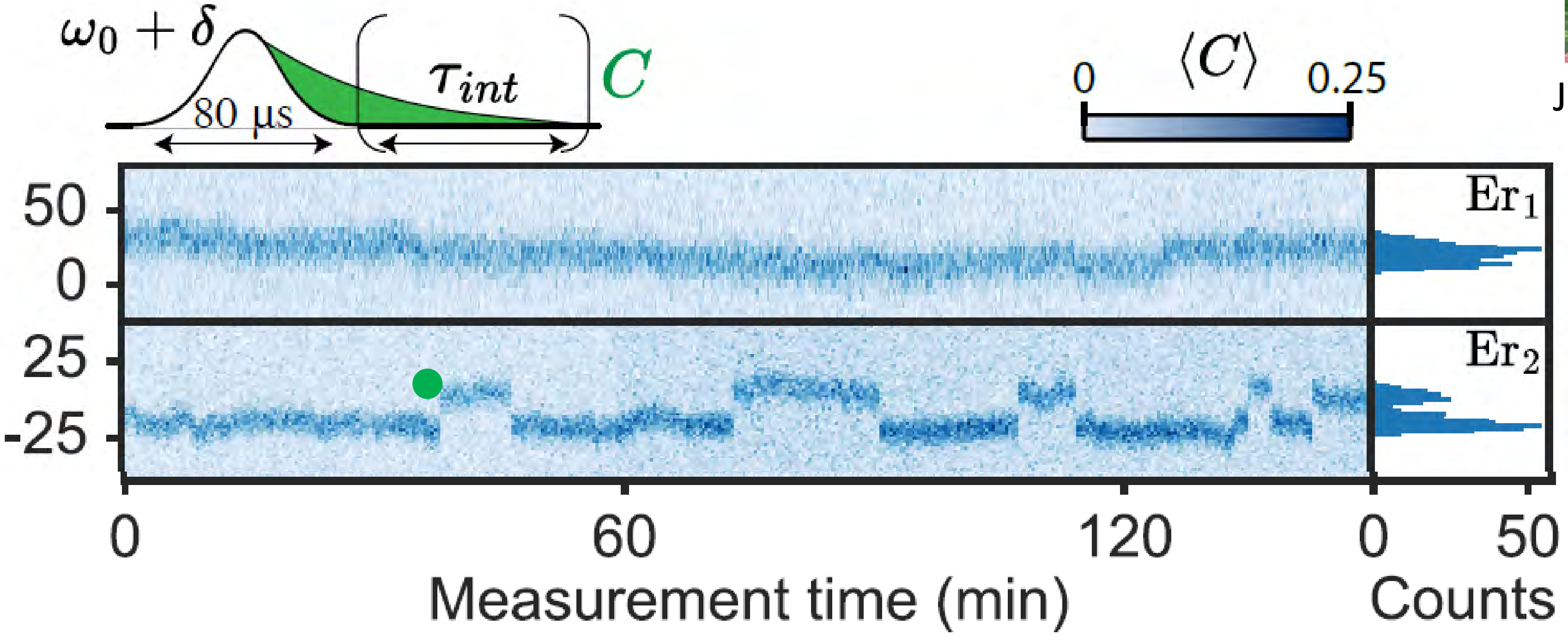

$$\hat{H} = \omega_S \hat{S}_z + \omega_I \hat{I}_z + A_\parallel \hat{S}_z \cdot \hat{I}_z + A_\perp \hat{S}_z \cdot \hat{I}_x$$

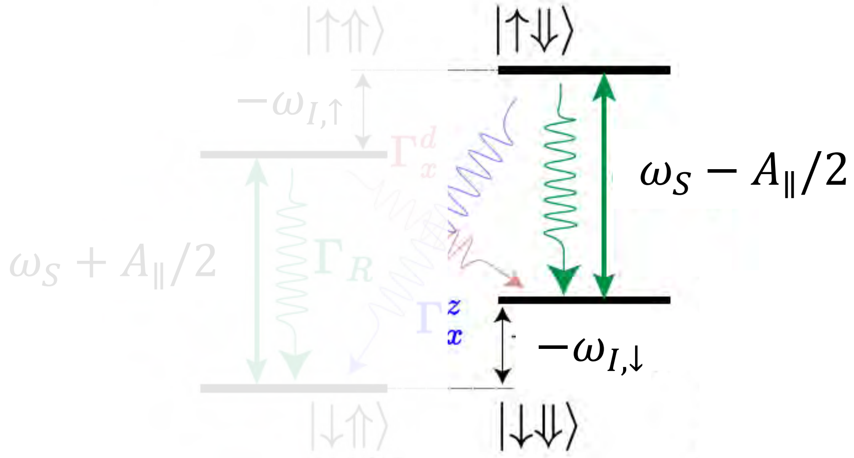

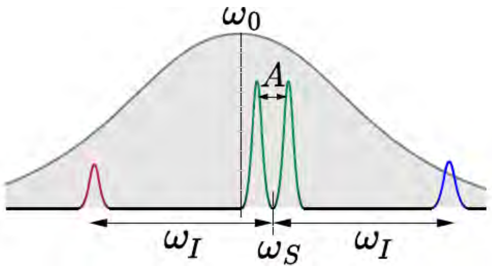

$$\frac{\Gamma_x^{z,d}}{\Gamma_R} = \frac{A_\perp^2}{4\omega_I^2} \frac{1}{1 + 4[\omega_I \pm (\omega_S - \omega_0)]^2/\kappa^2}$$

Quantum jumps of individual ^{183}W nuclear spins

J. Travesedo

J. O'Sullivan

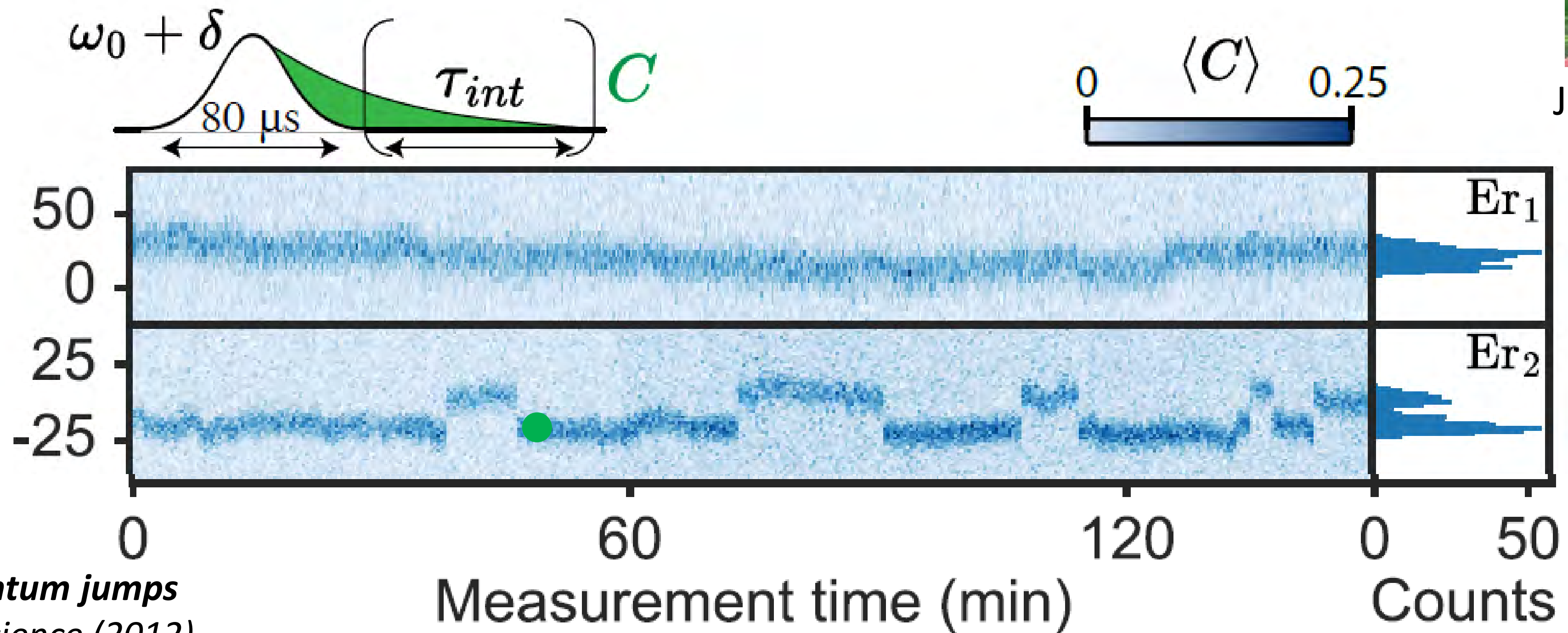

Nuclear Spin Quantum jumps

Neumann et al., Science (2012)

Vincent et al., Nature (2012)

Pla et al., Nature (2013)

Dréau et al., PRL (2013)

Hesselmeier et al., PRL (2024)

$$\hat{H} = \omega_S \hat{S}_z + \omega_I \hat{I}_z + A_\parallel \hat{S}_z \cdot \hat{I}_z + A_\perp \hat{S}_z \cdot \hat{I}_x$$

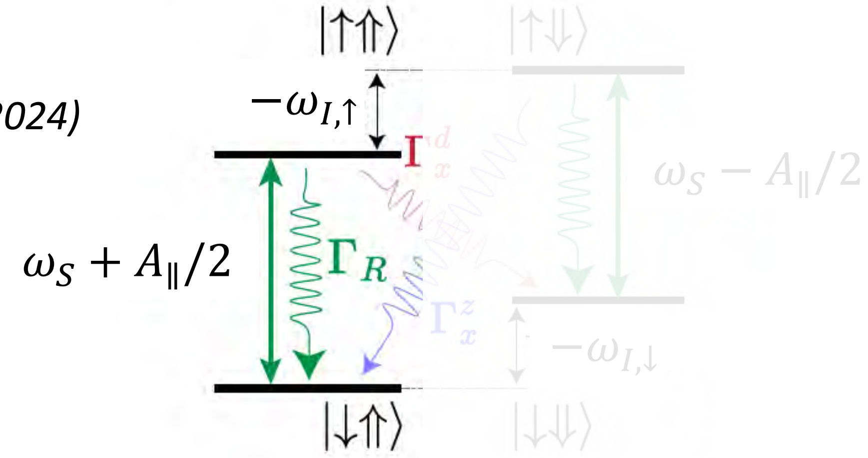

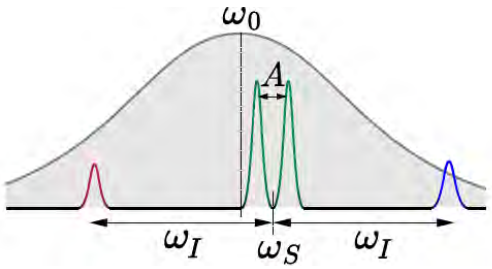

$$\frac{\Gamma_x^{z,d}}{\Gamma_R} = \frac{A_\perp^2}{4\omega_I^2} \frac{1}{1 + 4[\omega_I \pm (\omega_S - \omega_0)]^2/\kappa^2}$$

Quantum jumps of individual ^{183}W nuclear spins

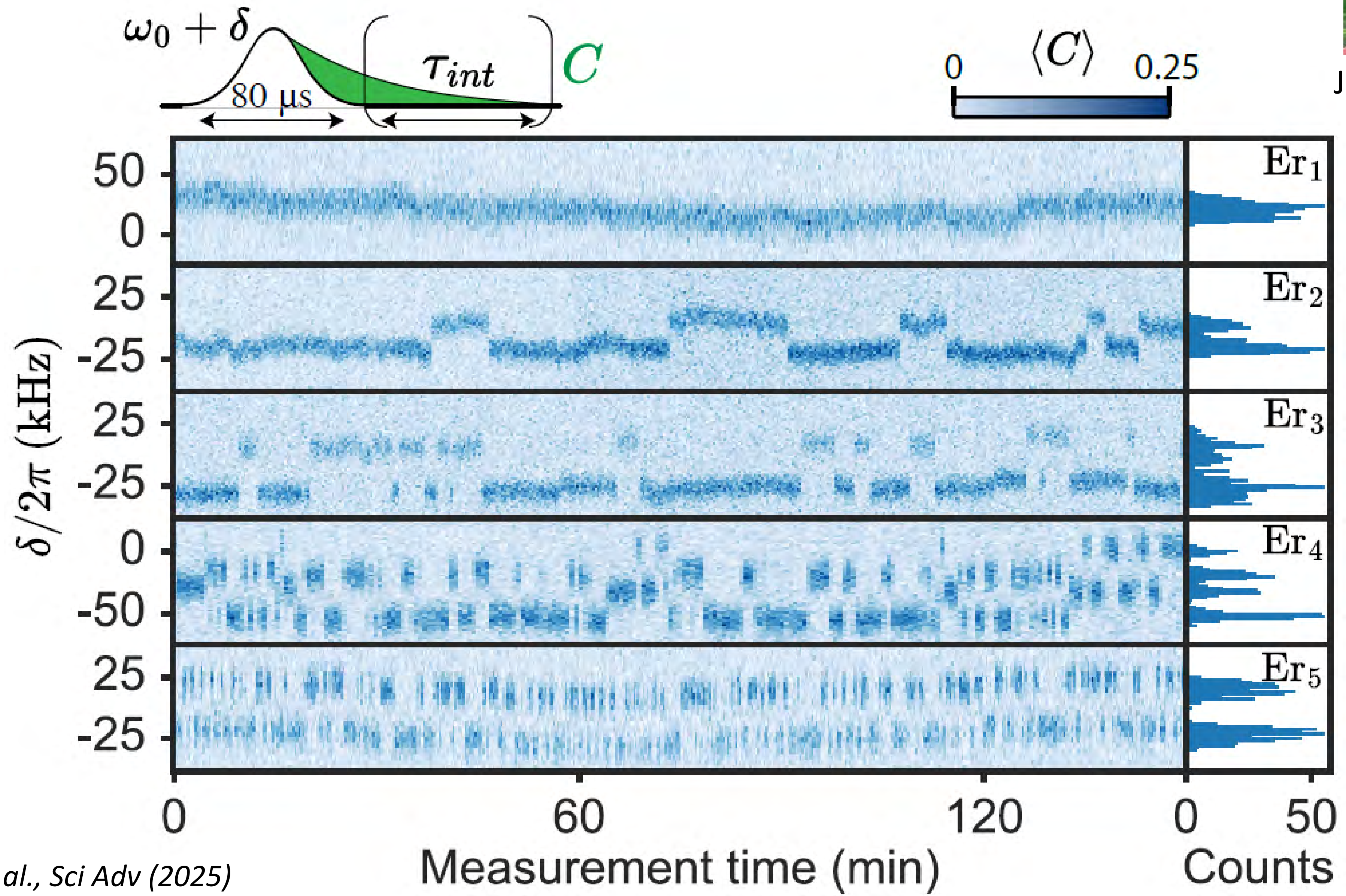

J. Travesedo

J. O'Sullivan

Travesedo et al., Sci Adv (2025)

All-microwave Nuclear spin quantum jumps and Single-Shot Read-Out

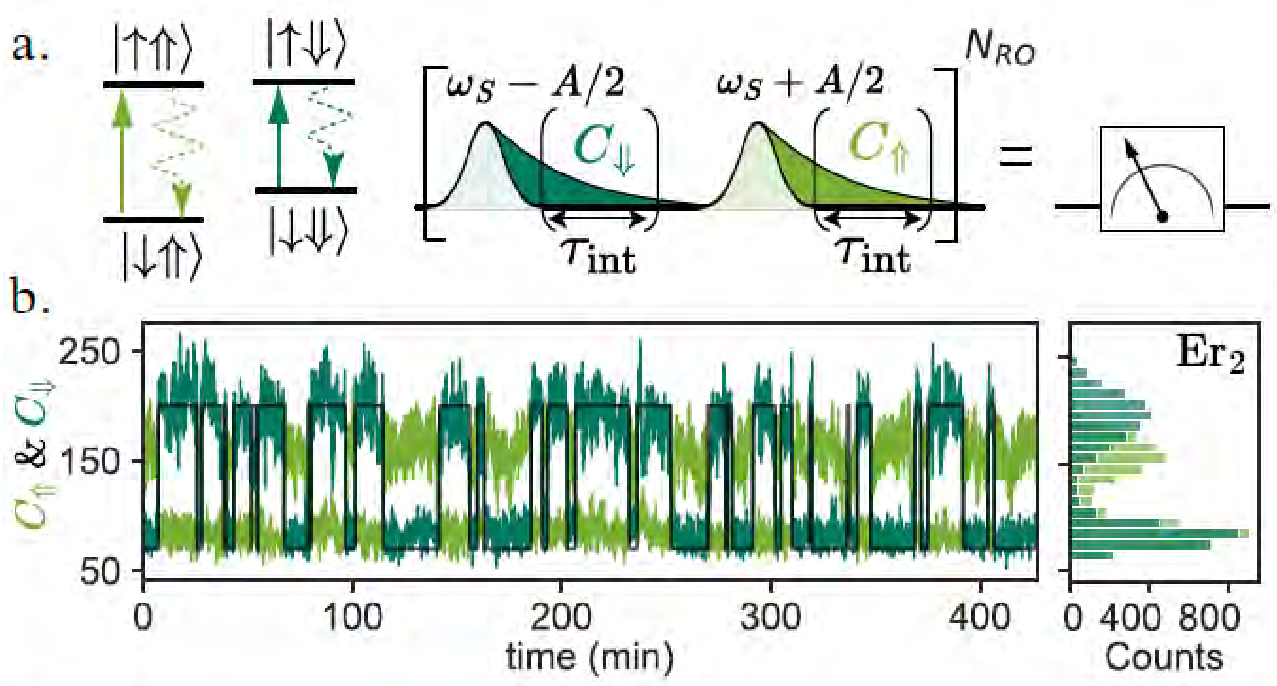

Nuclear Spin Quantum jumps
Neumann et al., Science (2012)
Vincent et al., Nature (2012)
Pla et al., Nature (2013)
Dréau et al., PRL (2013)
Hesselmeier et al., PRL (2024)

Travesedo et al., Sci. Adv. (2025)

All-microwave Nuclear spin quantum jumps and Single-Shot Read-Out

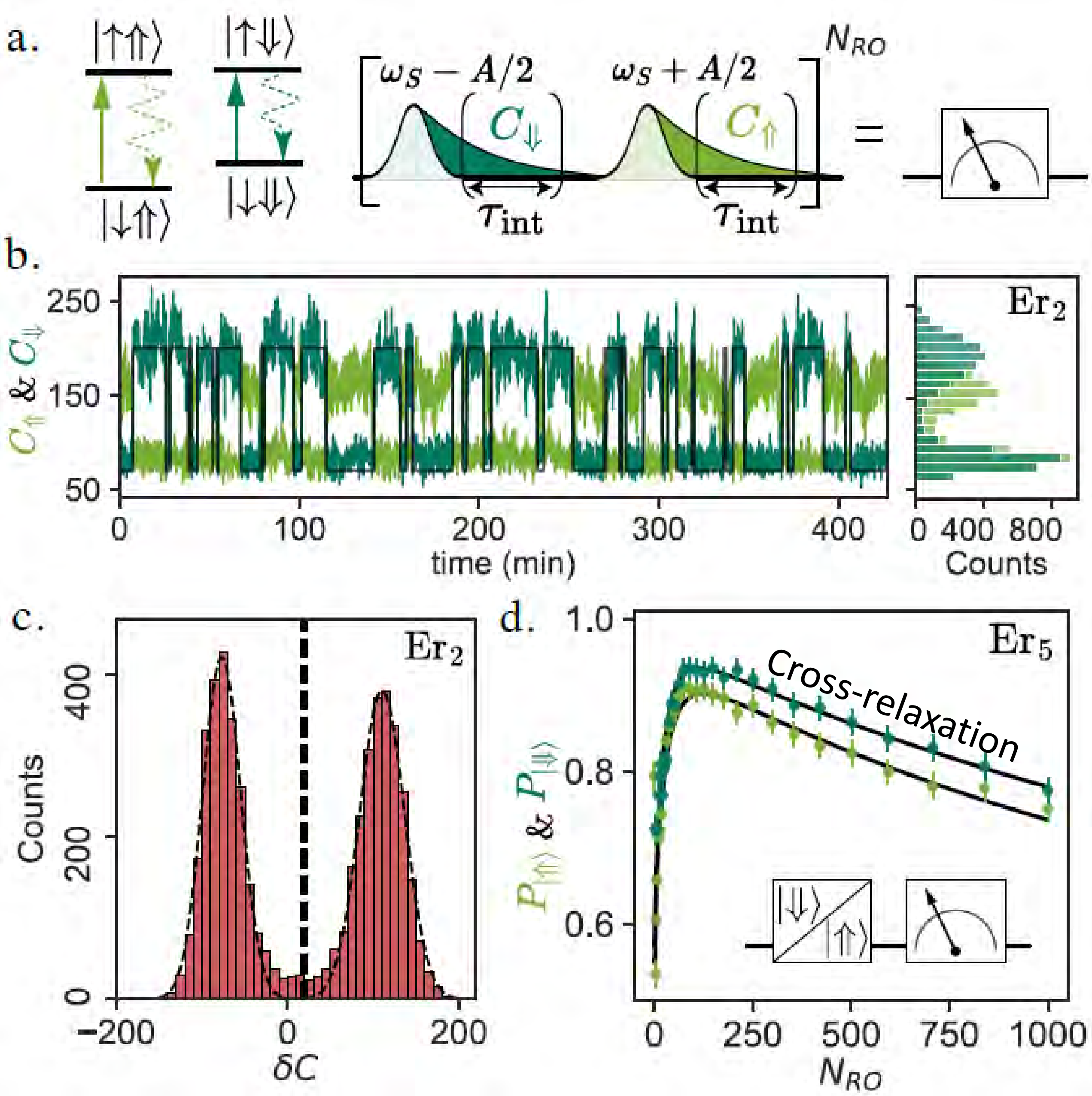

Nuclear Spin Quantum jumps

Neumann et al., Science (2012)
Vincent et al., Nature (2012)
Pla et al., Nature (2013)
Dréau et al., PRL (2013)
Hesselmeier et al., PRL (2024)

Travesedo et al., Sci. Adv. (2025)

Forbidden transition spectroscopy

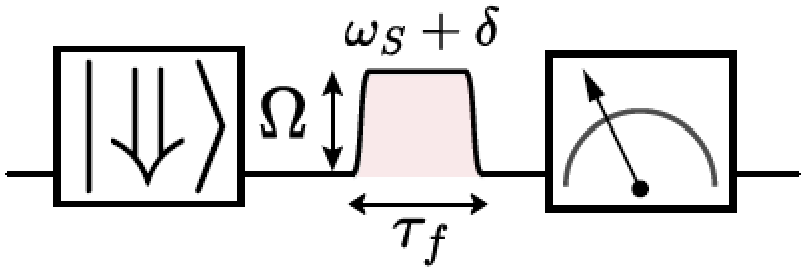

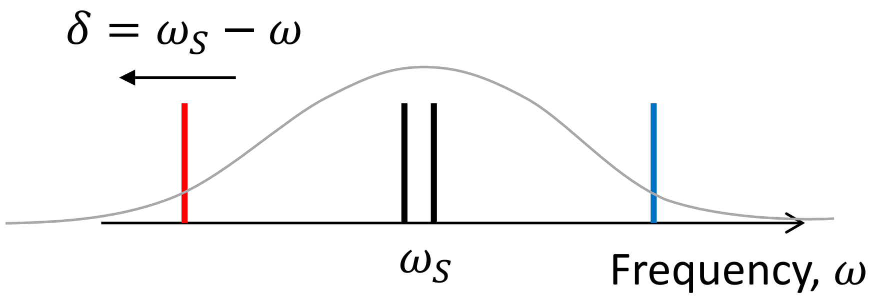

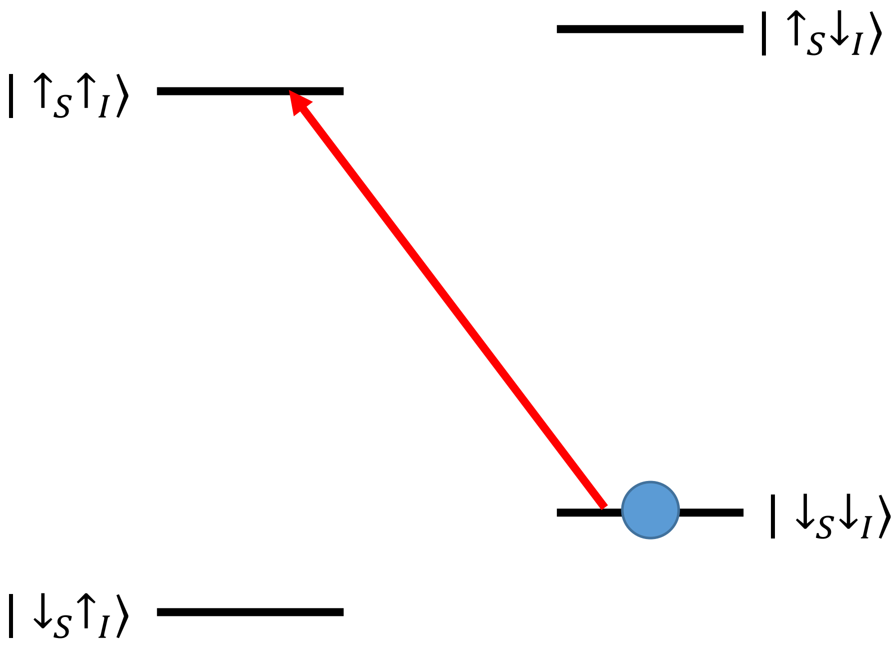

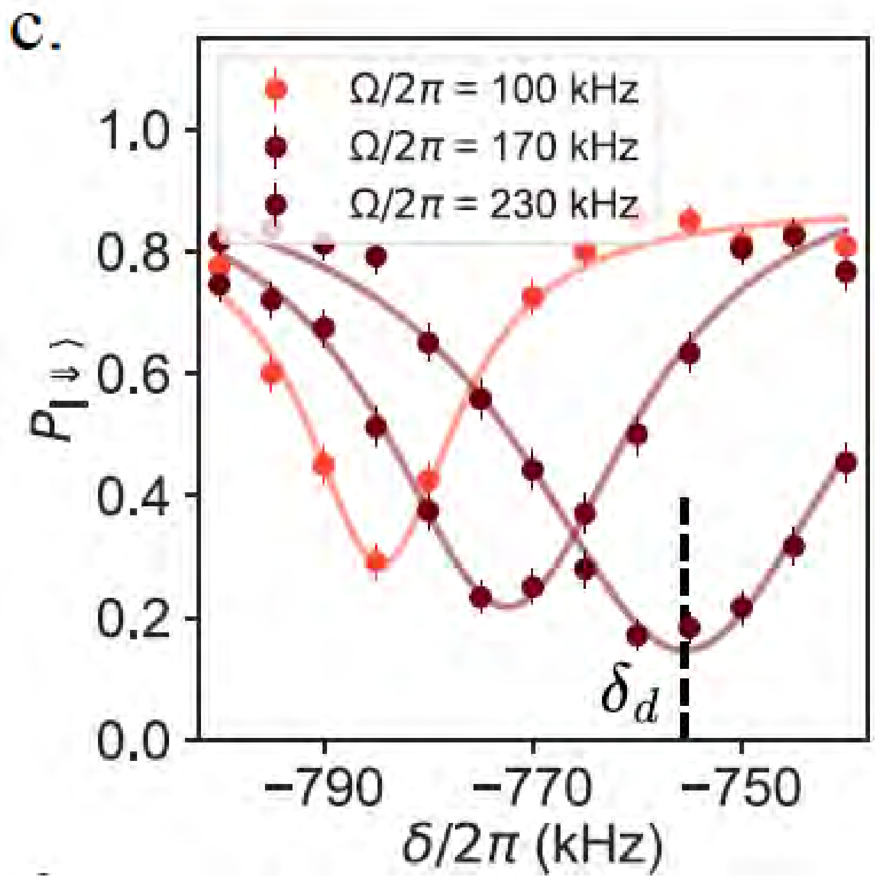

Forbidden transition spectroscopy

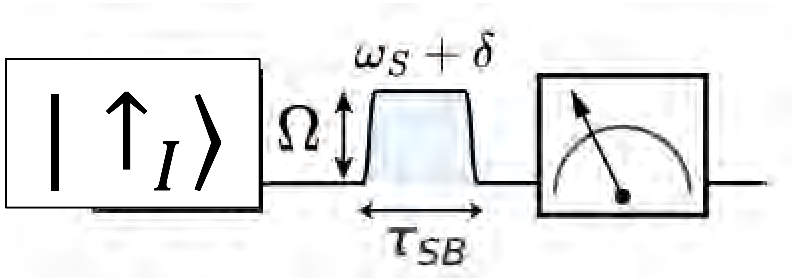

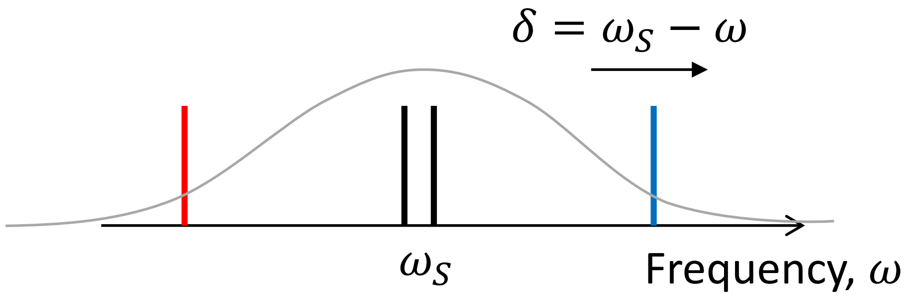

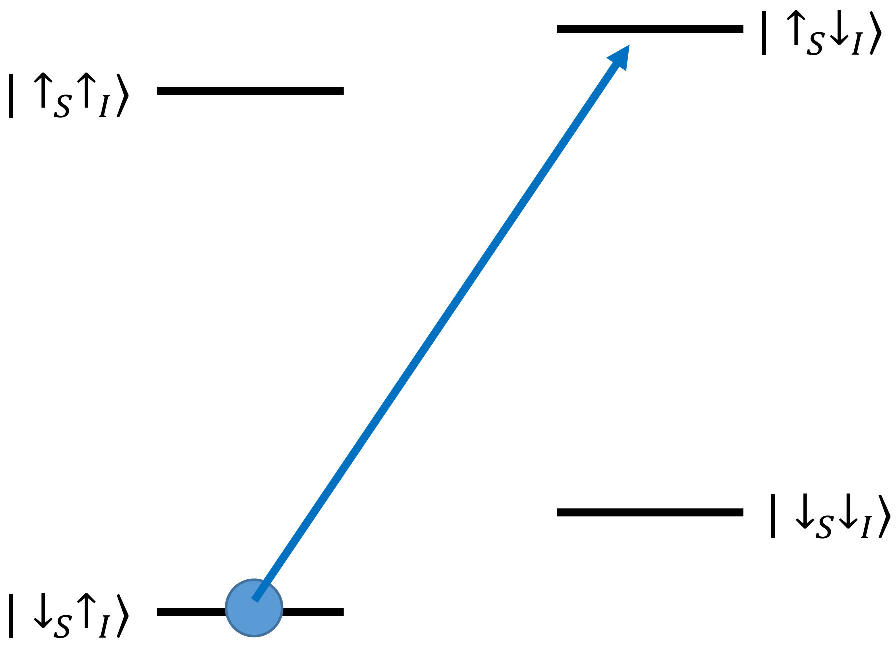

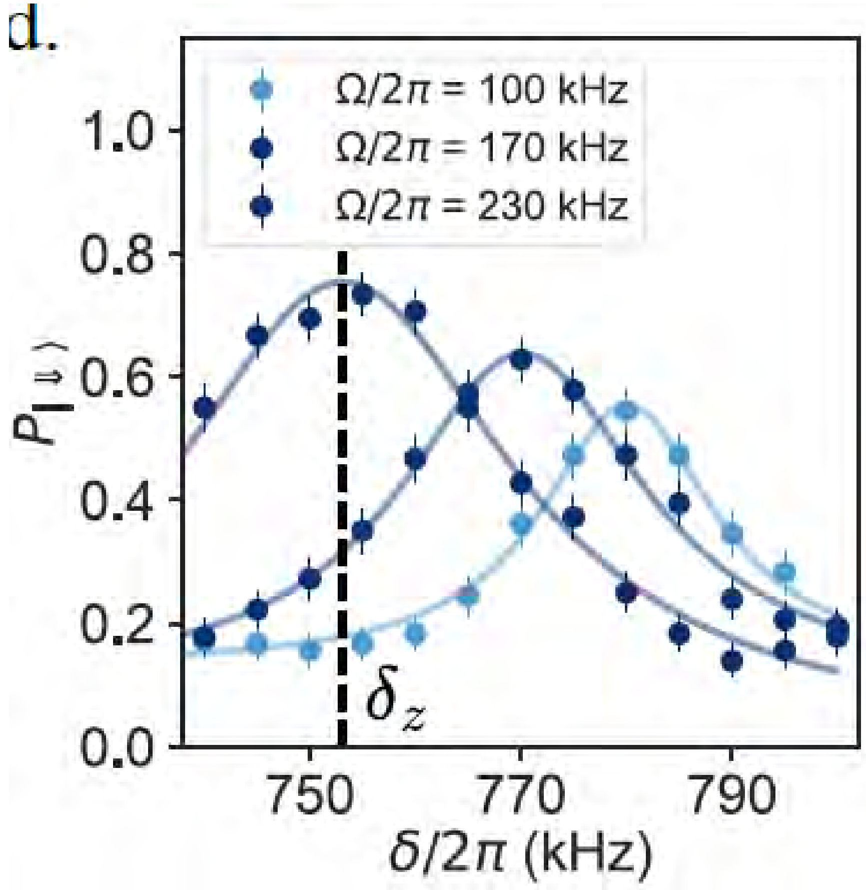

Forbidden transition spectroscopy

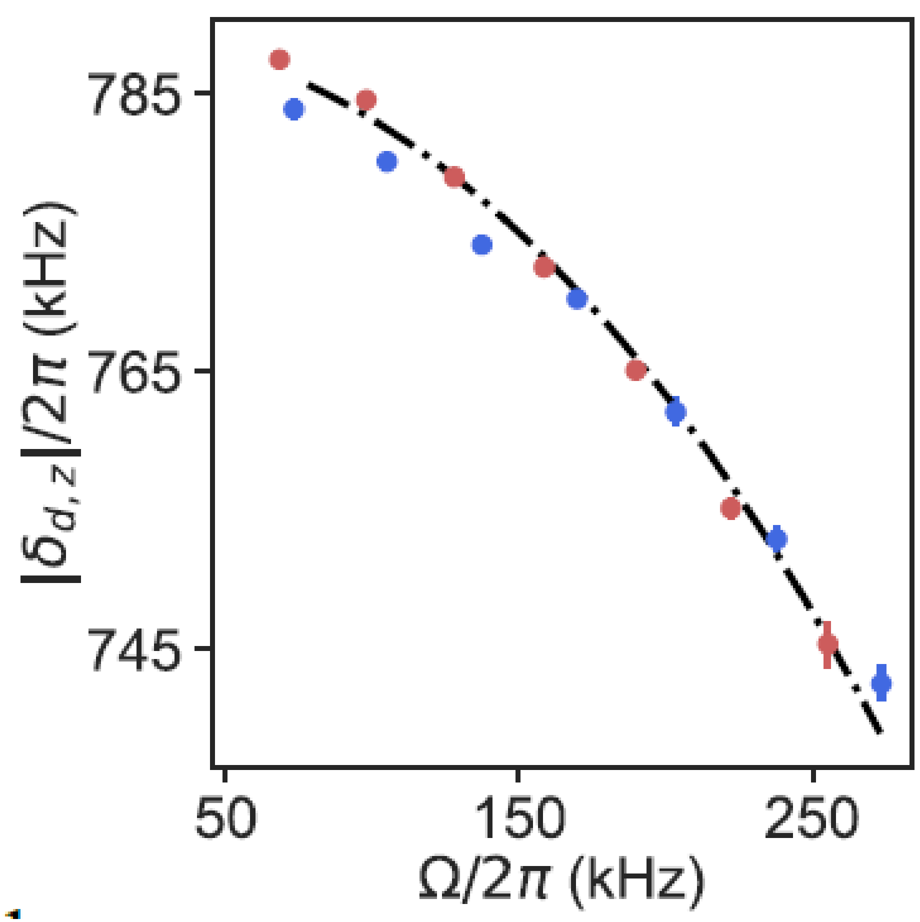

Travesedo et al., Sci. Adv. (2025)

- Fitted $\frac{\omega_I}{2\pi} = \frac{-|\delta_{d,z}(\Omega=0)|}{2\pi} = -788.1$ kHz@446mT. Matches expected ^{183}W $\frac{\gamma_W}{2\pi} = 1.774$MHz/T
- Evidence for power-dependent frequency shifts in ELDOR-detected NMR

Nuclear spin State Preparation / Single-atom Solid-Effect DNP

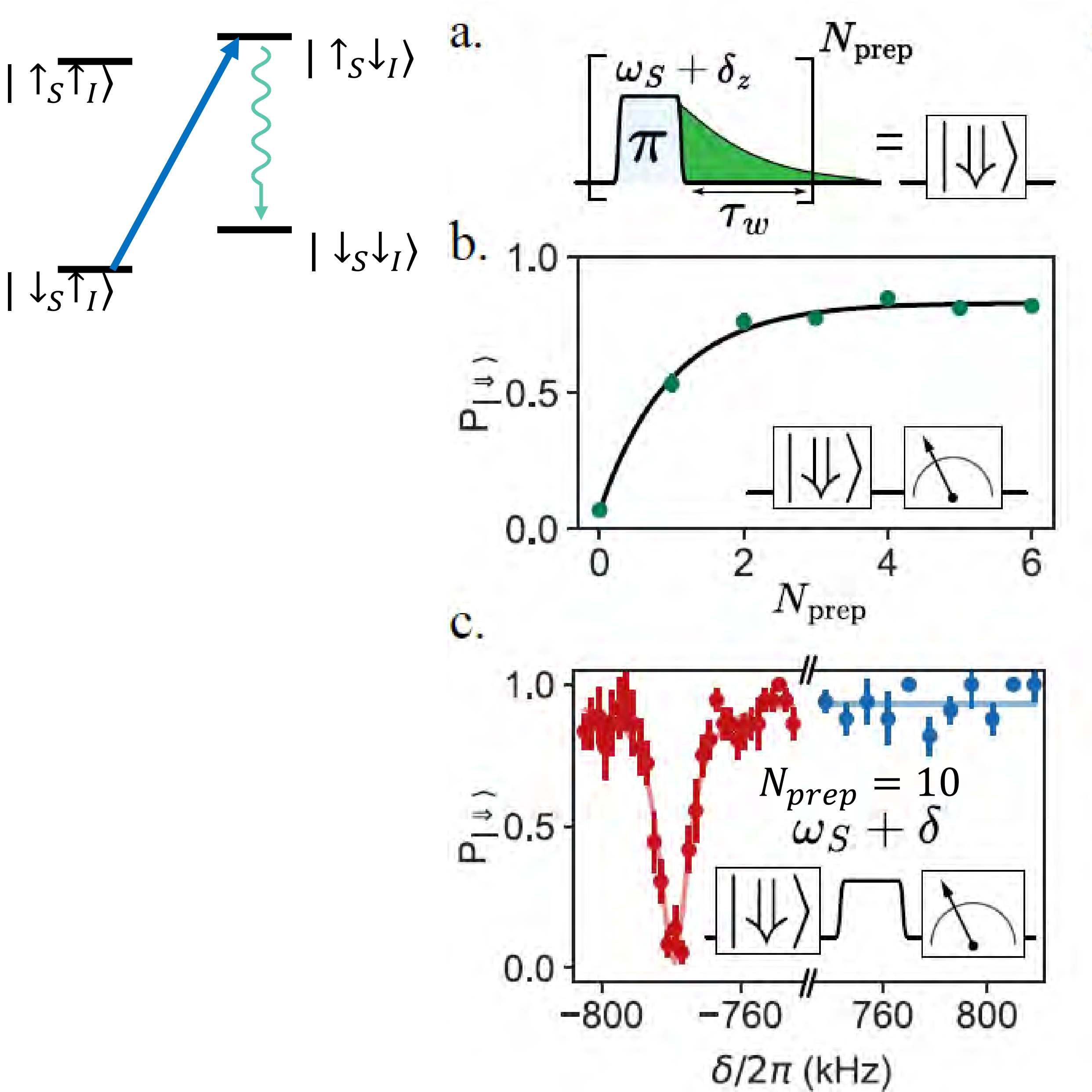

Travesedo et al., Sci. Adv. (2025)

Nuclear spin State Preparation / Single-atom Solid-Effect DNP

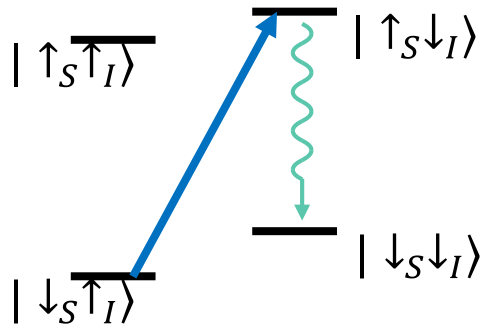

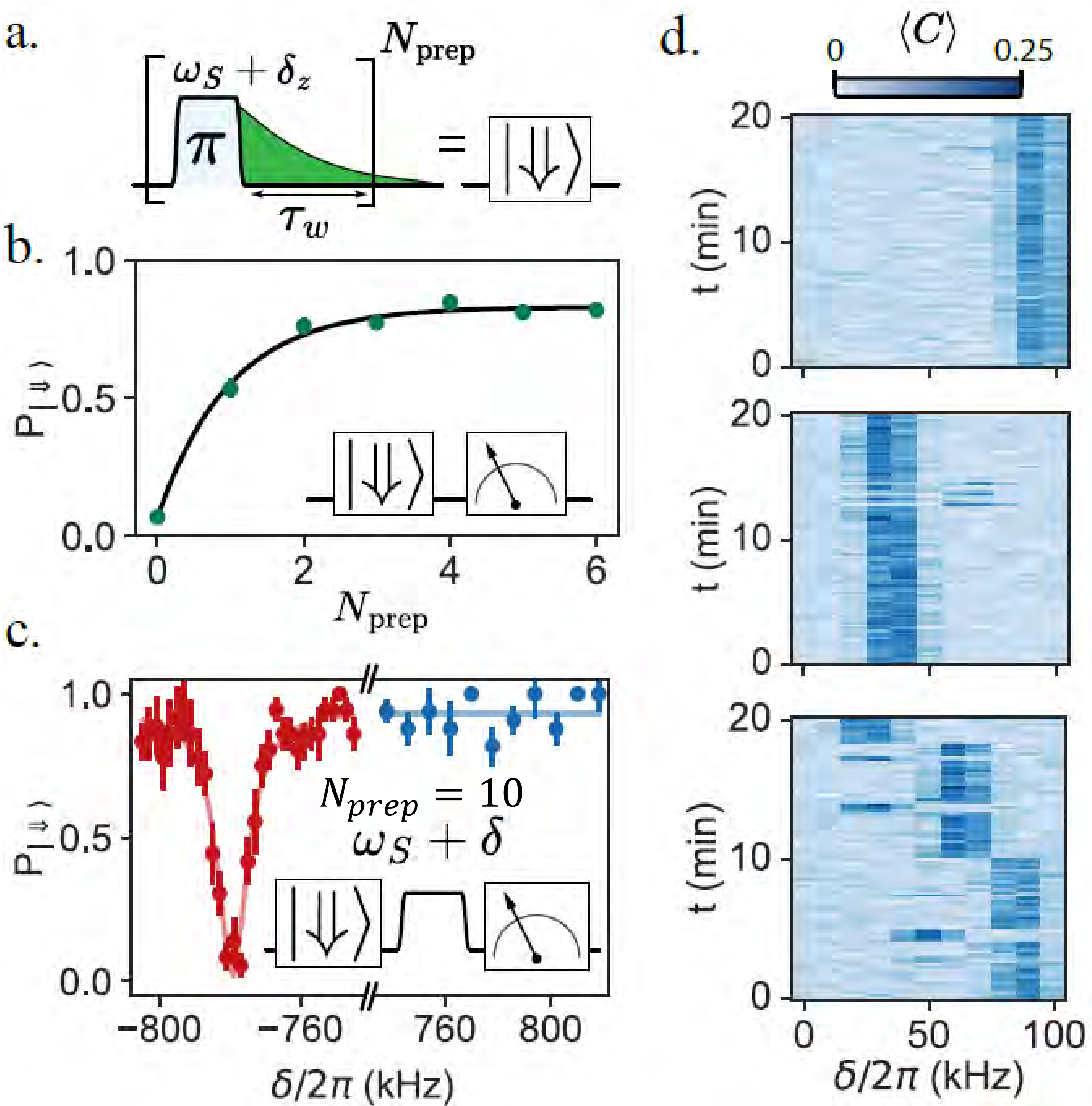

Preparation in $|\downarrow\downarrow\rangle$
at the beginning of each sweep

Preparation in $|\uparrow\uparrow\rangle$
at the beginning of each sweep

No preparation

Travesedo et al.,
Sci. Adv. (2025)

Nuclear spin driving by stimulated Raman transitions

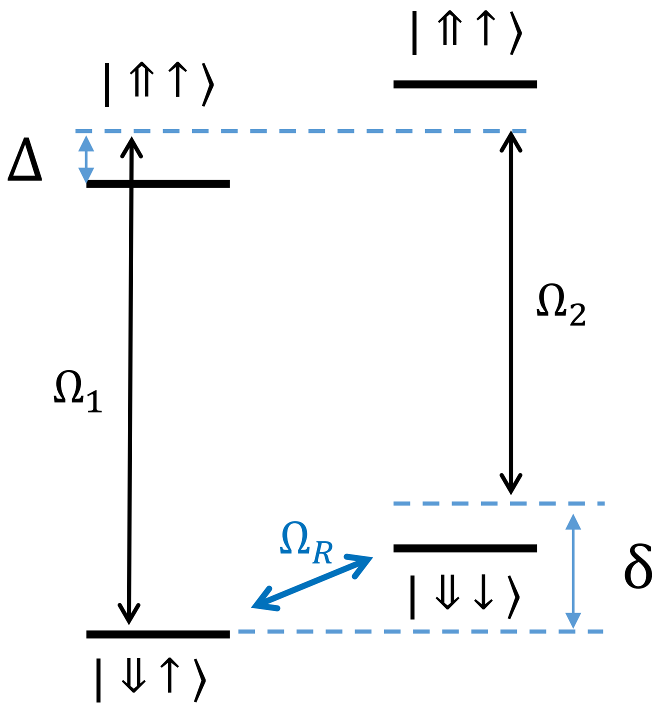

- **2-photon** process
- **Virtual** → not limited by electron coherence

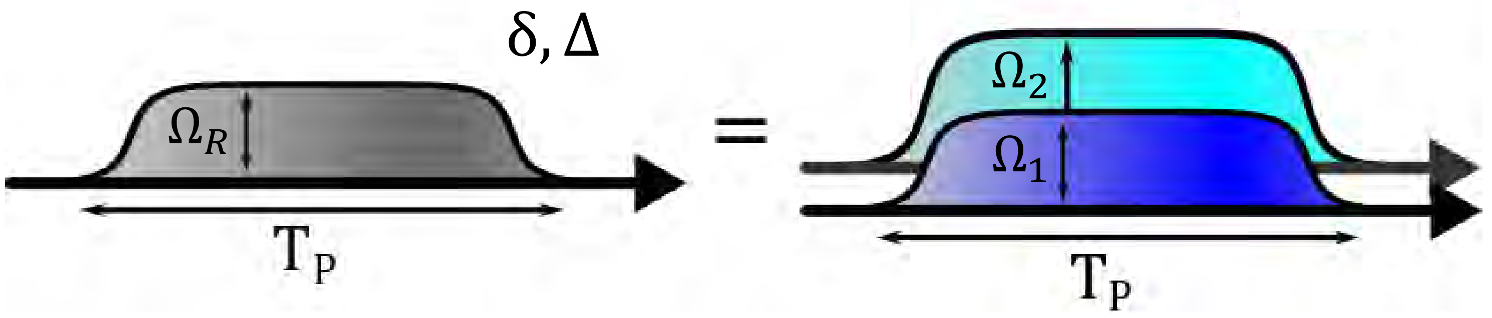

Nuclear spin driving by stimulated Raman transition

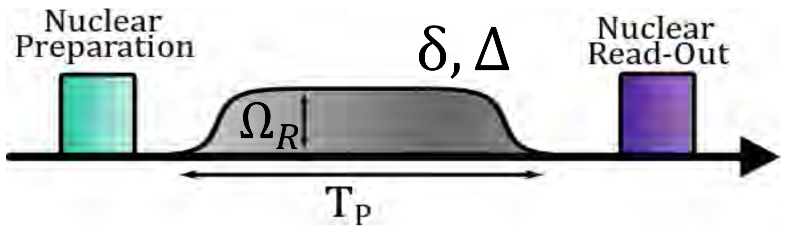

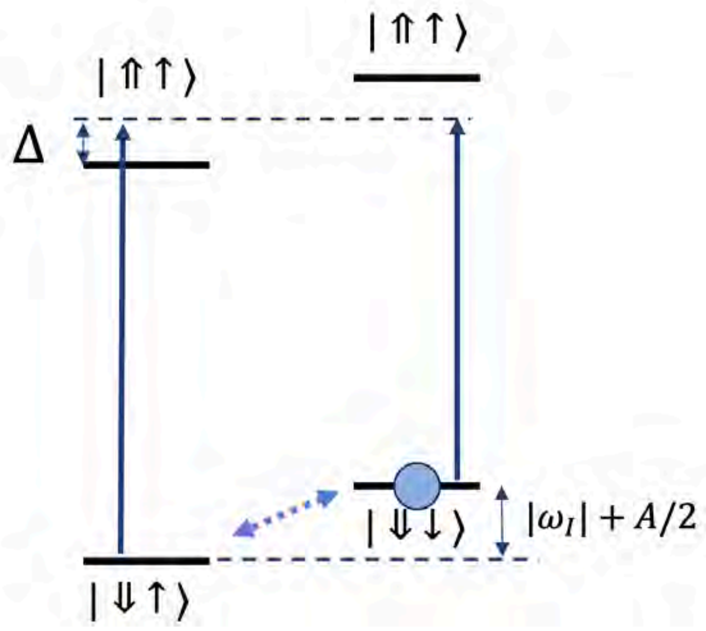

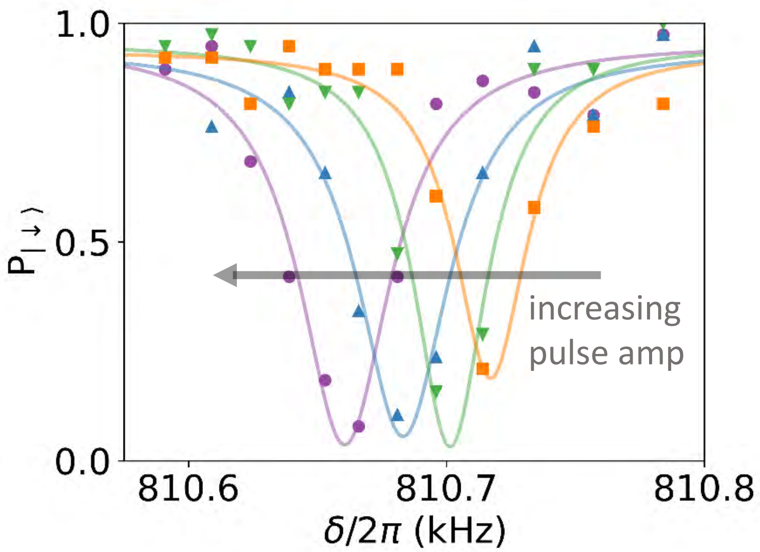

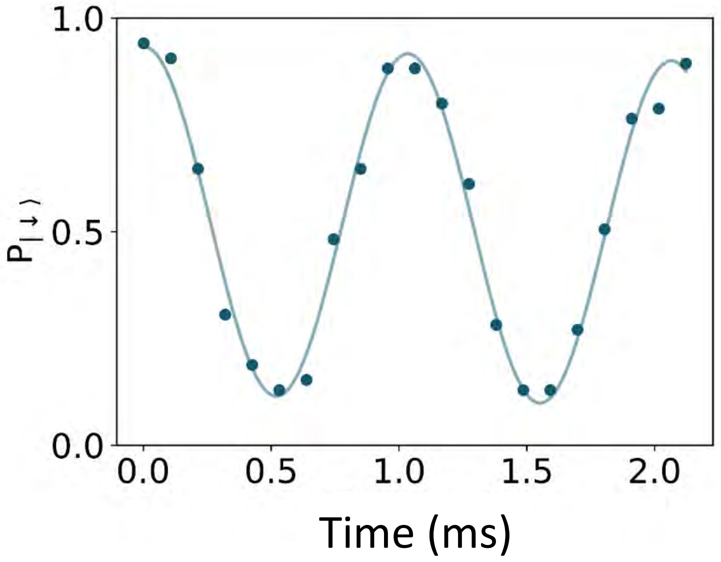

- AC-Zeeman shifts
- $\simeq$ kHz Rabi frequencies

Coherence time and high-resolution spectroscopy

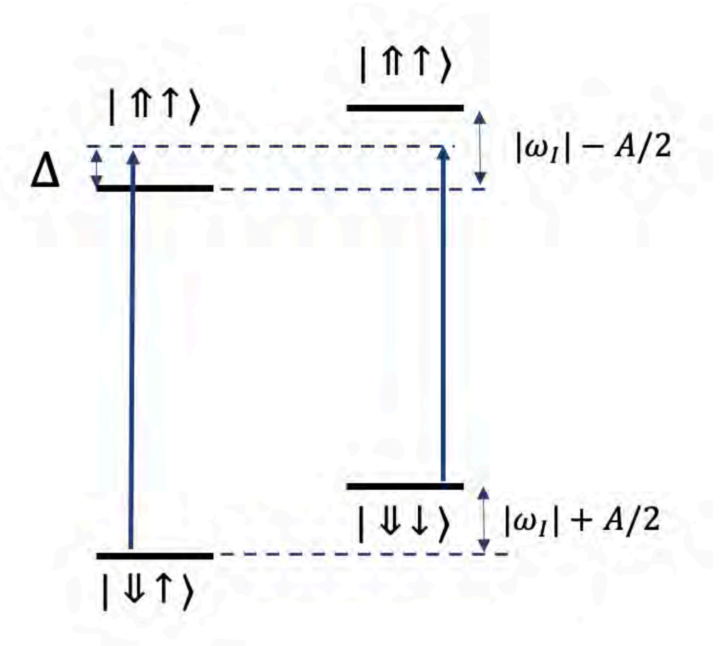

Ground state Ramsey

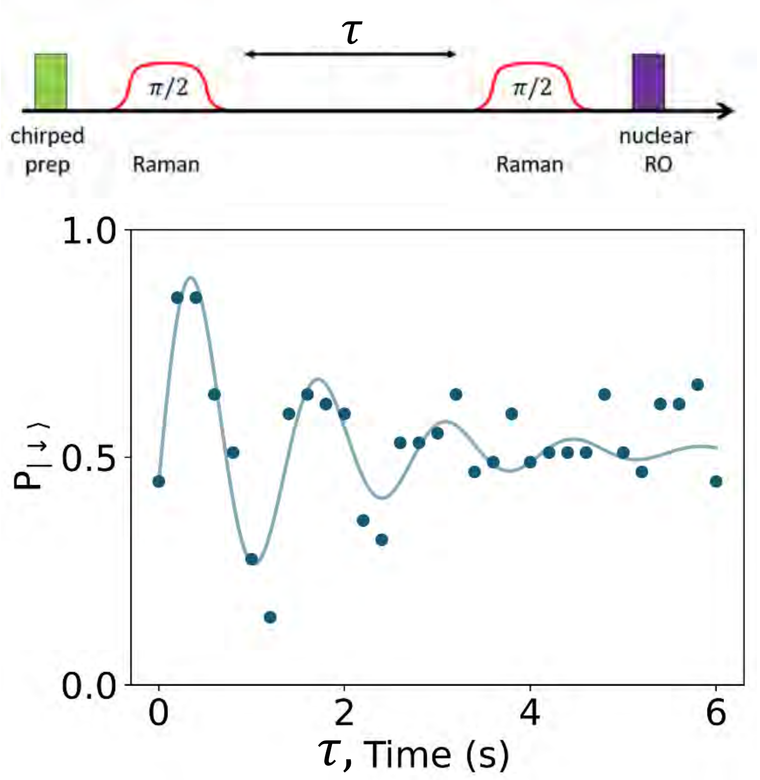

Excited state Ramsey

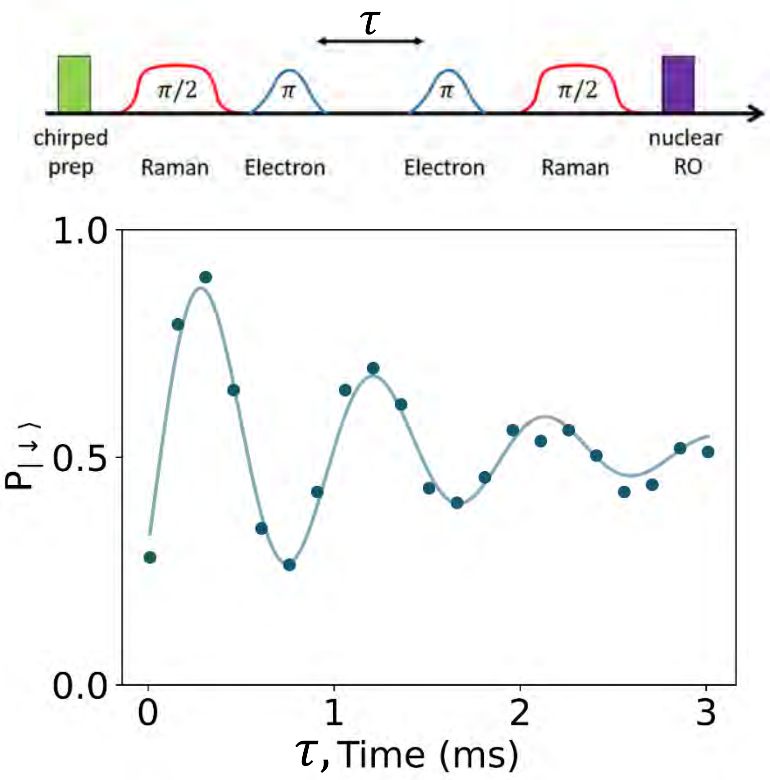

- High-resolution spectroscopy : $A/2\pi = 22.9\ kHz, \frac{\omega_I}{2\pi} = -798.1\ kHz$
- Coherence time $T_2^* \simeq 1$s. Record for nuclear spins in solid-state, even in isotopically enriched crystals

Electron coupled to 2 nuclear spins

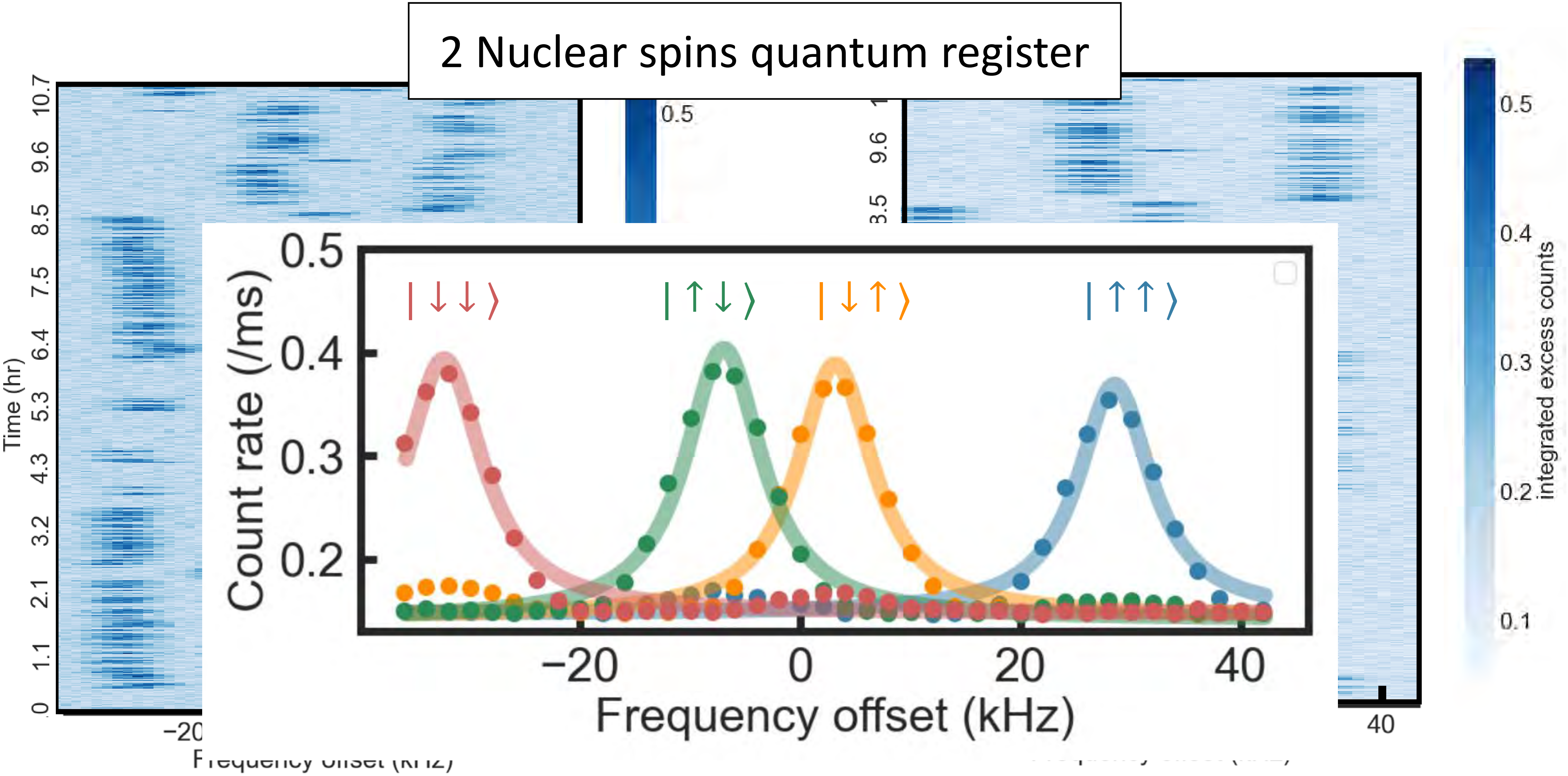

2 nuclear spin register : Read-Out

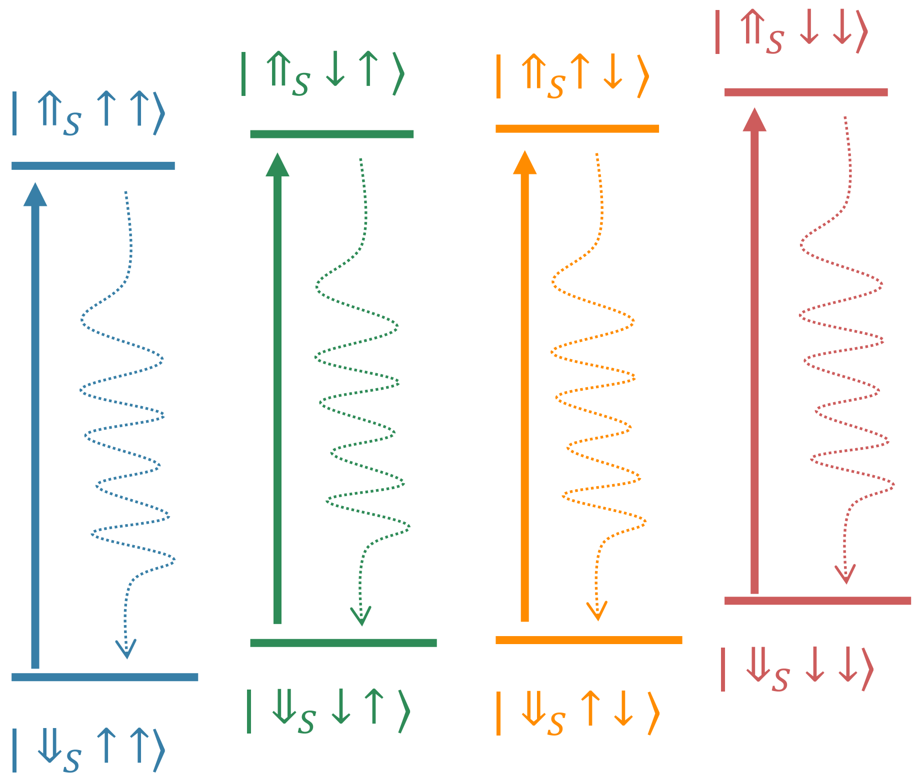

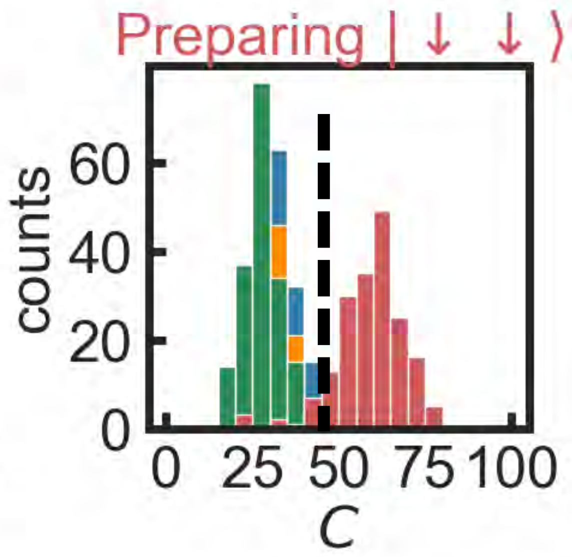

2 nuclear spin register : State initialization

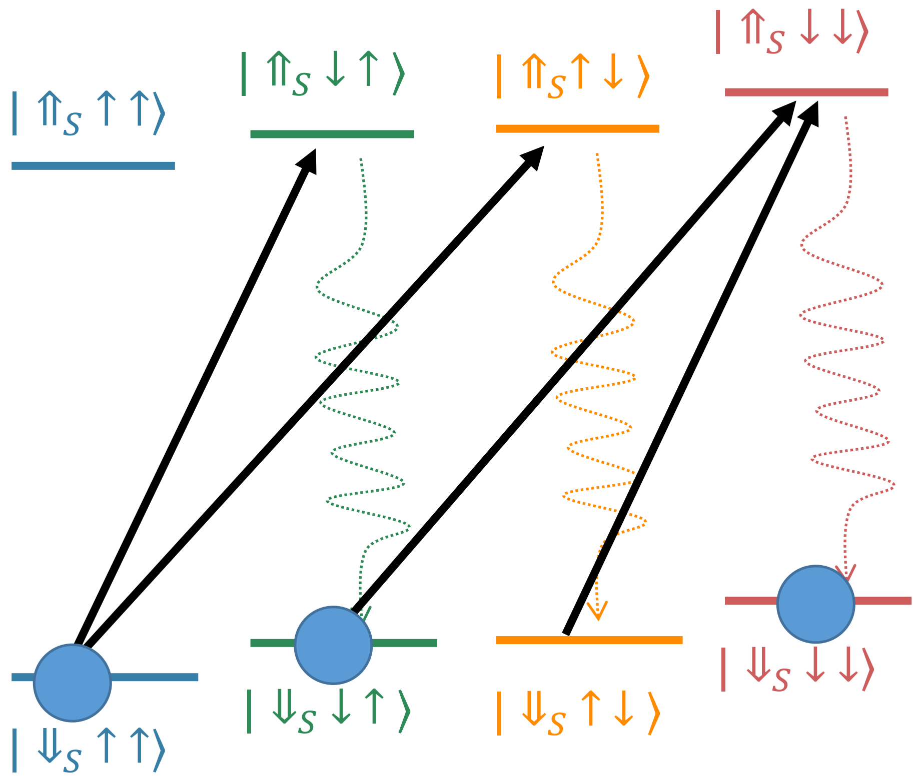

N_{prep} **chirped** preparation pulses, covering all sideband frequencies

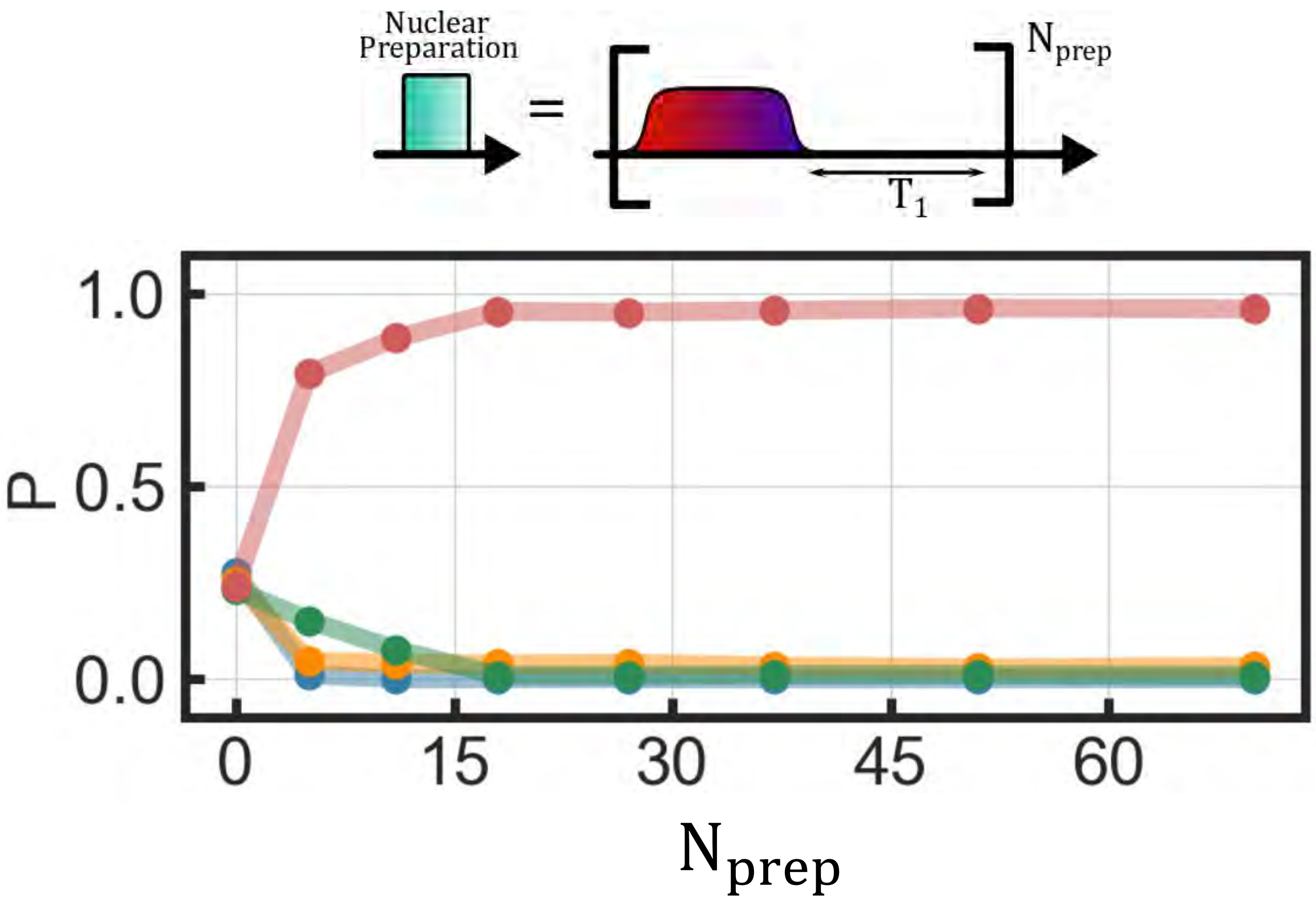

Two-nuclear-spin spectroscopy

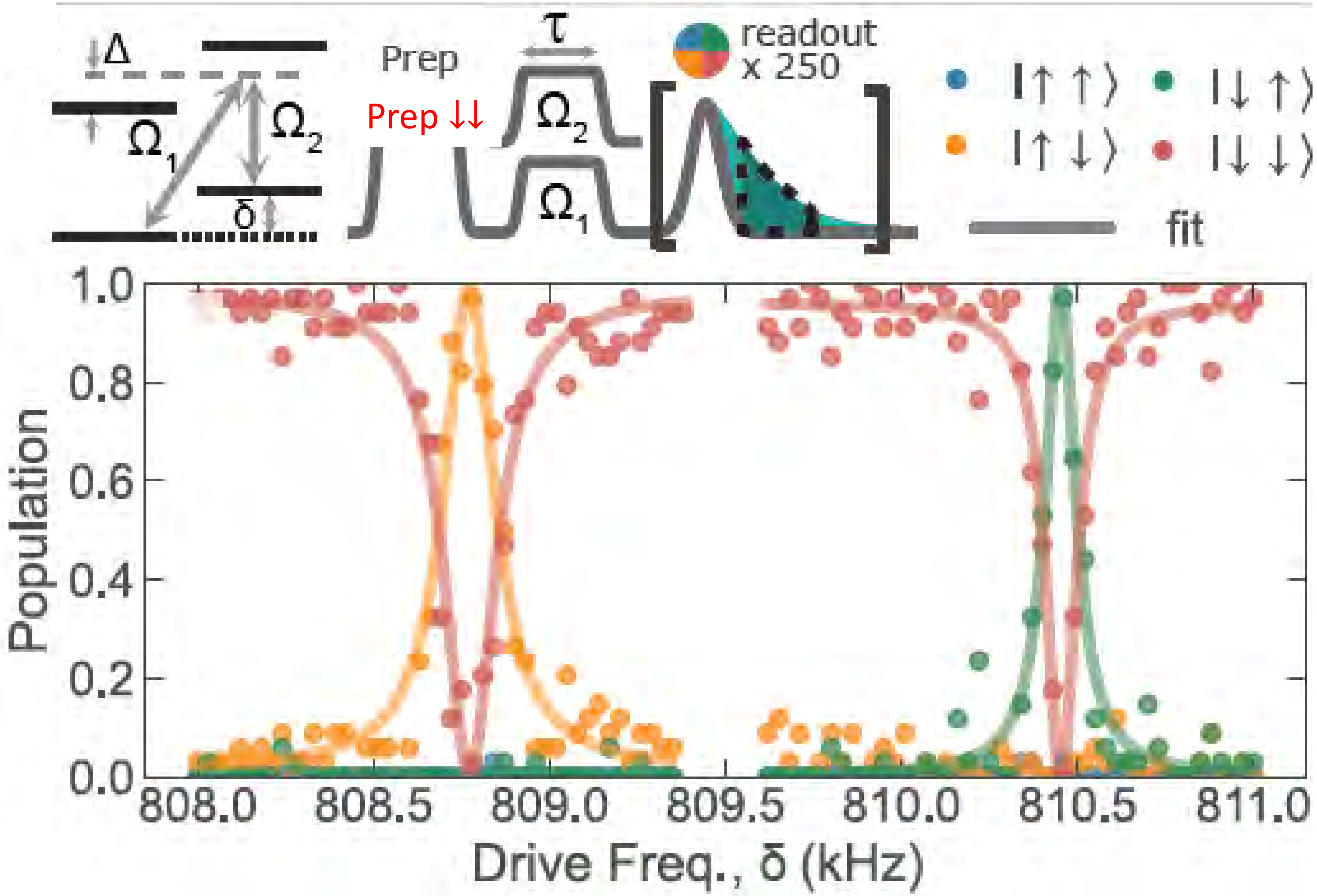

J. O'Sullivan et al., arxiv (2024)

Single-qubit gate on each qubit

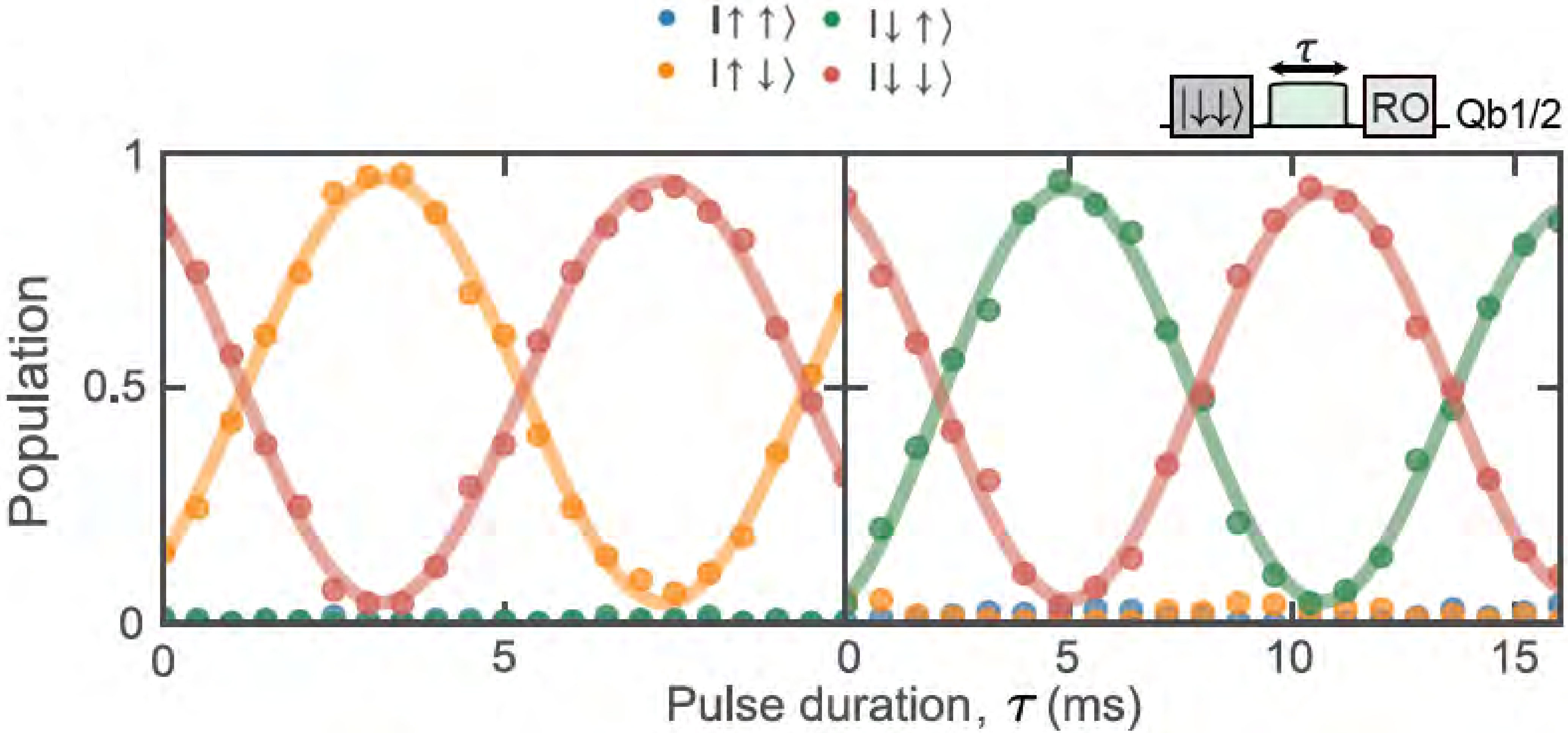

J. O'Sullivan et al., arxiv (2024)

Coherence times

Ramsey

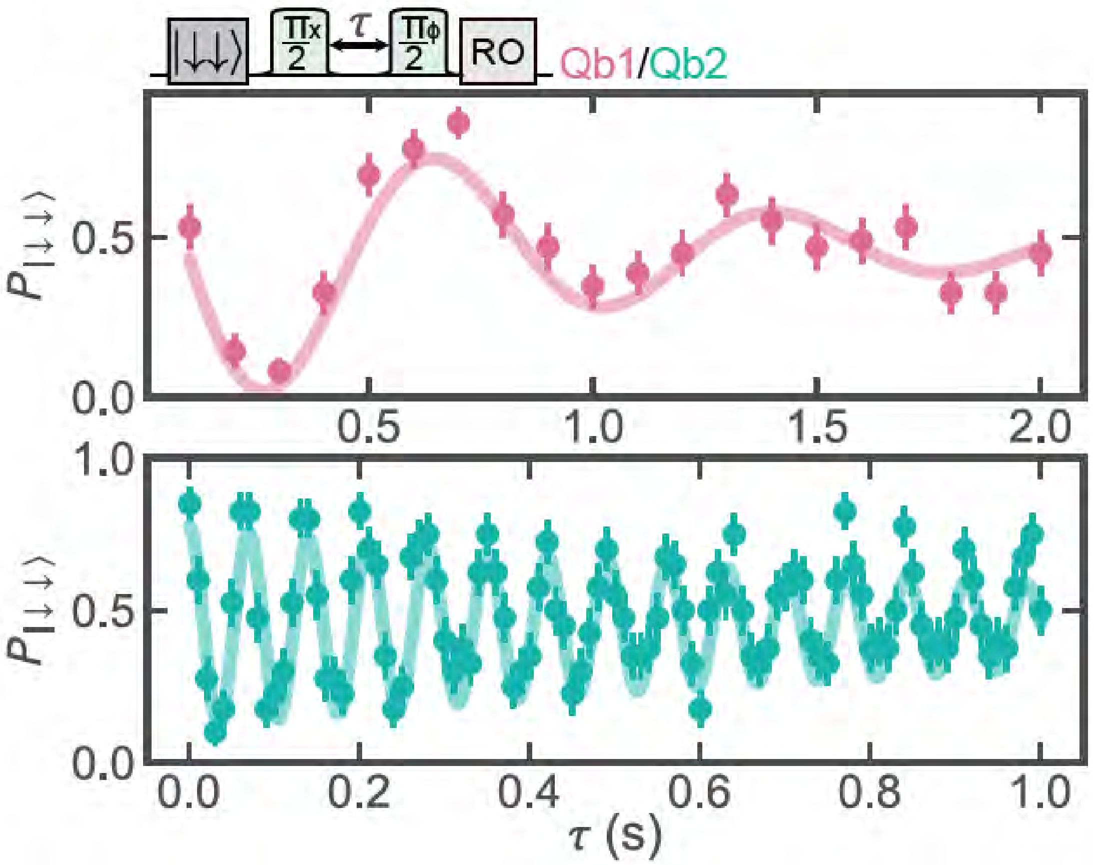

Hahn echo

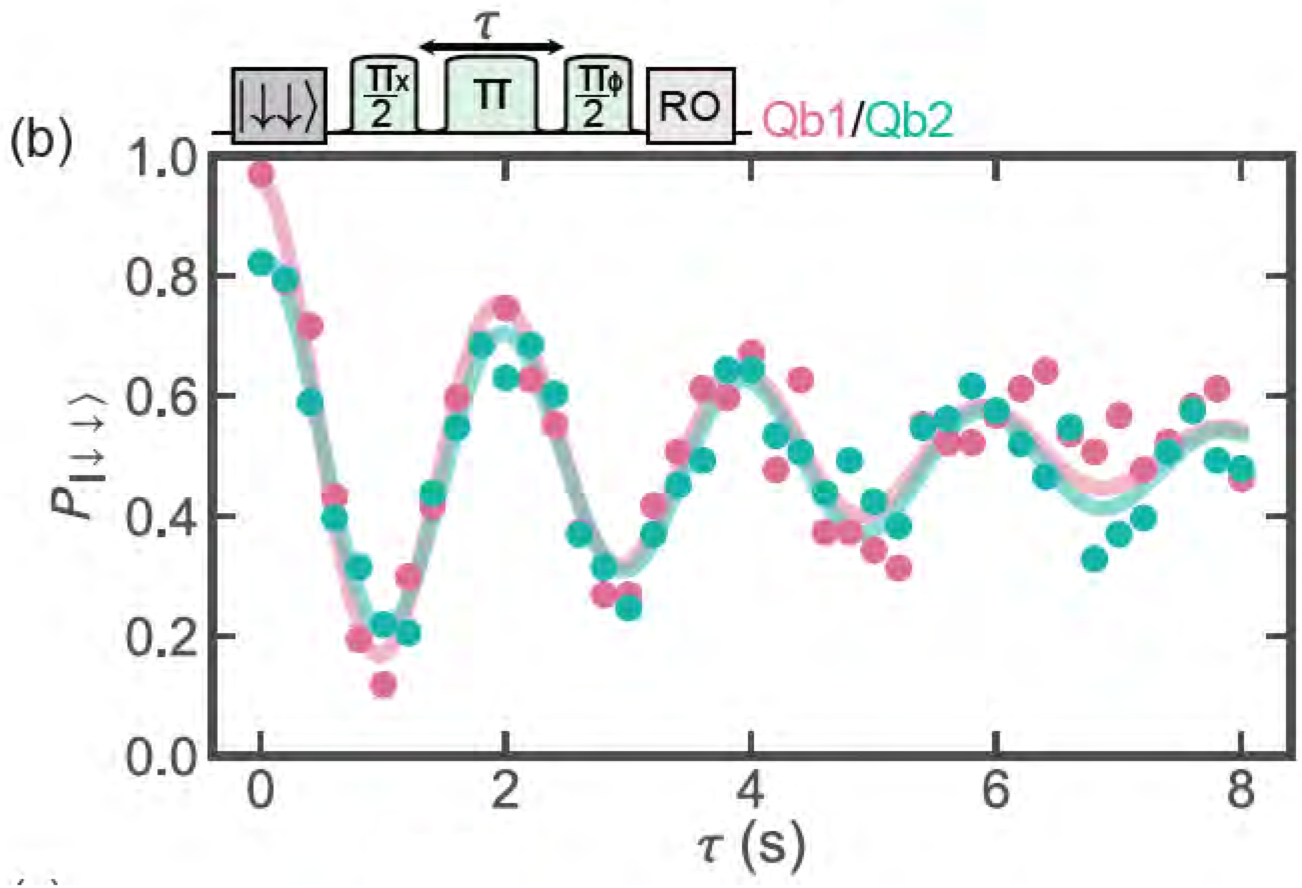

$T_2^* \simeq 1\text{s}$, $T_2 = 4\text{s}$ for both nuclear spins

J. O'Sullivan et al., arxiv (2024)

Direct spin-spin coupling

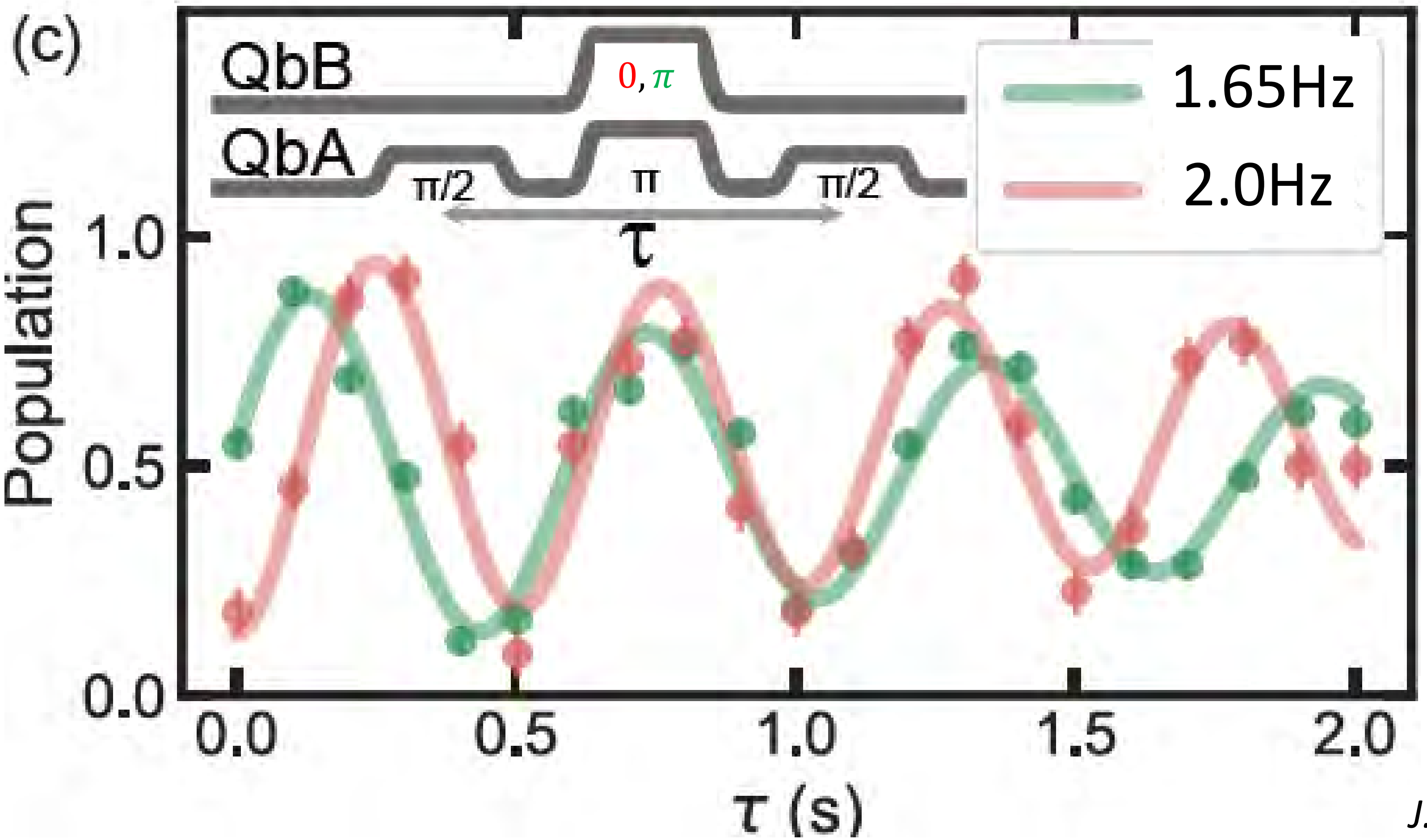

J. O'Sullivan et al., arxiv (2024)

^{183}W-^{183}W dipolar coupling $\frac{C}{2\pi} = 2 \times 0.35 = 0.7$Hz, too small for two-qubit gate

Conditional ac-Zeeman shift of Raman transitions

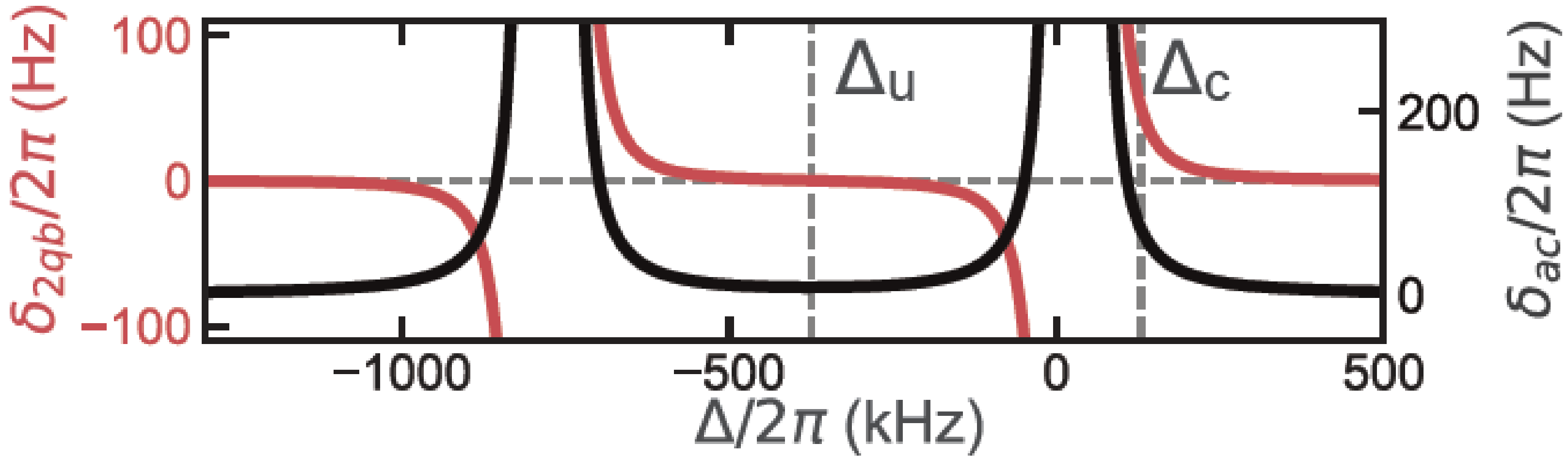

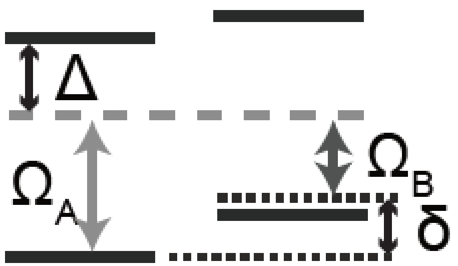

- During Raman driving, the ac-Zeeman shift of qubit 2 is $\delta_{ac} + \delta_{2q} I_{z1}$
- If $\Delta = \Delta_u$, $\delta_{2q} = 0$ -> Unconditional driving
- If $\Delta \neq \Delta_u$, the ac-Zeeman shift becomes conditional to q1 state

Conditional ac-Zeeman shift of Raman transitions

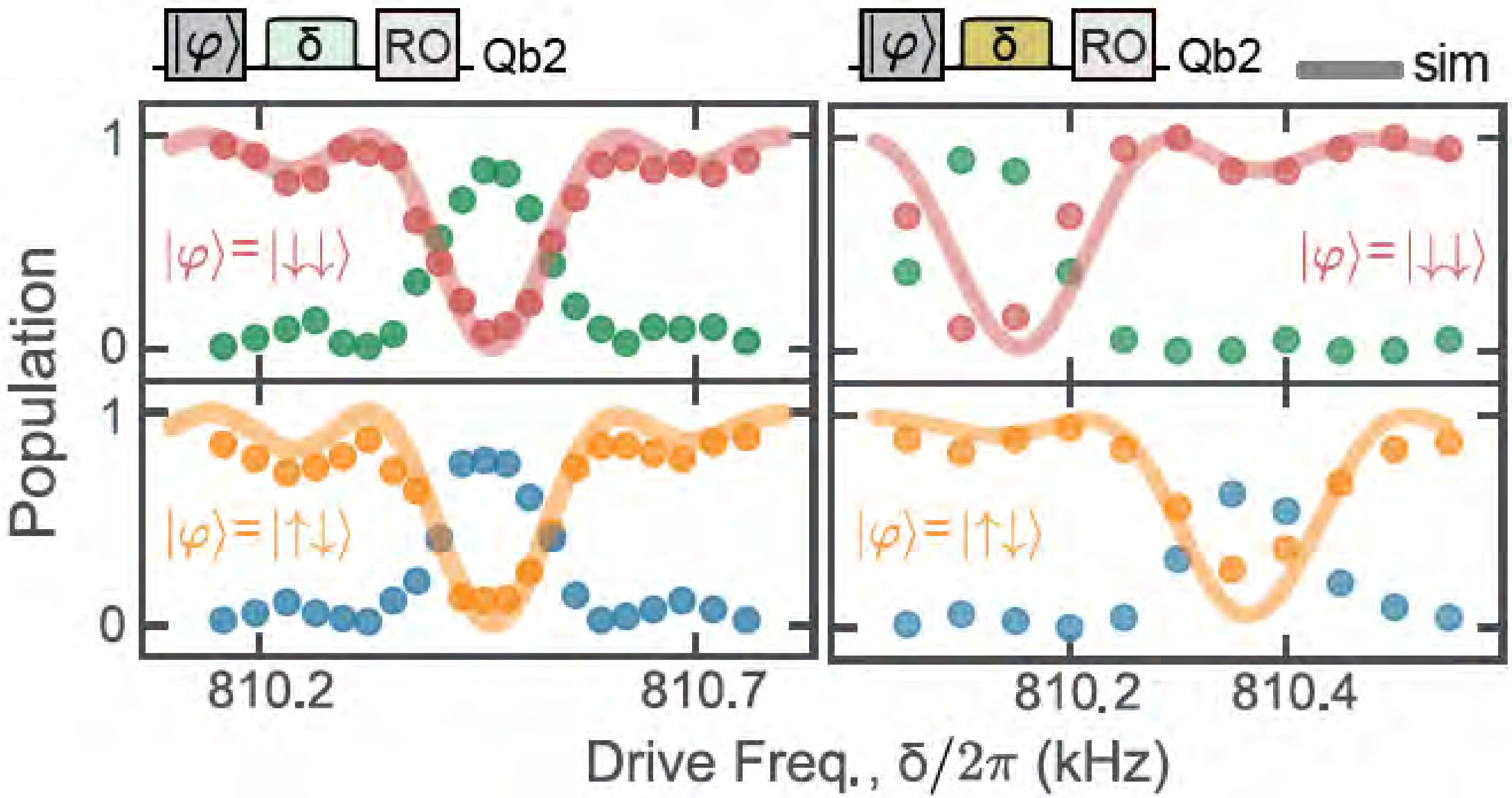

J. O'Sullivan et al., Nature Phys. (2025)

CNOT via conditional ac-Zeeman shifts

Preparing |↓↓⟩

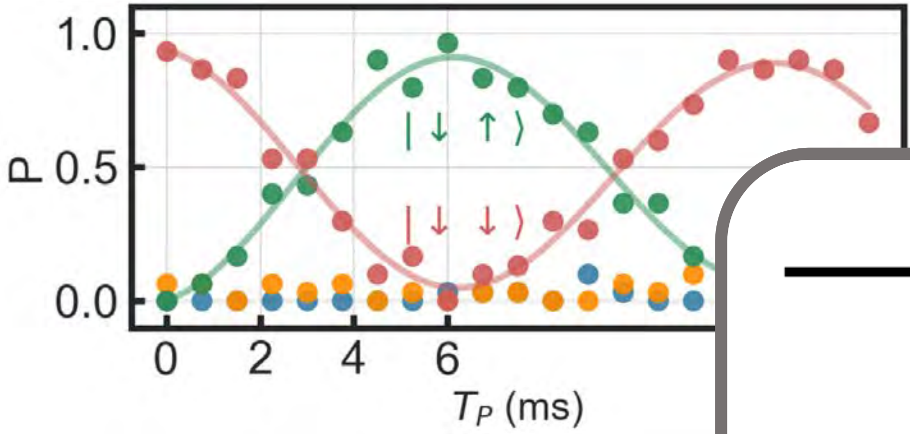

Preparing |↓↑⟩

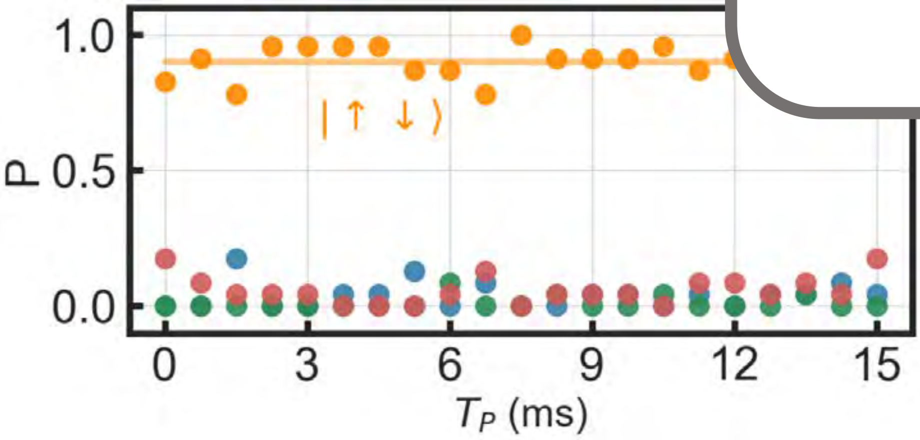

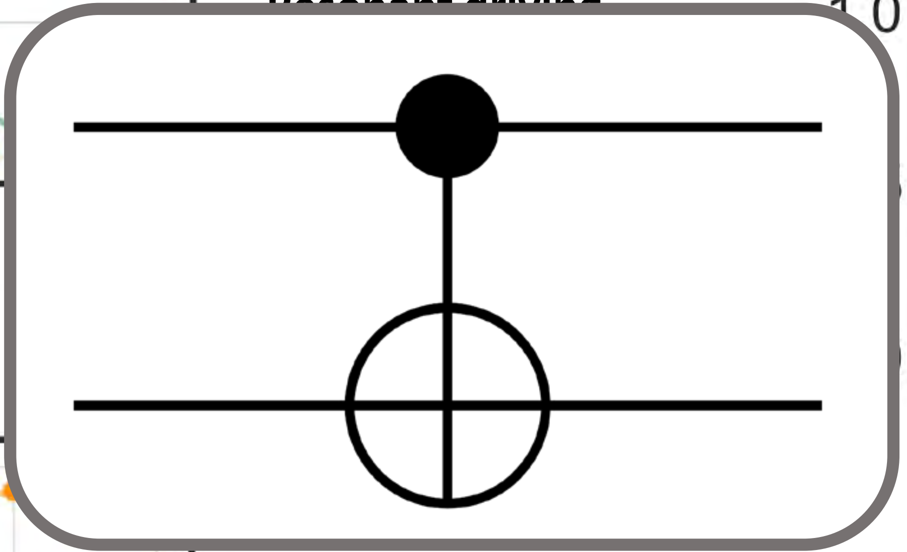

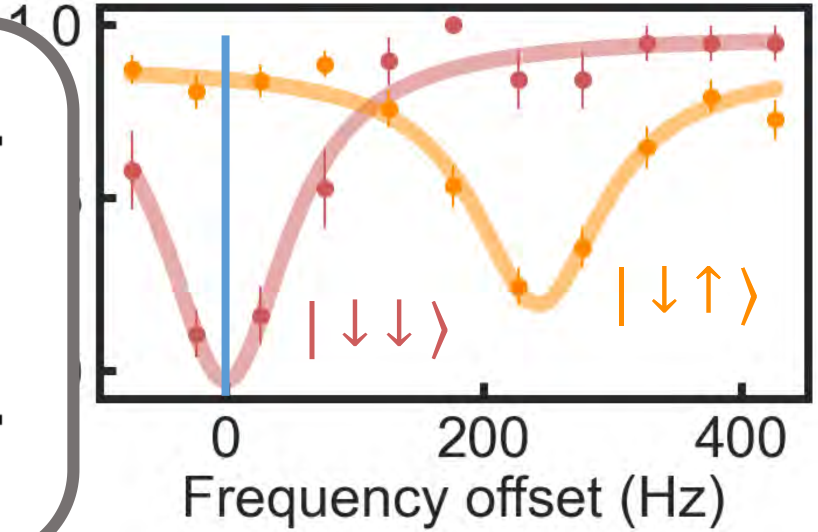

No driving

Bell state preparation and tomography

$$\frac{1}{\sqrt{2}}\left(|\downarrow\downarrow\rangle + |\uparrow\uparrow\rangle\right)$$

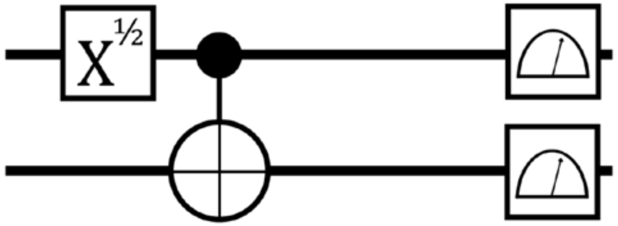

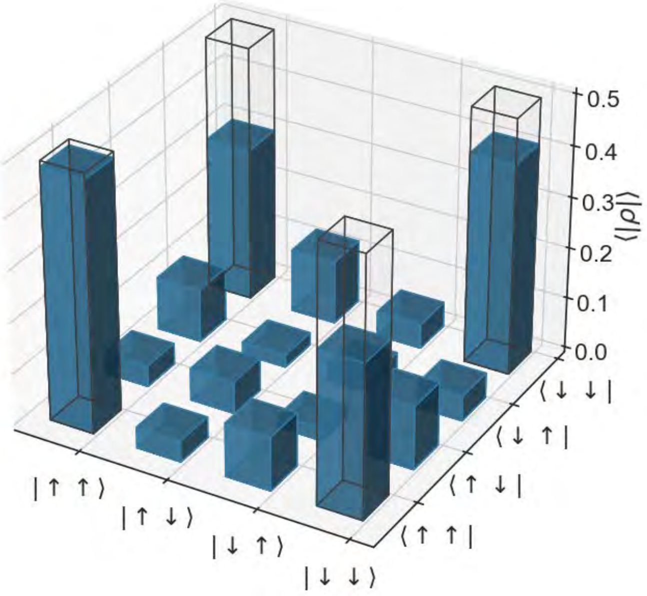

$$\frac{1}{\sqrt{2}}\left(|\downarrow\uparrow\rangle + |\uparrow\downarrow\rangle\right)$$

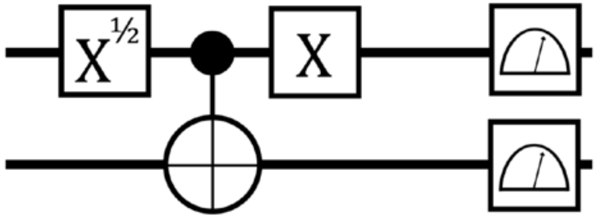

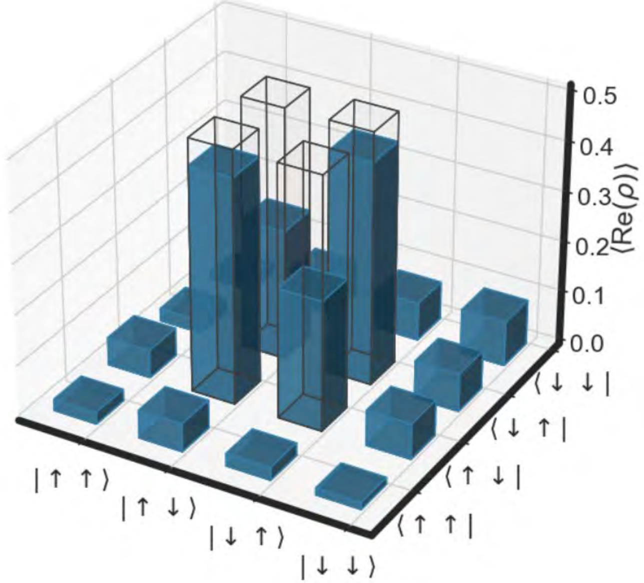

Two-qubit entangled states with second-long lifetime

$$\frac{\mathbf{1}}{\sqrt{\mathbf{2}}}(|\downarrow\downarrow\rangle + |\uparrow\uparrow\rangle)$$

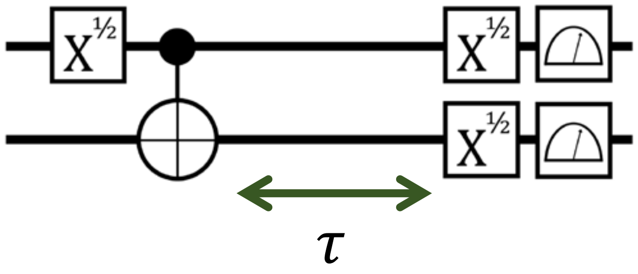

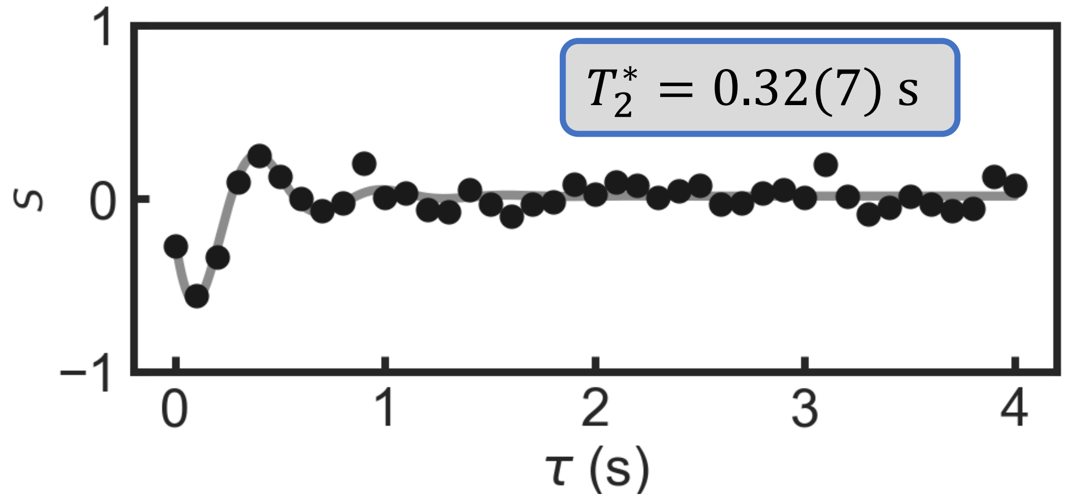

$$\frac{\mathbf{1}}{\sqrt{\mathbf{2}}}(|\downarrow\uparrow\rangle + |\uparrow\downarrow\rangle)$$

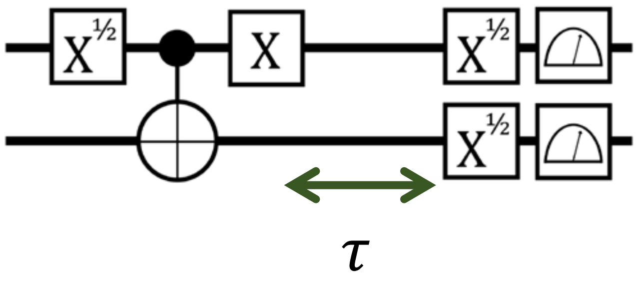

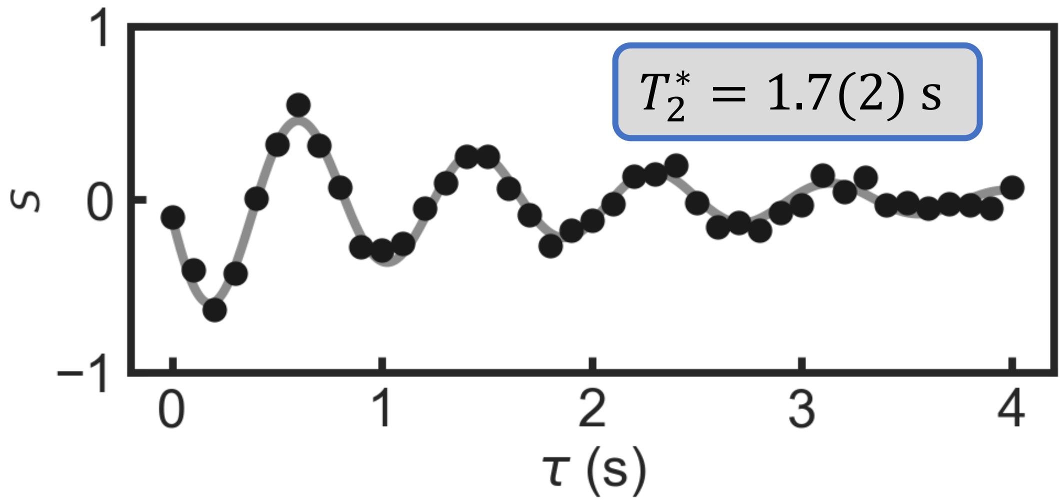

State $\frac{|\uparrow\downarrow\rangle + |\downarrow\uparrow\rangle}{\sqrt{2}}$ has longer coherence time than individual nuclear spins T_2^*

because it is insensitive to correlated magnetic noise (Decoherence-Free Subspace)

An unexpected nuclear spin

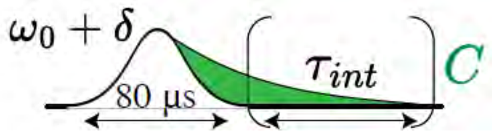

J. Travesedo Z. Huang

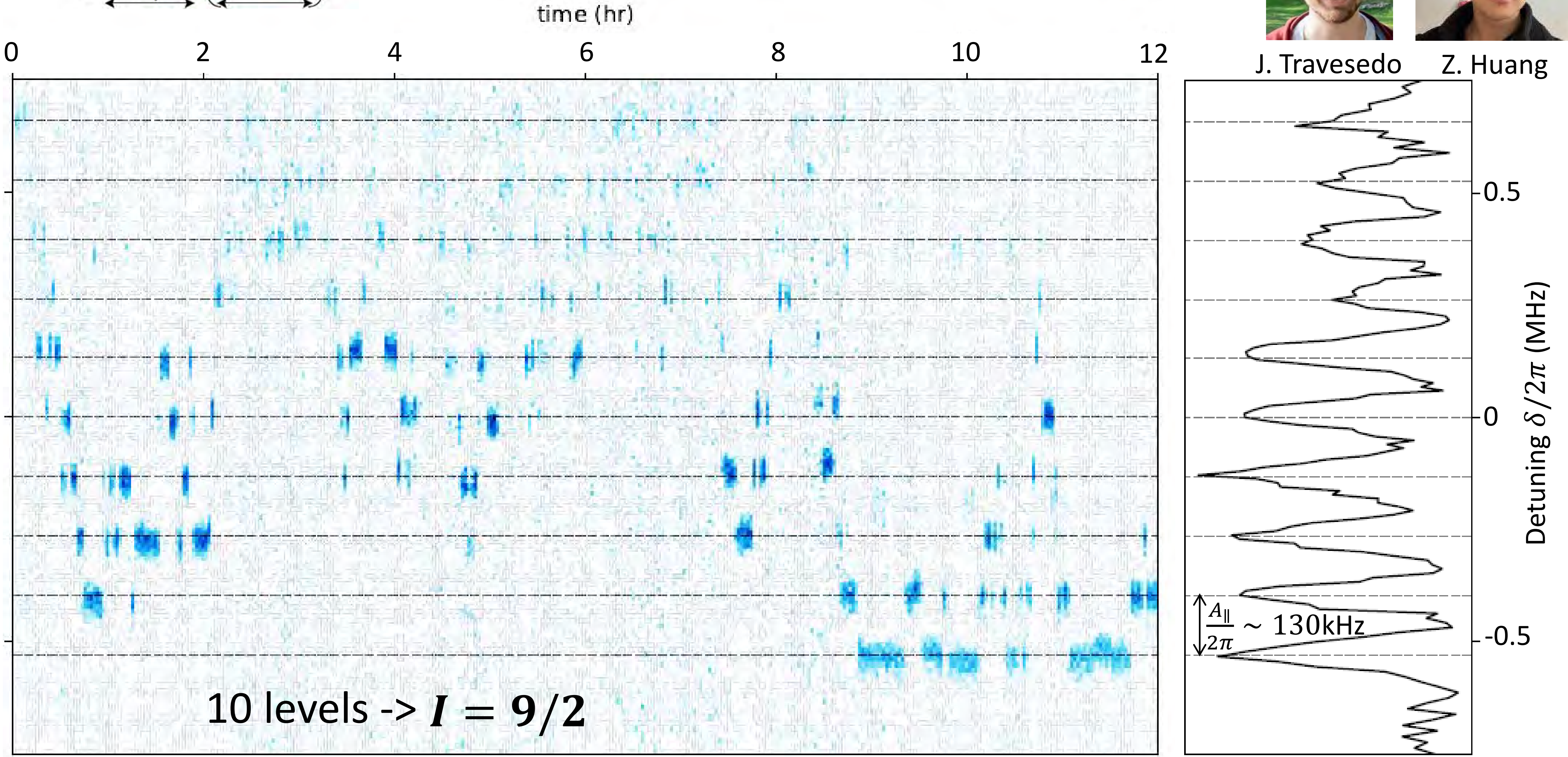

Interacting paramagnetic impurity and 9/2 nuclear spin : Spin Hamiltonian

$$\mathcal{H} = \mathcal{H}_{eZ} + \mathcal{H}_{hf} + \mathcal{H}_{nZ} + \boldsymbol{\mathcal{H}_{Q}}$$

Electron spin 1/2

$$\mathcal{H}_{eZ} = \omega_S S_z$$

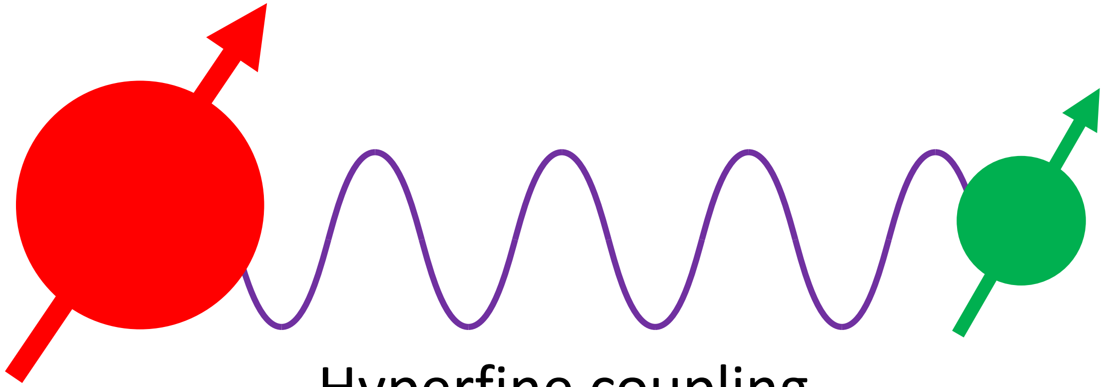

Nuclear spin

$$\mathcal{H}_{nZ} = \omega_I I_z$$

Hyperfine coupling
(dipolar + Fermi contact)

$$\mathcal{H}_{hf} = S \cdot \bar{\bar{A}} \cdot I$$

Quadrupolar interaction
if $I > \frac{1}{2}$

$$\mathcal{H}_{Q} = I \cdot \bar{\bar{Q}} \cdot I$$

Detailed study of quadrupolar interaction at the single-nucleus level

Breitweiser et al., Nano Lett. (2024)
Bartling et al., PR Appl. (2024)
Fernandez de Fuentes et al., Nature Com (2024)

Nuclear spin quadrupole interaction

Electrostatic energy of a non-spherical (I>1/2) nucleus in an electric-field gradient

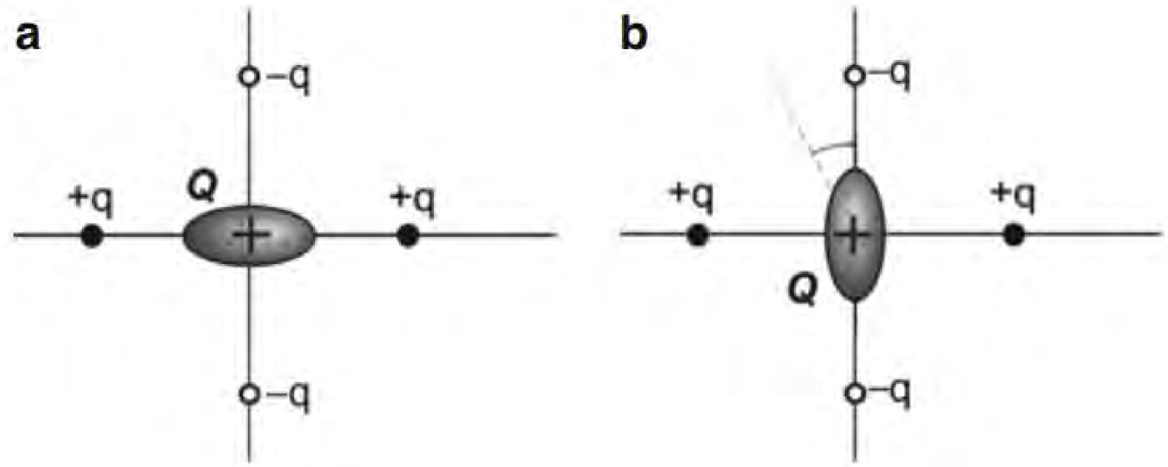

Slichter,
Principles of Magnetic Resonance

$H = \Sigma_{i,j=\{x,y,z\}} Q_{ij} I_i I_j$ Q_{ij} proportional to $\frac{\partial^2 V}{\partial r_i \partial r_j}$, traceless and symmetric

5 parameters

In the principal axis basis (X,Y,Z)

$$H_Q = Q_X I_X^2 + Q_Y I_Y^2 + Q_Z I_Z^2, \text{ with } Q_Z = -Q_X - Q_Y$$

$$H_Q = \frac{C_Q}{4I(2I-1)}[3I_Z^2 - I(I+1) + \eta(I_X^2 - I_Y^2)]$$

Two principal values (Q_X, Q_Y)
3 Euler angles

Quadrupolar constant C_Q
Biaxiality parameter η
3 Euler angles

Precision spectroscopy : motivation

$$\mathcal{H} = \mathcal{H}_{eZ} + \mathcal{H}_{hf} + \mathcal{H}_{nZ} + \mathcal{H}_{Q} + \cdots ???$$

Electron spin 1/2

$$\mathcal{H}_{eZ} = \omega_S S_z$$

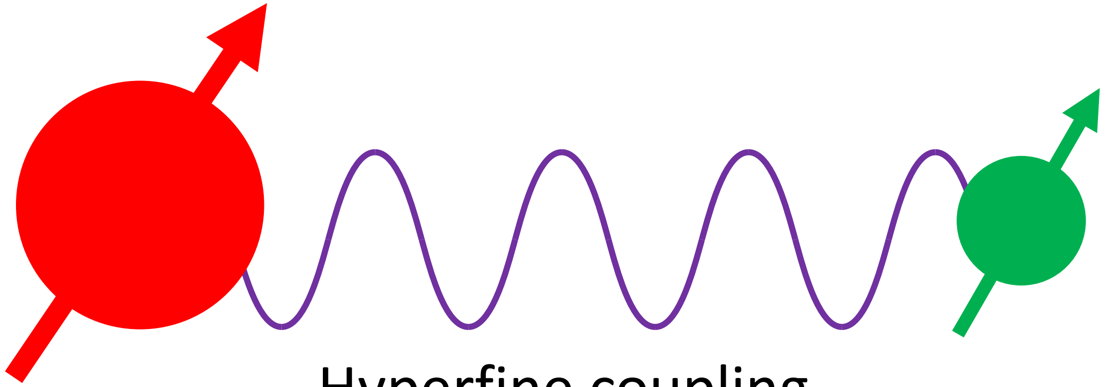

Nuclear spin

$$\mathcal{H}_{nZ} = \omega_I I_z$$

Quadrupolar interaction

if $I > \frac{1}{2}$

$$\mathcal{H}_Q = I \cdot \bar{\bar{Q}} \cdot I$$

Hyperfine coupling
(dipolar + Fermi contact)

$$\mathcal{H}_{hf} = S \cdot \bar{\bar{A}} \cdot I$$

Possible extra terms ?

- Octupolar interaction with magnetic field 2nd derivative: $\Sigma_{i,j,k=\{x,y,z\}} O_{ijk} I_i I_j I_k$
- Hexadecapolar interaction with electric field 3rd derivative: $\Sigma_{i,j,k,l=\{x,y,z\}} H_{ijkl} I_i I_j I_k I_l$
- Higher-order interactions between electron and nuclear spin

NEED HIGH SPECTRAL RESOLUTION (Hz)

Energy levels

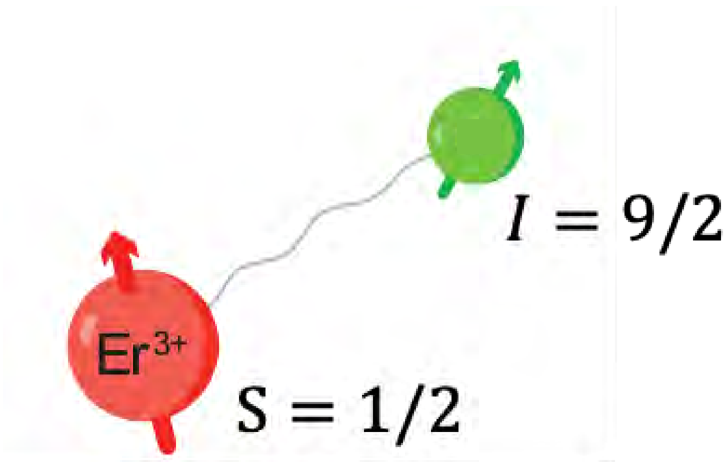

$$\hat{H}/\hbar = \omega_S \hat{S}_z + \omega_I \hat{I}_z + A_\parallel \hat{S}_z \hat{I}_z + A_\perp \hat{S}_z \hat{I}_x + \hat{I} \cdot \bar{\bar{Q}} \cdot \hat{I}$$

$|\uparrow 0\rangle$ $|\uparrow 1\rangle$ $|\uparrow 2\rangle$ $|\uparrow 3\rangle$ $|\uparrow 4\rangle$ $|\uparrow 5\rangle$ $|\uparrow 6\rangle$ $|\uparrow 7\rangle$ $|\uparrow 8\rangle$ $|\uparrow 9\rangle$

$|\downarrow 0\rangle$ $|\downarrow 1\rangle$ $|\downarrow 2\rangle$ $|\downarrow 3\rangle$ $|\downarrow 4\rangle$ $|\downarrow 5\rangle$ $|\downarrow 6\rangle$ $|\downarrow 7\rangle$ $|\downarrow 8\rangle$ $|\downarrow 9\rangle$

Detailed spectroscopy needed

Nuclear spin readout

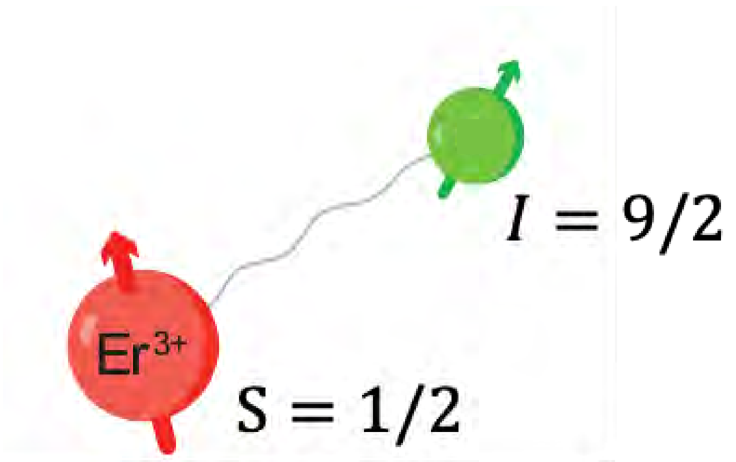

$$\hat{H}/\hbar = \omega_S \hat{S}_z + \omega_I \hat{I}_z + A_\parallel \hat{S}_z \hat{I}_z + A_\perp \hat{S}_z \hat{I}_x + \hat{I}\cdot\bar{\bar{Q}}\cdot\hat{I}$$

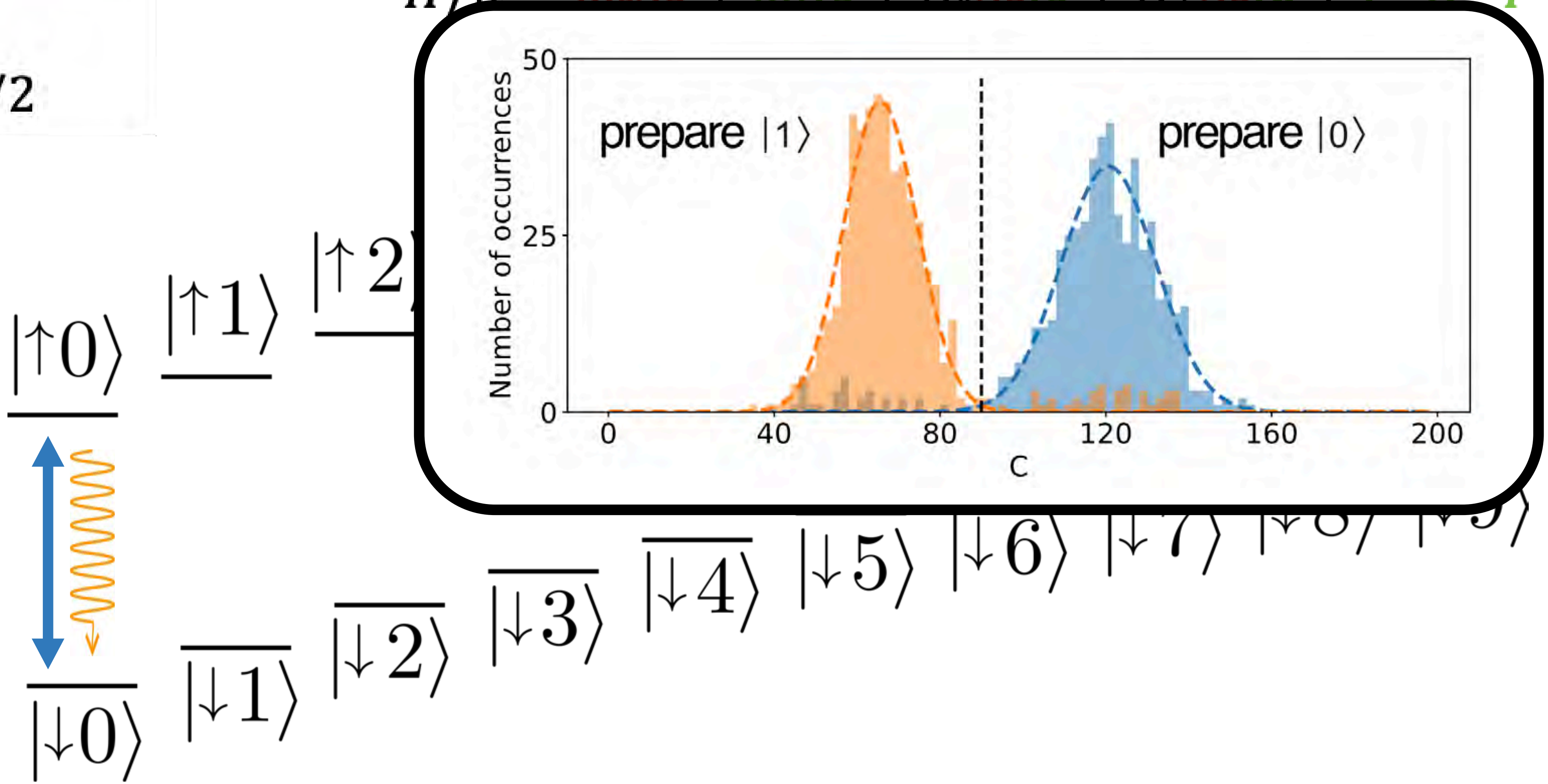

Nuclear spin preparation

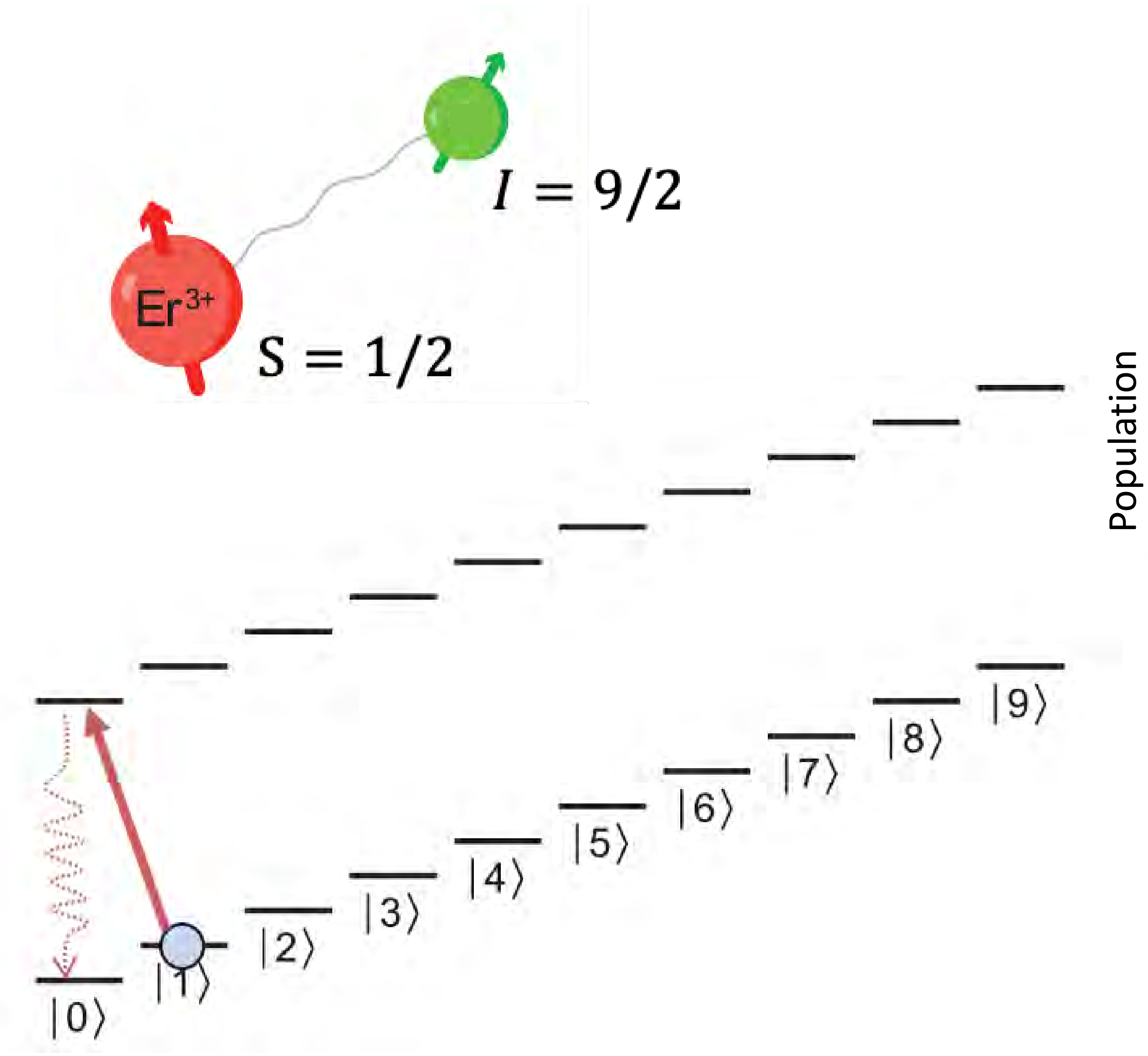

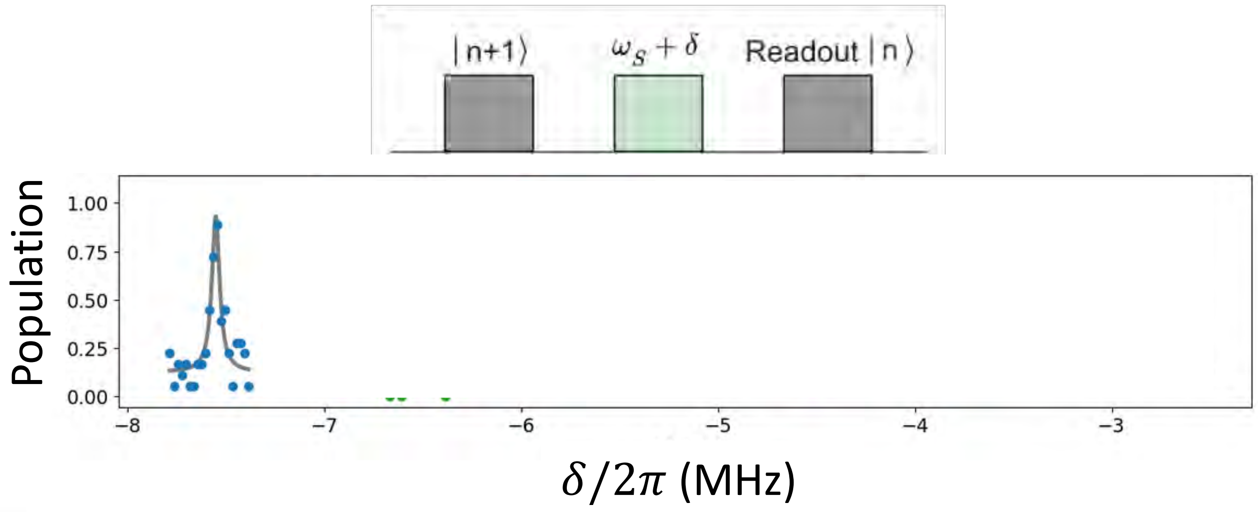

Nuclear spin preparation

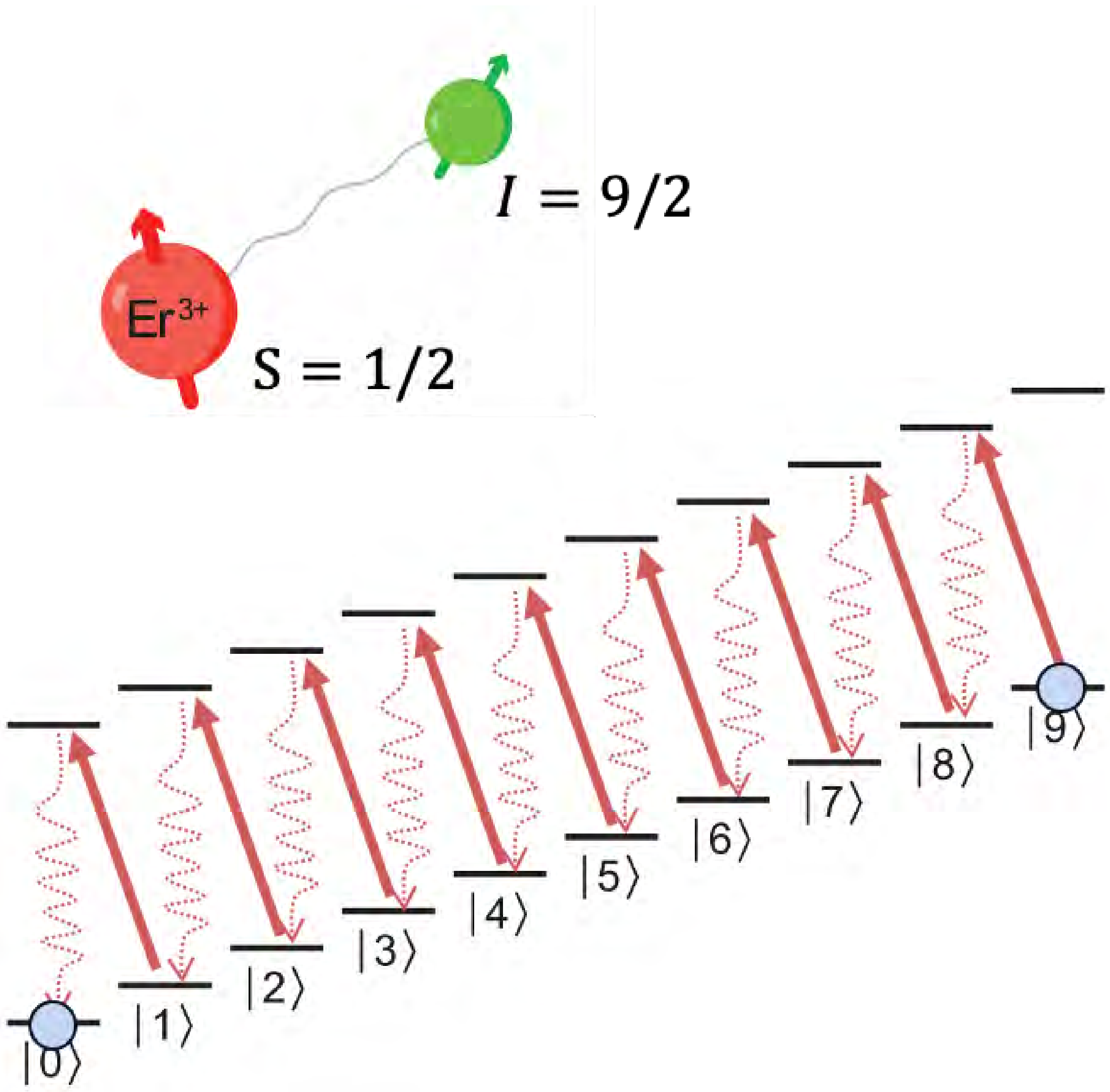

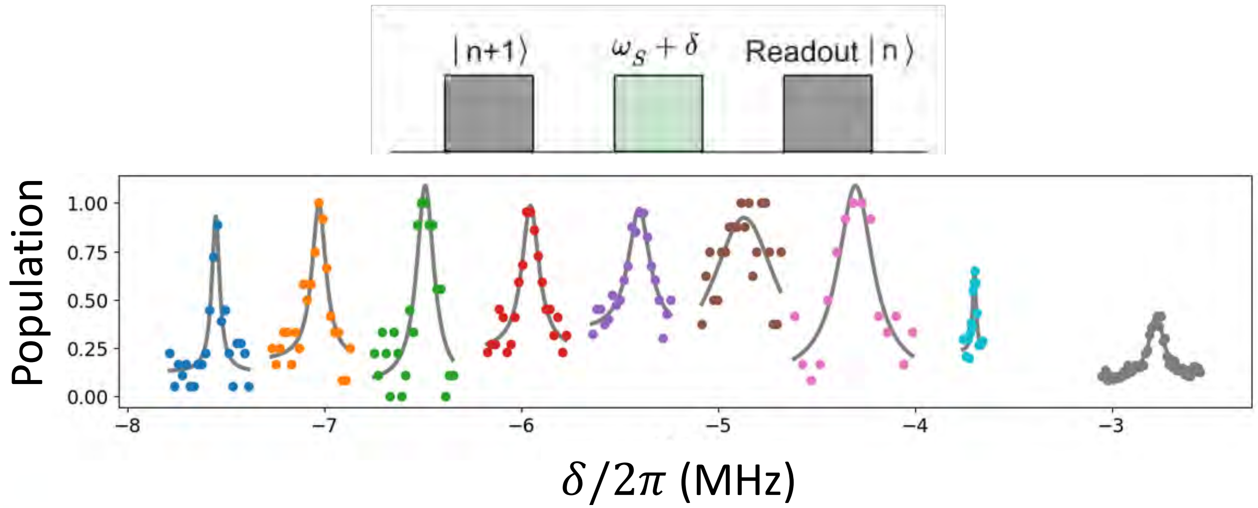

Nuclear spin identification by the gyromagnetic ratio (Er3+ in $|\downarrow\rangle$)

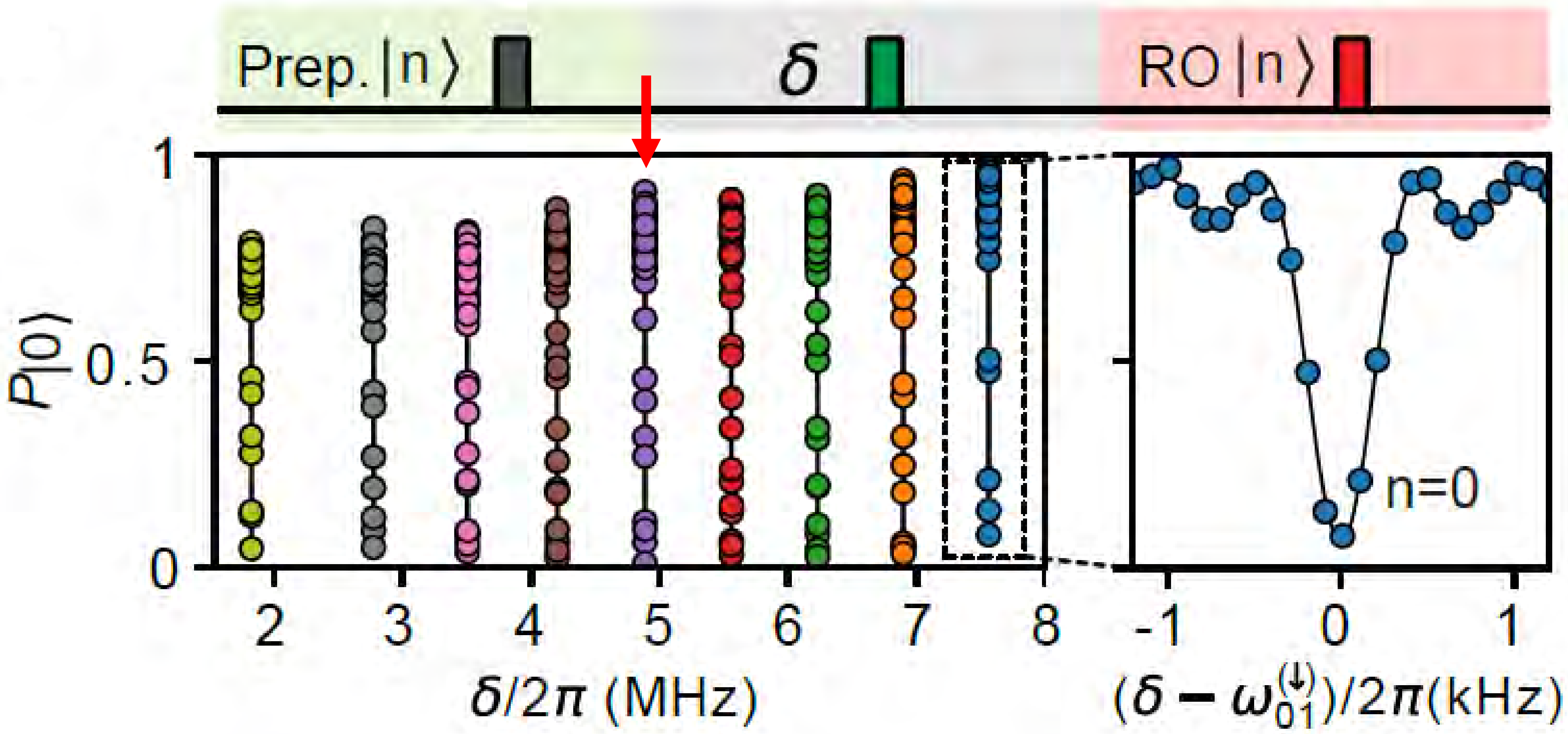

$\left|-\frac{1}{2}\right\rangle \leftrightarrow \left|+\frac{1}{2}\right\rangle$ is 2nd-order insensitive to quadrupole $\Longrightarrow$ $\omega_{45,\downarrow} \sim \gamma_I B_0$

$\frac{\omega_{45}}{B_0} = 2\pi \times 10.83\text{MHz/T}$ is close to ^{93}Nb gyromagnetic ratio, $\gamma_{^{93}Nb} = 2\pi \times 10.45\text{MHz/T}$

Possible origin of the ^{93}Nb impurity

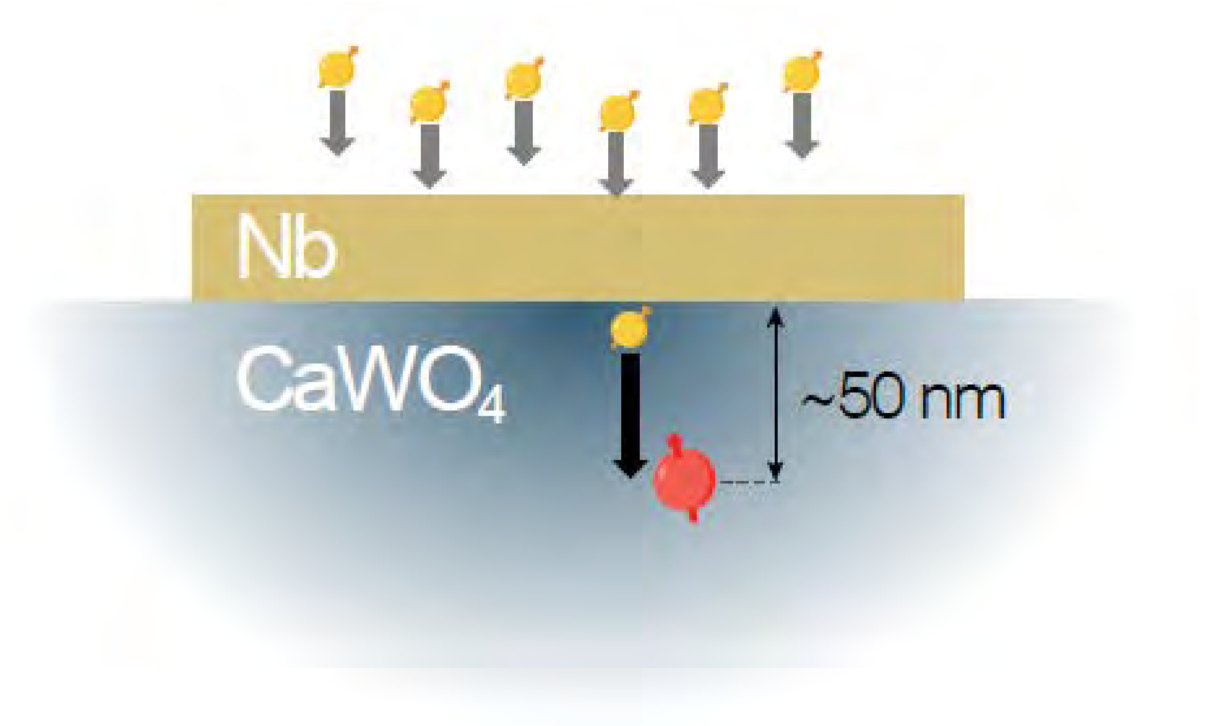

- Origin : either sputtering, or as-grown impurity
- Likely replaces a W^{6+}

^{93}Nb impurity site assignment

$A_{\parallel}$ and $A_{\perp}$ are measured and compared to
magnetic dipole coupling in the point-dipole approximation

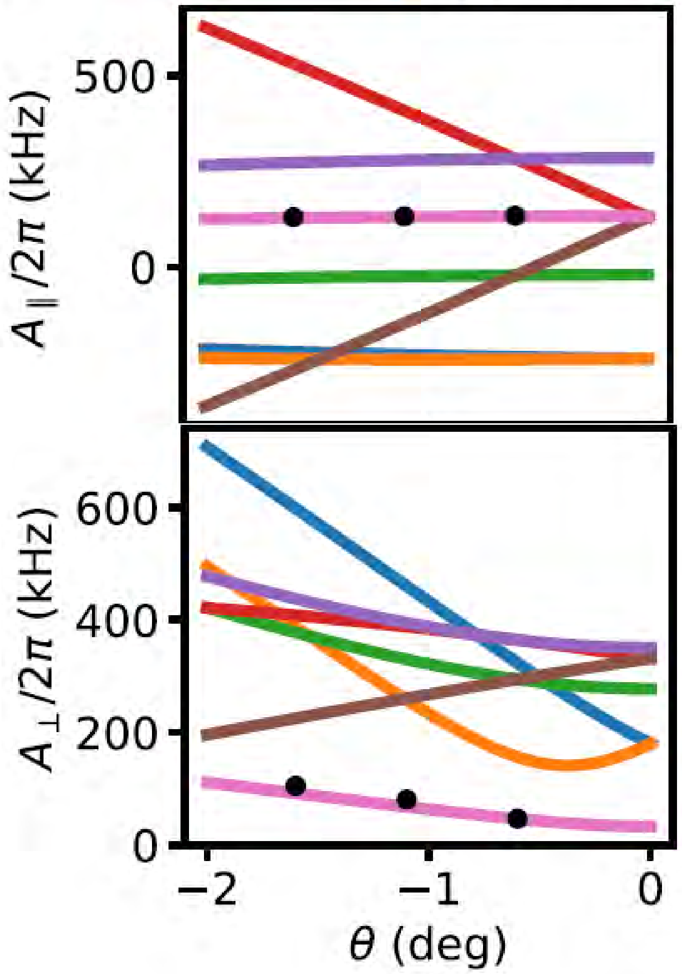

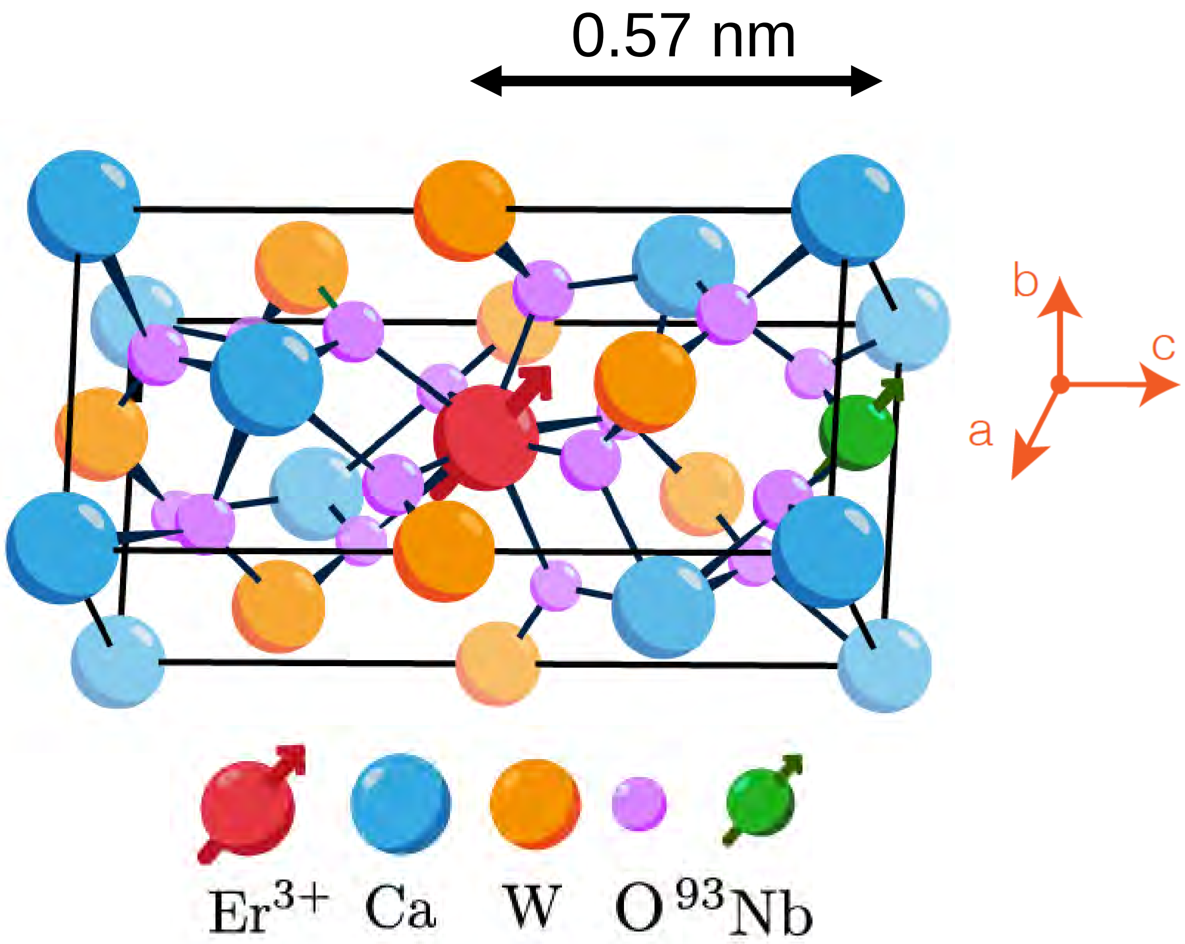

Narrowing linewidth by Dynamic Nuclear Polarization

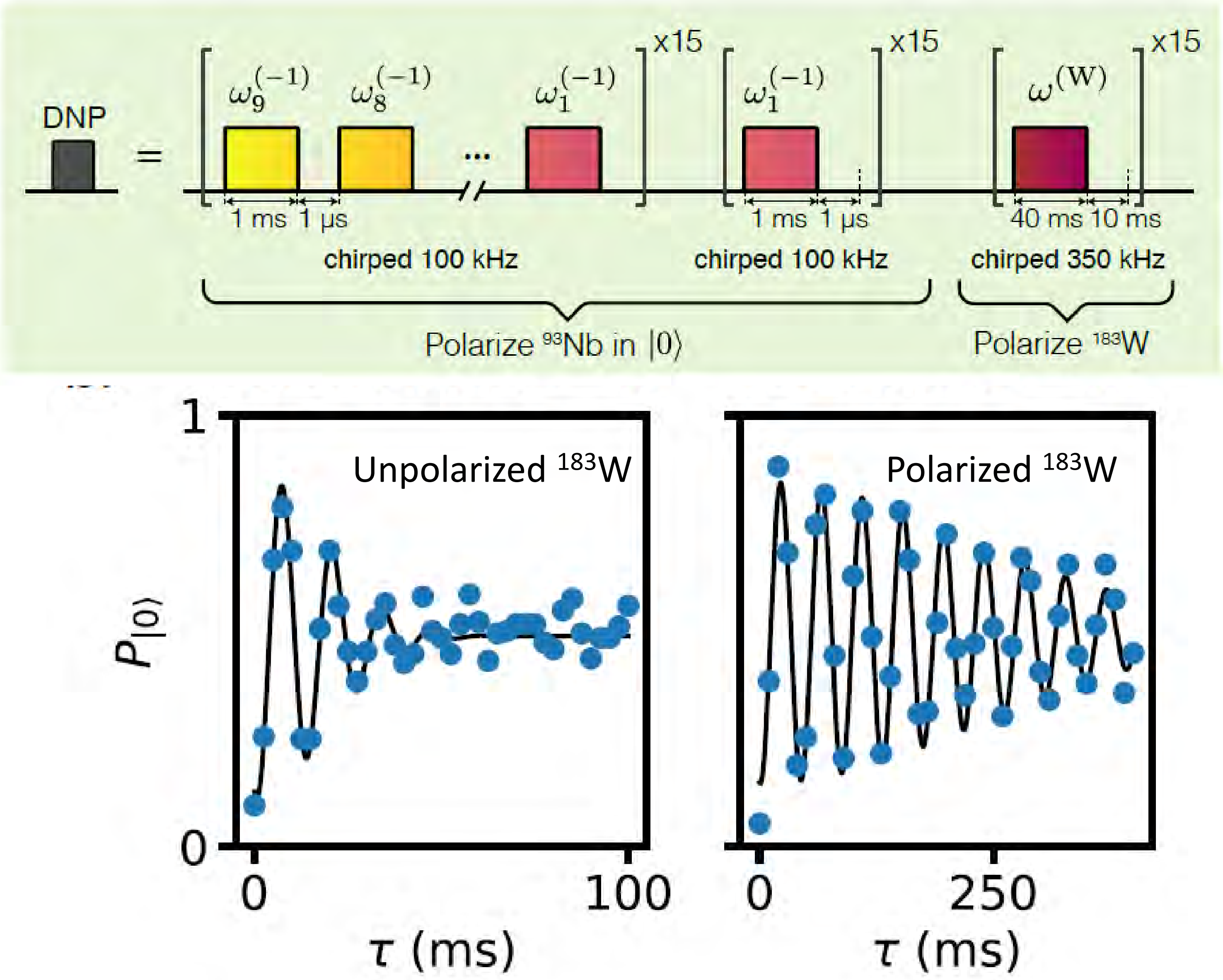

^{93}Nb spectroscopy, Er^{3+} in $|\downarrow\rangle$

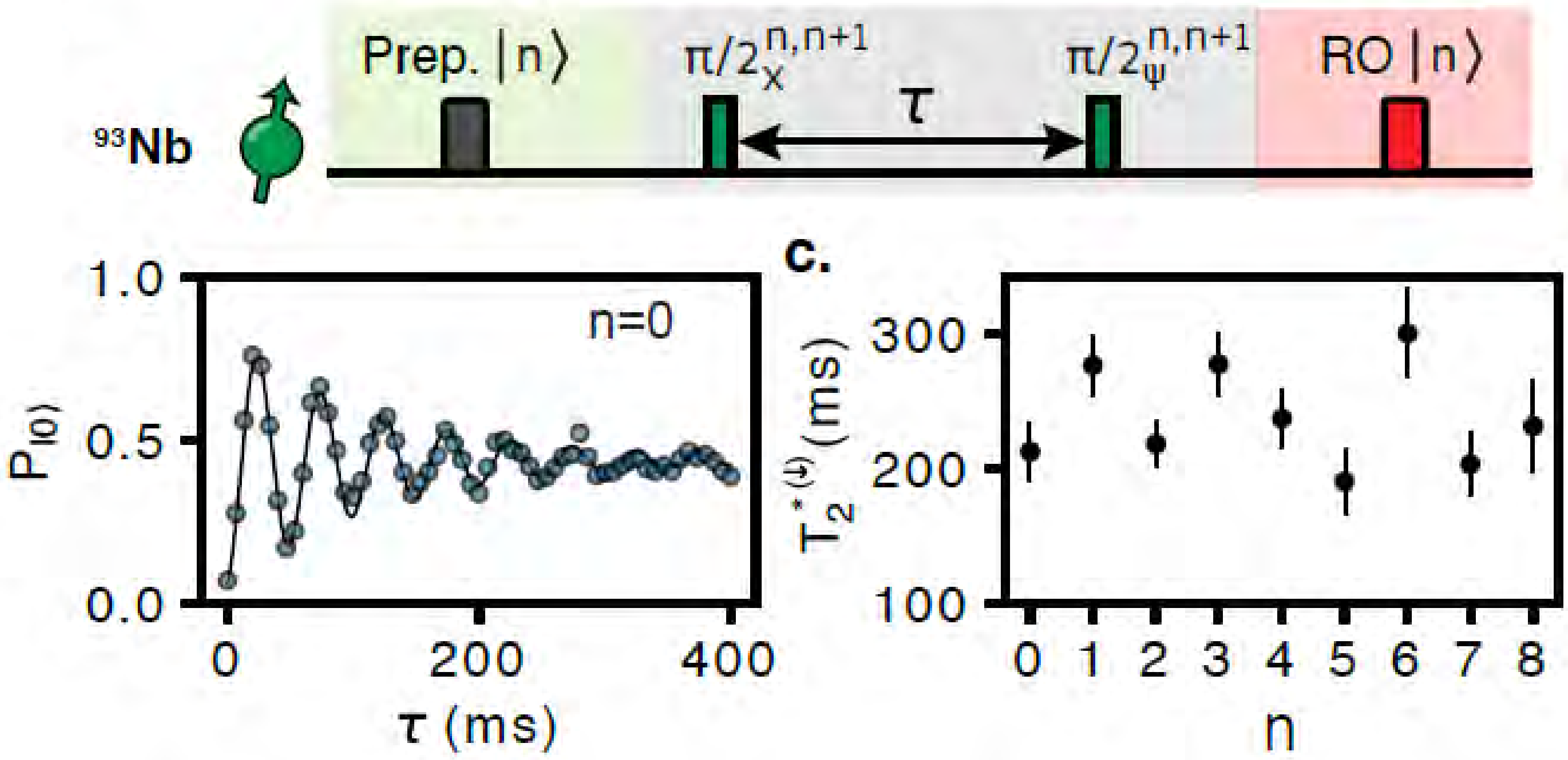

$T_2^* = 200 - 300\text{ms}$ → 1-1.5 Hz linewidth when Er3+ is in $|\downarrow\rangle$

^{93}Nb spectroscopy, Er^{3+} in $|\uparrow\rangle$

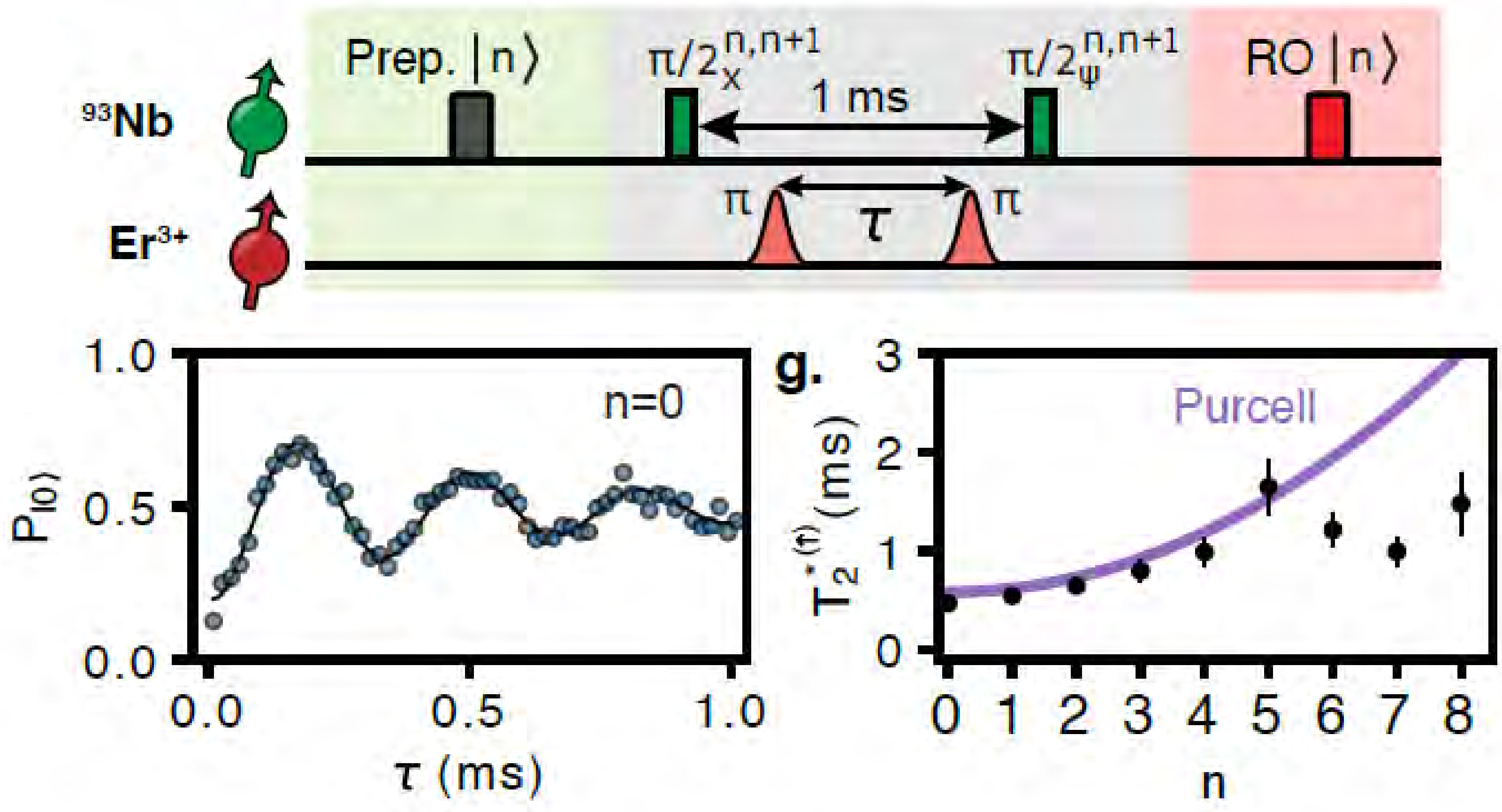

$T_2^* = 0.5 - 1.5\text{ms}$ → 300 - 700 Hz linewidth when Er3+ is in $|\uparrow\rangle$

Hamiltonian parameters fitting

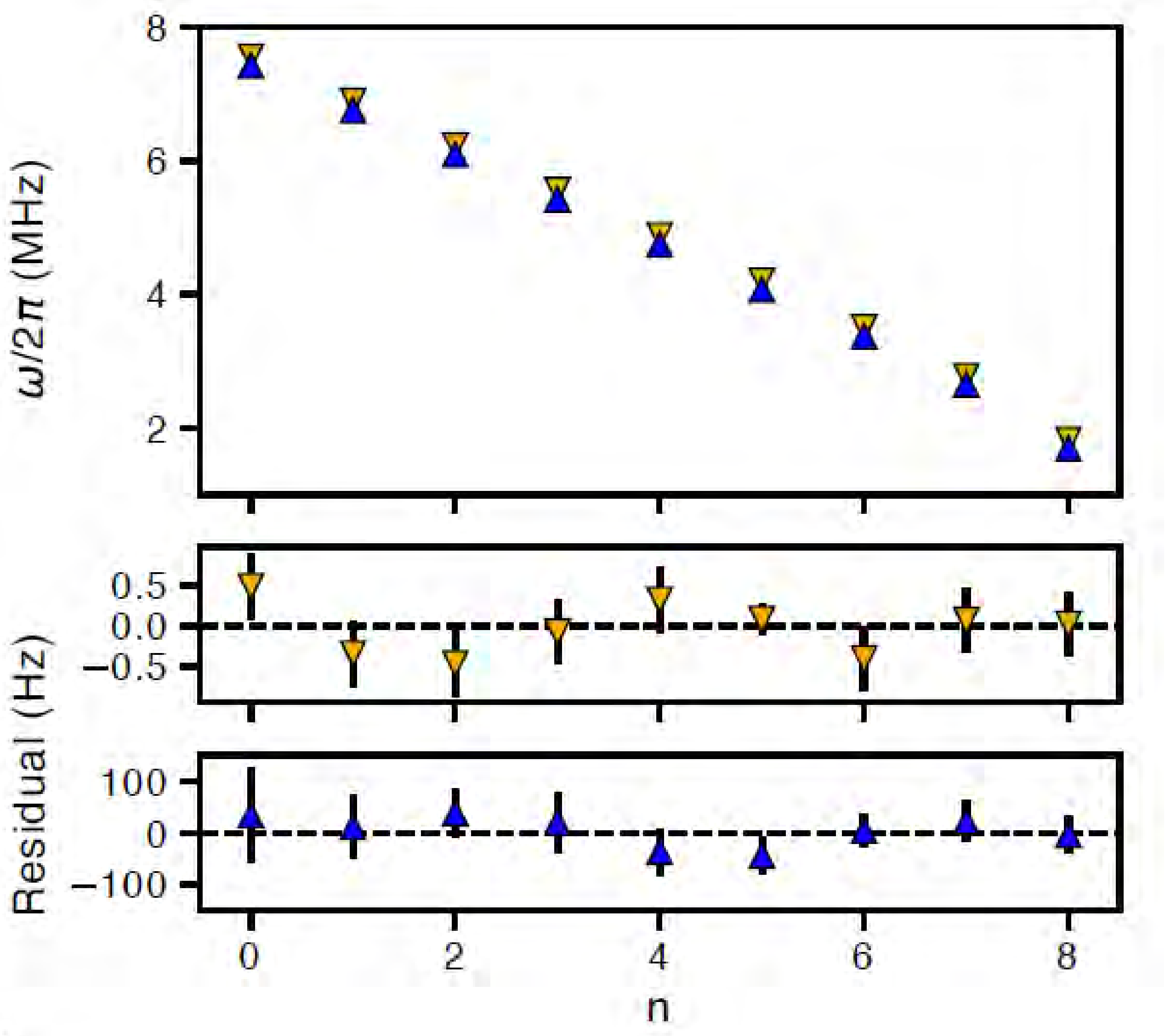

$$H = \omega_I^{(m_S)} I_z^{(m_S)} + H_Q^{(m_S)}$$

5 fitting parameters
$\omega_I^{(m_S)}$ and 4 quadrupolar terms
(angular symmetry around B_0)
for 9 frequencies

Agreement with quadrupolar model
to statistical uncertainty

Fitted $\frac{C_Q}{2\pi} = 19.3059(7)$ MHz and $\eta = 0.77026(7)$
in agreement with DFT (T. Charpentier)

Quadrupolar principal values, ground/excited

Comparison of fitted quadrupolar principal values for $m_S = \downarrow$ and $m_S = \uparrow$

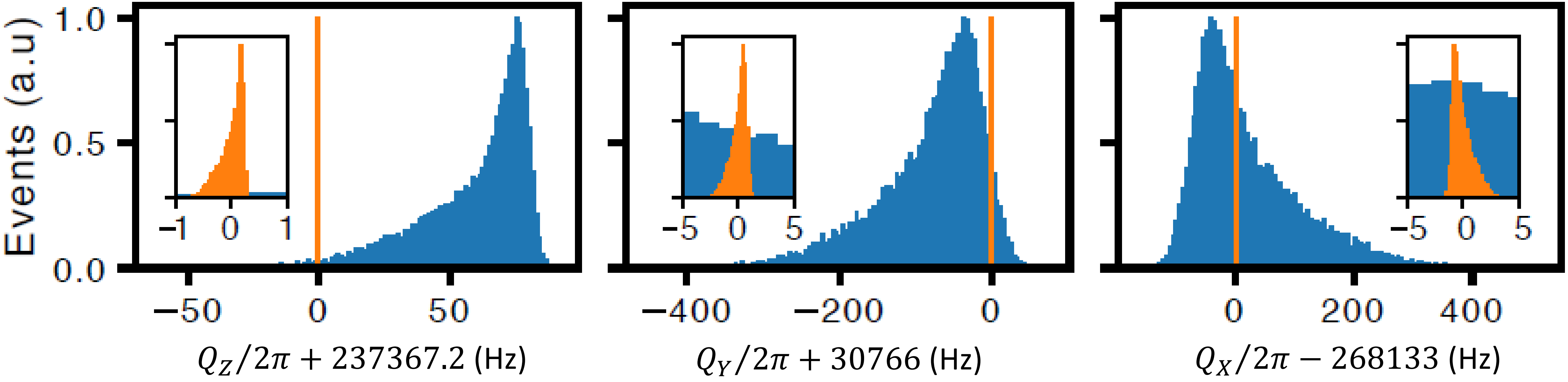

- Uncertainty on Q_Z is much lower than $Q_{X/Y}$ because Z coincides approx. with B_0 (also approx. along c axis)
- Q_Z depends on the Er^{3+} spin state with high statistical significance

New Spin-Dependent-Quadrupole term $\mathcal{H}_{SDQ} = \frac{Q_{zzz}^{(SDQ)}}{6} S_z[3I_z^2 - I(I+1)]$ with $\frac{Q_{zzz}^{(SDQ)}}{2\pi} = 76\text{Hz}$

Attributed to electrostatic coupling between Er^{3+} and ^{93}Nb

What limits the spectral resolution in the ground state ?

Repeated Ramsey measurements on 0-1 transition

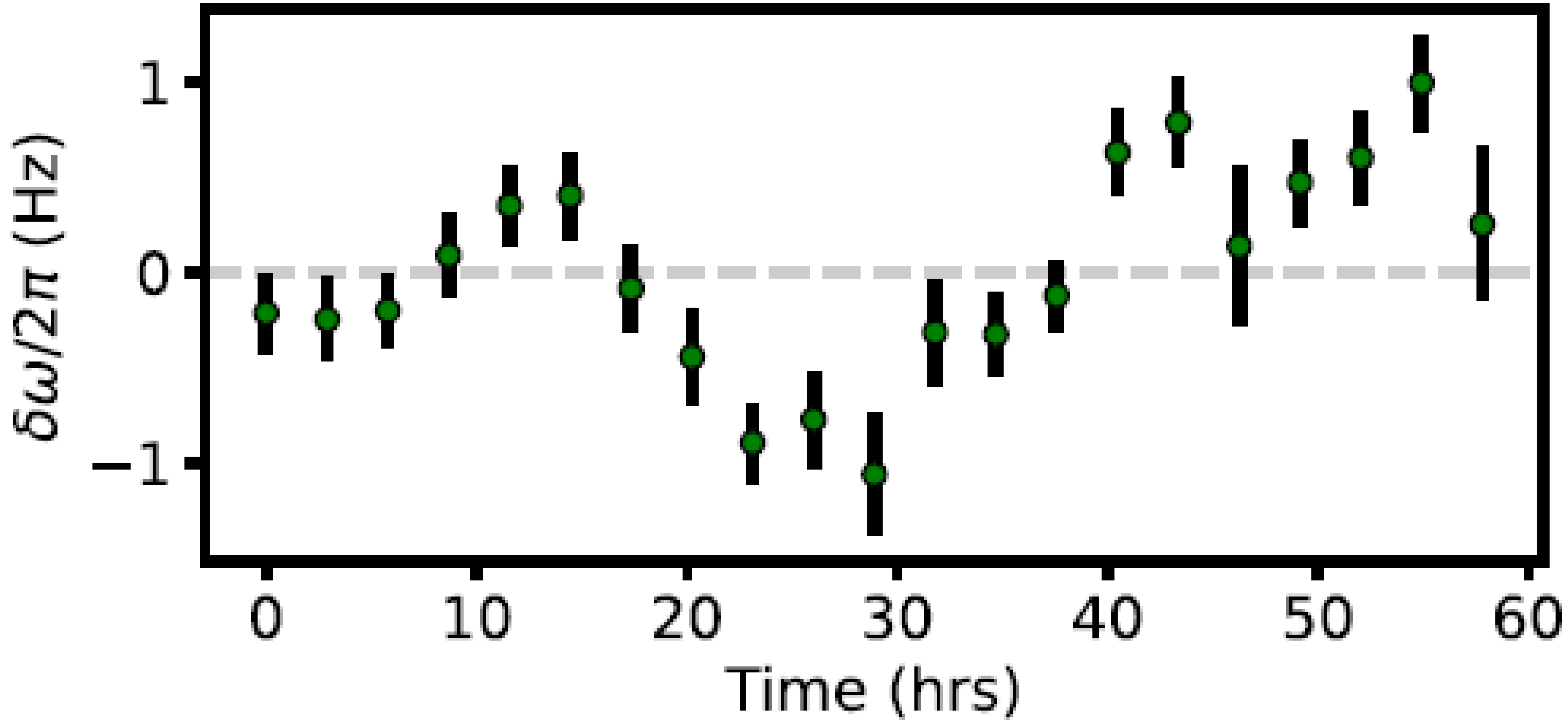

- Long-term drifts possibly due to nuclear spin bath, or B_0 drift
- Stability ± 1Hz over 60 hours

Enhancing ground-state spectral resolution with differential measurements

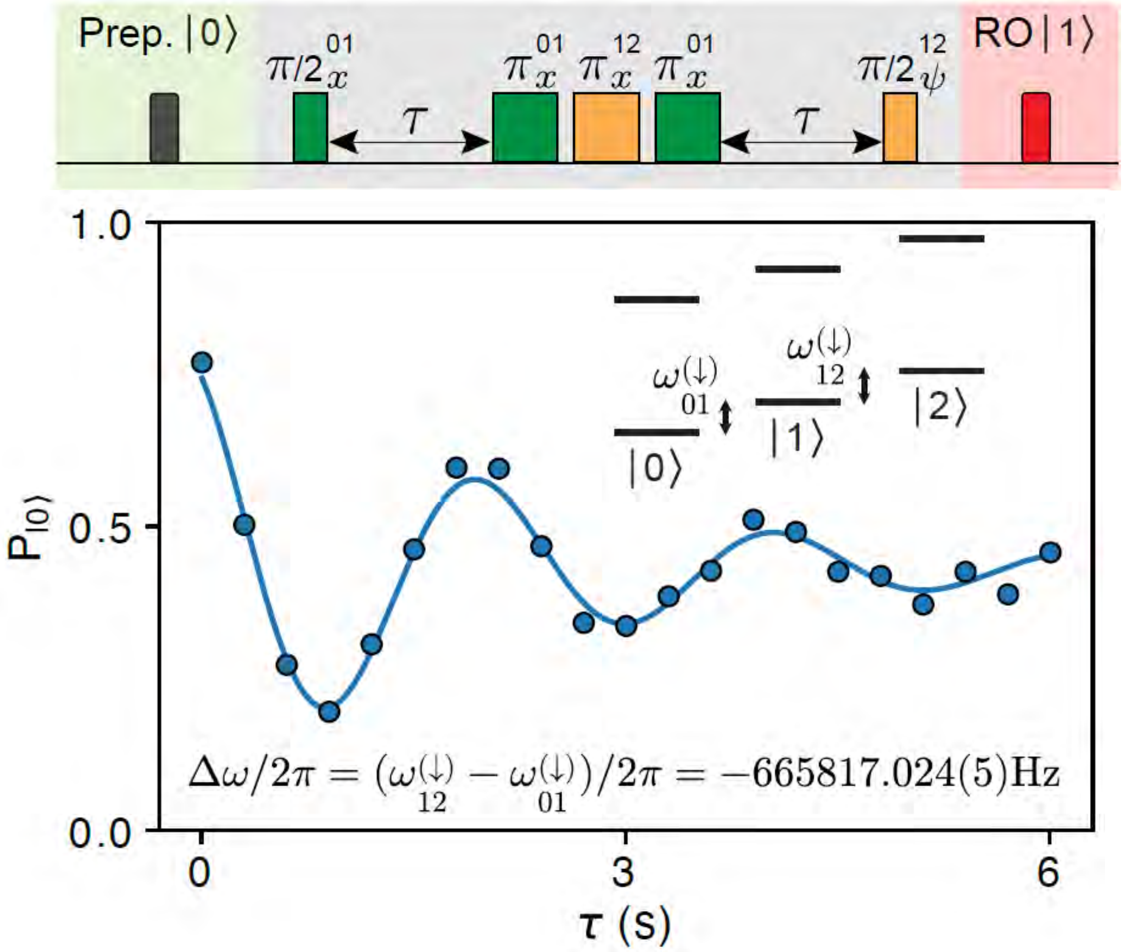

$T_2 = 3\mathrm{s}$

Linewidth = 0.1Hz

Ten-fold increase in spectral resolution

- Magnetic noise impact reduced by differential measurement (analog. correlation spectroscopy in NMR)
- Eight-digit ground-state differential frequency measurements

Fitting the differential ground-state data

3 models

Quadrupole only (Q)

$$\mathcal{H}^{(Q)} = \omega_I I_z + I \cdot Q \cdot I$$

Quadrupole + Octupole (Q+O)

$$\mathcal{H}^{(Q+O)} = \omega_I I_z + I \cdot Q \cdot I + \frac{C_3}{I(2I-1)(I-1)} C_3 I_z^3$$

Quadrupole + Hexadecapole (Q+H)

$$\mathcal{H}^{(Q+H)} = \omega_I I_z + I \cdot Q \cdot I + \frac{C_4}{I(2I-1)(I-1)(2I-3)} C_4 I_z^4$$

- Quadrupole-only is ruled-out
- Best agreement with hexadecapole term

$$C_4/2\pi = 9.4(3)\text{Hz}$$

First observation in solid-state

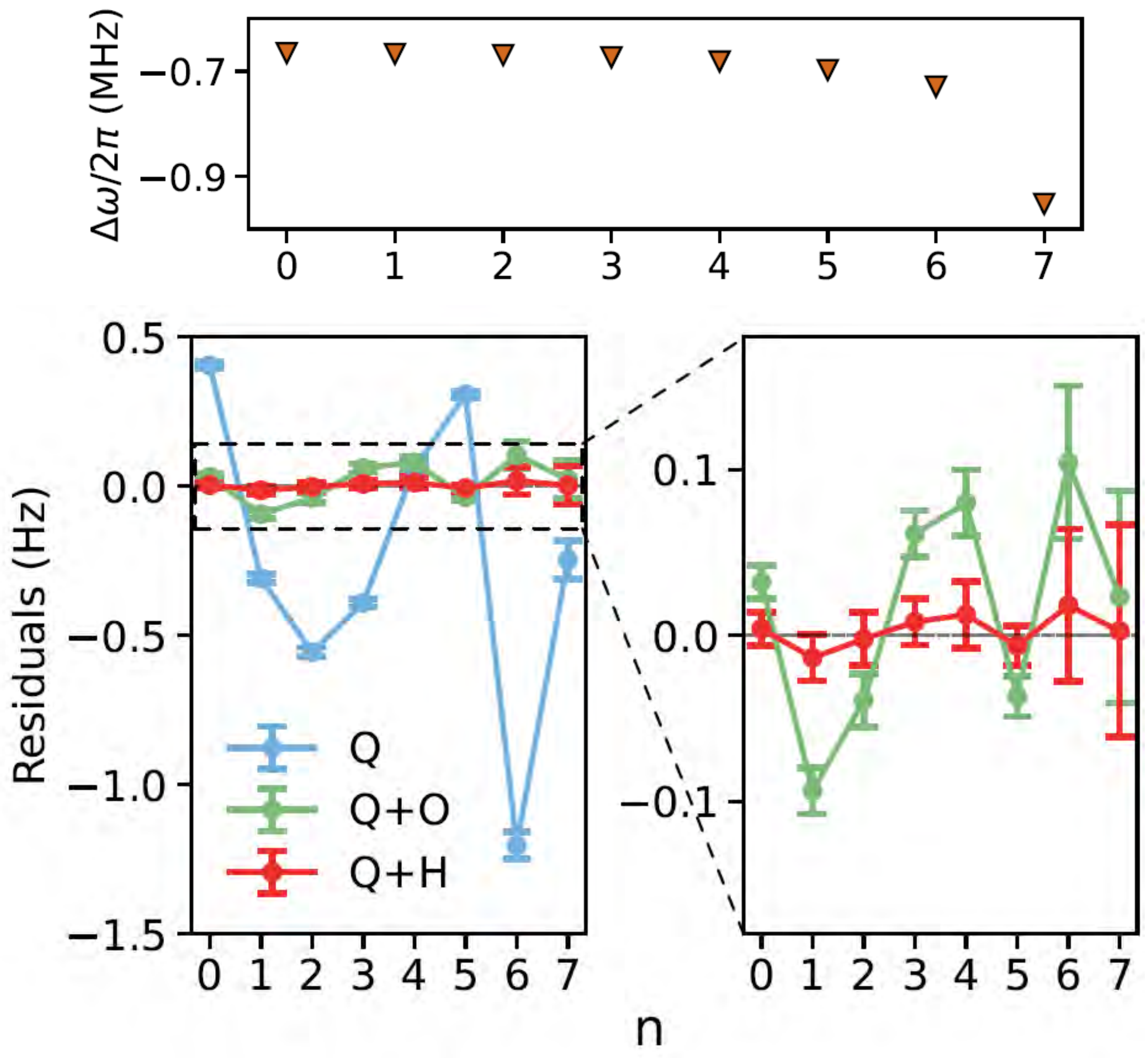

Conclusions

- Single-electron spin detection using microwave photon counting at 10mK
- Quantum jumps, readout, polarization and spectroscopy of individual nuclear spins

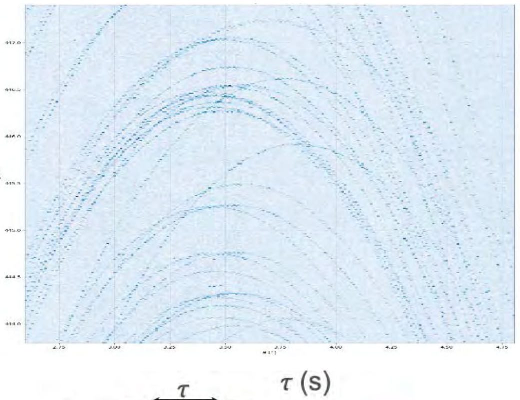

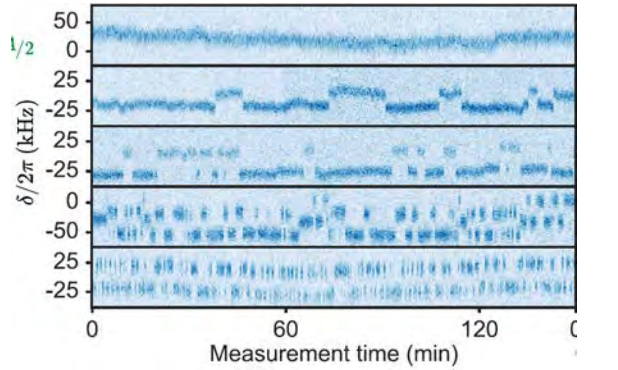

- Nuclear-spin qubits with second-long coherence time
- Two-nuclear-spin-qubits gate

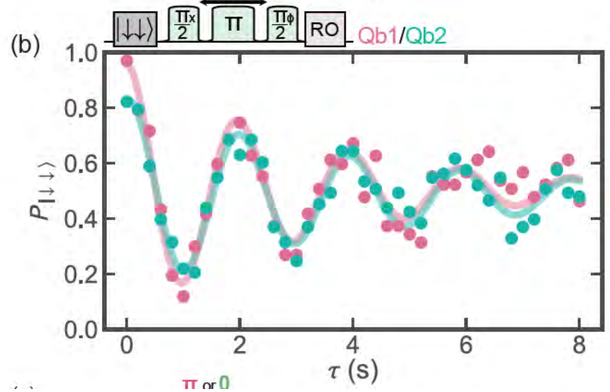

High spectral resolution yields two previously unobserved terms in the Hamiltonian of a Er^{3+} coupled to a ^{93}Nb spin :

- Er^{3+} spin-dependent quadrupole term prop. to $S_z I_z^2$
- Hexadecapolar nuclear spin interaction prop. to I_z^4

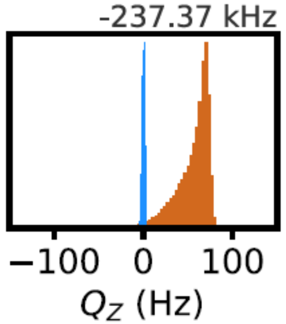

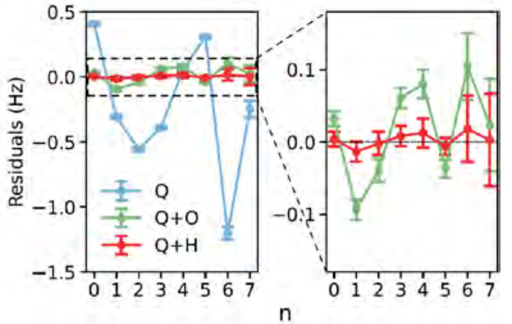

THANKS !

J. Travesedo

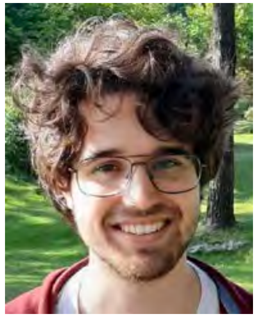

D. Haegi

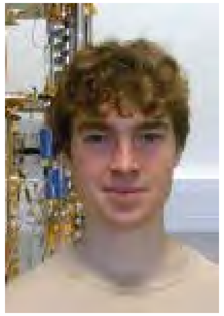

W. Huang

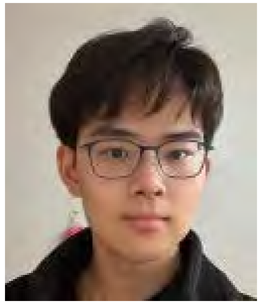

L. Suteveski

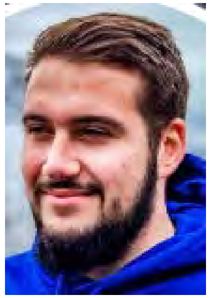

N. Thill

L. Mykolyshyn

M. Le Gall

J. Liersch

S. Palmiotto

L. Pallegoix

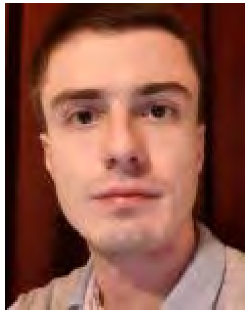

A. May

X. Zhou

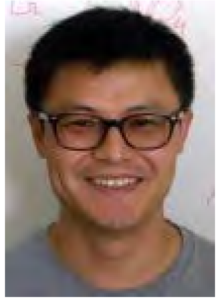

A. Pscherer

L. Balembois

J. O'Sullivan

E. Flurin

D. Vion

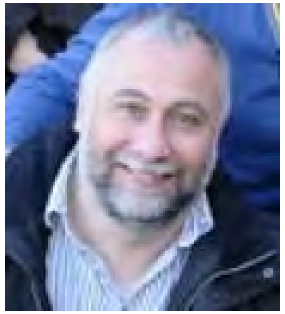

P. Abgrall

P. Simon

cea iramis ROBUST SUPERQ erc

cnrs spec ANR AGENCE NATIONALE DE LA RECHERCHE